2006-10-05

A Study on Pulsation In Runehamar Tunnel Fire Tests With Forced Longitudinal Ventilation

Mihyun Esther Kim
Worcester Polytechnic Institute

A STUDY ON PULSATION IN RUNEHAMAR TUNNEL FIRE TESTS WITH FORCED LONGITUDINAL VENTILATION

by

Mihyun Esther Kim

A Thesis

Submitted to the Faculty

of the

WORCESTER POLYTECHNIC INSTITUTE

in partial fulfillment of the requirements for the

Degree of Master of Science

in

Fire Protection Engineering

by

_____

June 2006

APPROVED:

_____

Professor John P. Woycheese, Major Advisor

_____

Professor Nicholas A. Dembsey, Co-Advisor

_____

Professor, Kathy A. Notarianni, Head of Department

ABSTRACT

Fire tests involving heavy goods vehicles (HGVs) in a road tunnel with forced ventilation in Norway, conducted by SP, demonstrated a pulsation phenomena that is similar to oscillating flames and thermo-acoustic instabilities previously observed in vitiated compartments and resonant systems that meet the Rayleigh criterion, respectively. This current study investigates whether the causal phenomena can be determined using either a simple, one-dimensional fluid dynamics model or a computation fluid dynamics program. It is assumed that the leading cause for pulsation is a locally under-ventilated fire.

Theoretical analysis shows that this assumption is valid and how such conditions can cause the flow field to change. A simple model is developed for a tunnel fire with forced, longitudinal ventilation. The results qualitatively represent the test data and support the assumption of a locally vitiated fire. A more sophisticated analysis, involving the Fire Dynamics Simulator (FDS) Version 4.0, provides similar results. Although FDS calibration, using similar experiment data from the Memorial Tunnel Ventilation Test Program, demonstrates model limitations in predicting smoke layers near the solid boundaries under forced flow field, the qualitative results from both models indicates that pulsation in large tunnel fires under forced ventilation conditions results from poor mixing of the bulk flow in the near field of the fire.

ACKNOWLEDGEMENT

First of all, I would like to thank God and my family for their support and encouragement. I thank Prof. Woycheese, my thesis advisor, for his guidance throughout the years that I have worked on this project. He told me right from the beginning that there will be peaks and valleys along the way. He reminded me that I was only at one of those valleys every time I had felt that my research was going nowhere. I would also like to thank Prof. Dembsey, my co-advisor, who helped me find the big picture of my research. Without his support, it would have been more challenging for me to finish this research. I thank Prof. Notarriani, the head of our department, for being on my thesis committee. I thank Prof. Rangwala for helping me develop my simple model for tunnel fires with forced longitudinal ventilation. Finally, I would like to thank Joel Sipe for his encouragement and help with my research.

TABLE OF CONTENTS

LIST OF TABLES

LIST OF FIGURES

NOMENCLATURE

$A_{CV_{fire}}$	cross-sectional area of the fire control volume
A_{tot}	total cross-sectional area
c_p	heat capacity of air
$c_{p,s}$	heat capacity of fuel
D	diameter
D^*	characterization length
E	energy
e/D	relative roughness
f	friction factor
f_0	initial friction factor
f_{down}	friction factor for downstream control volume
f_{up}	friction factor for upstream control volume
ΔH_{ch}	heat of combustion
M	molecular weight
m_d	mass of downstream control volume
m_f	mass of fire control volume
$\dot{m}_{net\ inflow,O_2}$	net mass inflow rate of fire control volume oxygen
$\dot{m}_{net\ inflow,s}$	net mass inflow rate of fire control volume fuel
$m_{O_2,f}$	mass of fire control volume oxygen
$\dot{m}_s$	mass flow rate of specified and stored fire control volume fuel supply
$m_{s,f}$	mass of fire control volume fuel
$\dot{m}_{s,fire}$	mass flow rate of specified fire control volume fuel supply
$\overline{P}$	average pressure
P_f	pressure at the fire control volume
P_{in}	pressure at the entrance of the upstream control volume
P_∞	ambient pressure
ρ	density
ρ_f	density for fire control volume
ρ_d	density for downstream control volume

ρ_{up}	density for upstream control volume
ρ_{∞}	ambient density
$\dot{Q}_{actual}$	actual heat release rate
R	universal gas constant
Re	Reynolds number
γ	ratio of the heat capacity at constant pressure to that at constant volume
r	stoichiometric ratio of fuel to oxygen
T_f	temperature of the fire control volume
T_d	temperature of the downstream control volume
T_s	temperature of the fuel supply
T_{∞}	ambient temperature
τ_0	shear stress
$\overline{U}$	average velocity
$\overline{U}_d$	average velocity of downstream control volume
$\overline{U}_{up}$	average velocity of upstream control volume
V_{CV}	volume of fire control volume
V_d	volume of downstream control volume
X	ratio of cross-sectional area of the fire control volume to total cross-sectional area
$Y_{O_2,f}$	oxygen mass yield of fire control volume
$Y_{O_2,\infty}$	ambient oxygen mass yield
$Y_{s,f}$	fuel mass yield of fire control volume

1. INTRODUCTION

Over the past 10 years, fire accidents in tunnels demonstrated the serious consequences in such events. For example, in 1999, a fire accident involving multiple heavy goods vehicles (HGVs) and passenger cars in the Mont Blanc (France/Italy) tunnel [1]. The estimated peak HRR of this fire was between 300 to 380 MW. This fire cost the lives of over forty people and caused significant damage to the tunnel. Two years later, another catastrophic fire occurred in the St. Gotthard (Switzerland) tunnel which resulted in 11 fatalities [2]. As in these cases, most of the fires resulted in multiple fatalities. In addition to that, in most cases the fires affected the tunnel facilities, which led to an interruption of regular tunnel operations for fire investigations and repair. The closure of tunnels introduced disturbances to nearby traffic and additional financial damage to the economy due to poor road transportation conditions.

The increasing frequency of such fires has led to greater efforts to identify and reduce potential fire risks in tunnels.

After assessing recent tunnel fire accidents, engineers determined that the fires in these accidents developed up to several hundred MWs when HGVs were involved [1, 2]. These fire sizes were far in excess of those used in current practice to represent the fire hazard from vehicles in tunnels. The estimated heat release rate of a heavy goods truck fire in a tunnel is 20 ~ 30 MW [3] and that for a tanker fire is 100 MW [4]. These values are used to evaluate proposed fire protection measures for tunnels. Although these guidelines are currently in use, they under-estimate the possible amount of transported goods on HGVs. This is why a relatively lower heat release rate is recommended compared to the ones found in the actual tunnel fire accidents. Due to the development in the vehicle constructing technology, the amount of goods that a HGV can transport has increased. Therefore, there is a need for further research to understand the growth and behaviors of relatively large HGV fires in tunnels. Prior studies have included full-scale fire tests that were conducted to explore fires involving heavy goods vehicles (HGV) and trailers. These vehicles, used in Europe, are similar to the 18-wheel tractor-trailers in the United States except for the sides of the trailer, which are typically canvas. Under certain conditions, the air flow within the tunnel fluctuated during the fire tests [5].

In this study, the research goal is to suggest explanations for the cause of such pulsation, which was observed in Runehamar Tunnel fire tests, to better understand the dynamics of the tunnel fires and conditions near the fire. The following chapters consist of a detailed description of pulsations observed in the Runehamar tunnel tests and phenomena that might have certain relevance to pulsation, along with previous studies conducted on pulsation in tunnel fires (Chapter 2); a theoretical explanation of pulsation (Chapter 3); mathematical modelling of pulsation in a tunnel (Chapter 4); computational experiments using Fire Dynamics Simulator 4.0 (FDS) [14, 15] (Chapter 5, Chapter 6); and conclusions (Chapter 7).

2. BACKGROUND

In this section, background research is presented for a series of full-scale tunnel fire tests and for pulsation that occurred in the course of those tests. In addition, other scenarios with similar pulsation characteristics are presented. Finally, previous work directly related to the pulsation observed in the Runehamar tunnel fire is discussed.

2.1. Runehamar tunnel fire tests and pulsation

In 2003, four large scale tunnel fire tests were conducted in the Runehamar tunnel in Europe [5]. These tests were intended to evaluate the characteristics of tunnel fires with semi-trailers as the fuel source and with forced longitudinal ventilation to exhaust the smoke. The semi-trailers used in the tests were similar to the size of the recent fires in Mont Blanc Tunnel (France/Italy) [1] and St. Gotthard Tunnel (Switzerland) [2], which resulted in the maximum heat release rate (HRR) of approximately 100 MW.

In the Runnehamar Tunnel fire test sets [5], four large scale fire tests were conducted by the Swedish National Testing and Research Institute (SP) with different types of commodities: Test 1, wood and plastic pallets; Test 2, wood pallets and mattresses; Test 3, furniture and rubber tires; and Test 4, plastic cups in cardboard boxes on wood pallets. The fuel packages were placed on a rack to model heavy goods vehicle (HGV) trailer. The tunnel was 9 m wide, 6 m high and about 1600 m long with a semi-circular ceiling. The tunnel also had a 1 ~ 3% slope. The fire was located about 1 km from the entrance in an area with an approximately 1% downhill slope. Forced longitudinal ventilation using two large mobile fans placed in series at the entrance of the tunnel for smoke exhaustion, provided initial mean flow velocity of 2.9 ~ 3.1 m/s at the center of the tunnel before igniting the fuel. 458 m downstream of the fire, a measuring station was measured the gas species concentrations, temperatures, and velocity measurements. The species concentration was used in the oxygen consumption calorimetry technique to calculate HRR of each test.

The experiment results show that the peak heat release rates of the fires were in the range of 100 MW to 220 MW [5]. The first two fire tests in the Runehamar Tunnel tests, Test 1 and 2, had relatively large heat release rates (HRR) compared to the other two. In

both cases, when the HRR exceeded 130MW, the gas flow inside the tunnel, flowing downstream from the entrance to the exit, pulsed in a periodical manner; gas flow velocity ranging from minimum of 1 m/s to maximum of 5 m/s. Moreover, the amplitude of pulsation changed according to the changes in the HRR [6]. When the HRR was an increasing, the magnitude of the flow fluctuation also increased; the opposite also held true.

Figure 1. Still images from a video clip of pulsation (delta time ≈ 1.4 seconds); Short flames standing upright in the first clip. Then the flames lean towards the floor. As the longitudinal flow velocity reduces, the flames starts to stand up. The fire releases combustion products and its flame length becomes shorter as shown in the first clip.

Figure 1 shows the detailed changes in the fire during each pulsation cycle. As the HRR of the fire increases beyond 125 MW, the fire started to act with the pulsing ventilation flow. At the beginning of the cycle, where the velocity is at its minimum, the flames stand upright (first image). As the ventilation velocity increases, the flames are pushed further downstream, which essentially caused the flames to lean towards the floor (second image). When the velocity reduces, the flames start to be in an upright position again with the flame tip facing the ceiling (third image). In the last image, the smoke generated from the flames is filling up the space around the fire. The smoke is instantly accumulated around the fire area because there is least amount of blowing effect from the ventilation flow (forth image). Then the flame length becomes shorter as in the first clip. The process repeated itself until the fire size became smaller than 125 ~ 135 MW.

A reasonable explanation for the cause of pulsation in these two tunnel fire tests remained unknown throughout the test. Pulsation in tunnel fires was observed for the first time, though gas flow or pressure oscillation during fire conditions have been observed in vitiated compartment fires [7, 8] and in combustors [11, 12]. They will be discussed in the next section. In the following sections, theoretical explanations of pulsation, mathematical modeling and computational fluid dynamics (CFD) simulations for the Runehamar tunnel fire tests are presented.

2.2. Oscillating flames in vitiated compartment and thermo-acoustic instability

Although there were no other pulsations that were observed in tunnel fires, other than those found in the Runehamar tunnel fire tests, research for other scenarios have demonstrated flow or pressure oscillations. Oscillating flames observed in vitiated compartment fires [7, 8] and low frequency thermo-acoustic pressure waves generated in Rijke tubes or combustors [9, 10, 11, 12] are both similar to the phenomenon measured during the Ruhenamar tests.

From the experimental work of Utiskul [7], three different types of fire phenomena were identified in ventilation limited compartment fires: flame oscillations, ghosting flames and burning at the vent. The first case results in oscillating flames in the compartment that appear similar to those observed in the pulsation cycle in Figure 1. Utiskul found that under natural ventilation, when the cross sectional areas of the opened vents were small enough to provide oxygen limited condition within the compartment, the flames may find insufficient amount of oxygen to continuously burn all the existing fuel vapors, but may find enough to prevent complete extinction. When this happened, the fire size reduced until the flames were hardly visible, but cycled, producing an oscillating flame. The process continued until the fuel supply was totally consumed. The oscillating flames were also observed by Kim [8] during his study of the effects of ventilation factor and fuel surface area on compartment fires. He identified oscillating flames when a small ventilation factor was applied.

Systems with thermo-acoustic pressure waves are another example where flow and pressure oscillations in the mean flow were found. Thermo-acoustic waves are a pressure oscillation generated by an unsteady heat release in the system. According to Lord Rayleigh, the criterion for a sustained heat-driven acoustic oscillation is determined by comparing the total mechanical energy added to the oscillation cycle via unsteady heat addition and the total energy removed from the cycle by dissipation [9]: “If heat be given to the air at the moment of greatest condensation, or be taken from it at the moment of greatest rarefaction, the vibration is encouraged. On the other hand, if heat be given at the moment of greatest rarefaction, or abstracted at the moment of greatest condensation, the

vibration is discouraged." Therefore, an acoustic wave may increase in energy to a self excited oscillation with large amplitude when the following conditions are met: (1) The system is highly resonant. (2) The heat source is an efficient acoustic source, which has an oscillation cycle in phase with the system's natural frequency. (3) The heat source is placed near an anti-node of the system, where condensation and rarefaction of the medium, usually air, exists. These thermo-acoustic instabilities in the system are observed in Rijke tubes [10], an open ended tube with a flame torch or other type of heating element such as heated gauze placed within the tube, industrial furnaces [11], and rockets and gas turbine engines [12].

2.3. Previous research on pulsation

Previous studies on pulsation in the Runehamar tunnel were done by Lönnermark, Persson and Ingason [6, 13]. They have performed a frequency analysis of the tunnel system, based on the impedance, to compare the periods of the pulsation from the model results with the test data. Their work suggests that the pulsation in Runehamar tunnel tests were due to thermo-acoustic instabilities because the characteristics of the oscillations were similar with the resonance of the system. The pulsation period of the thermo-acoustic waves that may be easily vibrated in the Runehamar tunnel were found to be comparable to the ones from the actual test data; 18 and 4 seconds for the Test 1 and Test 2 tests. In their analyses, the excitation source of the vibration was assumed as a forced vibration. Although they briefly mentioned several factors that might have caused or gave a positive effect in sustaining pulsation, they did not conclude which of them was the initiating factor of the pulsation. The factors that were identified by Lönnermark and Ingason are the size of the fire and the tunnel set-up; the effect of thermal expansion due to heat release in the combustion zone; the local availability of the oxygen at the vicinity of the fuel package; the slope and geometry of the tunnel; and external forces, such as wind outside the tunnel, acting on the ends of the tunnel.

3. THEORETICAL APPROACH

In this study, the major focus was determination of the conditions that initiate pulsation in a tunnel fire with forced-ventillation. Among the possible pulsation excitation sources listed by Lönnermark and Ingason [6, 13], locally under-ventilated conditions near the fuel package is the most likely explanation, although this assumption cannot be verified owing to insufficient test data to support or to deny the theory. Below, arguments are made to provide reasoning why a locally under-ventilated condition could have occurred during Runehamar tunnel tests where pulsation was observed.

First, though the oxygen, carbon monoxide and carbon dioxide concentration data obtained from the measuring station located around 460 m downstream of the fuel package indicate that there was enough oxygen supplied to the fire during each test, there is a possibility of having an insufficient mixing between the fuel vapor and air near the fire location. The test data indicated that the minimum oxygen concentration in the first two tests, T1 and T2, which experienced pulsation, were 6.4% and 8.6%, respectively. The maximum carbon monoxide and carbon dioxide concentrations were 1810 ppm and 11.7 % in T1 and 2430 ppm and 9.2 % in T2, respectively [24]. These measurements were taken at the measuring station, 460 m downstream of the fuel location, and at the center of the tunnel cross-section. Therefore, from the gas concentration data it can be concluded that these two fires were globally well-ventilated. However, if there was a low degree of mixing in the gas phase, the mixing layer, which is within its flammable limit, would have reduced resulting in a locally under-ventilated condition. This would produce a fuel rich region with a sharp fuel concentration gradient near that area. The existence of locally under-ventilated fire in a globally well-ventilated condition was identified during a series of fire experiments conducted in a compartment [26].

Another supporting fact is that for the Runehamar tunnel fire case, the low carbon monoxide concentration data cannot be used as a reliable indication of under-ventilated fire. Even if the near-field of the combustion zone was locally under-ventilated, the maximum concentration of carbon monoxide, measured 460 m downstream of the fire, can be considerably low as in the actual measurements because the gas temperature at the combustion zone was too high to produce a significant amount of carbon monoxide. Also,

the measuring station was too distant from the combustion zone. According to the work of Gottuk [27] on the influence of gas temperature on the production of carbon monoxide in a compartment fire, an upper layer gas temperature above 900 K allows almost complete oxidation of carbon monoxide to carbon dioxide when the compartment is over-ventilated or slightly under-ventilated. The high temperature allows the gas layer to be reactive, and therefore, encourages further oxidation of carbon monoxide to dioxide. In addition to the high temperature factor, the traveling distance of the combustion products, flowing under turbulent condition, must be considered. During its travel, the air flow from the upstream of the fire, which was not involved in the combustion reaction, could have mixed together. The mixing can reduce the concentration of combustion products including carbon monoxide. These relationships between the gas temperature, gas travel distance and carbon monoxide concentration can be used as a supporting explanation for why measuring a low carbon monoxide concentration is possible when the near-fuel region is locally under-ventilated.

Third, in both tests, T1 and T2, the pulsation occurred when the heat release rate (HRR) of the fire exceeded 125 ~ 135 MW, within a range where the mass burning rate increases due to the heat feedback from the flames and the heated walls to the fuel package for further vaporization. If the ventilation air supply and the configuration of the flame confinement stay the same, which was true for the Runehamar tunnel tests, an increase in the mass burning rate would encourage a localized under-ventilated condition near the fuel source due to poor mixing between the fuel vapor and air at that region. Therefore, pulsation occurring where the fire size is greater than a certain HRR, for both T1 and T2, supports the assumption of locally under-ventilated condition at the vicinity of the fuel load causing the pulsation.

Last, the flame response during pulsation, which was found in the video recording (Figure 1), was similar to that of the oscillating flames observed in the vitiated compartment fires. (The oscillating flame was mentioned in Chapter 2, background section.) From the video recording, it was clearly shown that the volume occupied by the flame near the fuel location was cycling between small and large. This reduction and increase in the flame size during the cycle may exist due to the fire experiencing near-extinction condition as in the oscillating flames found in vitiated compartment fires. The

oscillating flames are also produced near the extinction limit and this flame behavior was explained by Rangwala [28] using a Damkohler number. (The Damkohler number is a ratio of residence time of the reactants to chemical reaction time.) To have an ignition, the Damkohler number must be greater than its critical value. This means that flame can exist only when the duration of flammable gaseous mixture remaining in the reaction zone exceeds the length of time needed for the combustion reaction to occur. The residence time depends on the fluid dynamics of the flame and its surroundings, while the reaction time is proportional to the inverse of the flame reaction rate, and hence, this depends on the flame characteristics [29]. According to his explanation, the oscillations are due to the changes in the residence time of the reactants in the compartment. He discusses that the heat added from the fire changes the gas temperature and pressure in the compartment, affecting the flows at the opened vents. The changes in the vent flows decide the residence time of the fuel vapors and oxygen near the flames, allowing the flame to have different flame sizes. When the changes are consistent and periodic, stable oscillating flames are observed. The similarity of the flame behaviors between the ones found in the Runehamar tunnel fire tests, T1 and T2, and the oscillating flames in vitiated compartment fires also provide supporting evidence that during pulsation, the reaction zone near the fuel package could have been locally under-ventilation condition.

These reasons discussed above shows that assuming a locally under-ventilated condition at the vicinity of the fuel package during pulsation is reasonable. With this assumption, an explanation of the pulsation phenomena can be given by considering the velocity field near the locally under-ventilated region within the combustion zone, the time necessary for proper mixing between the fuel and air supplied from forced ventilation, i.e., the residence time, and the boundary conditions of the surroundings near this region.

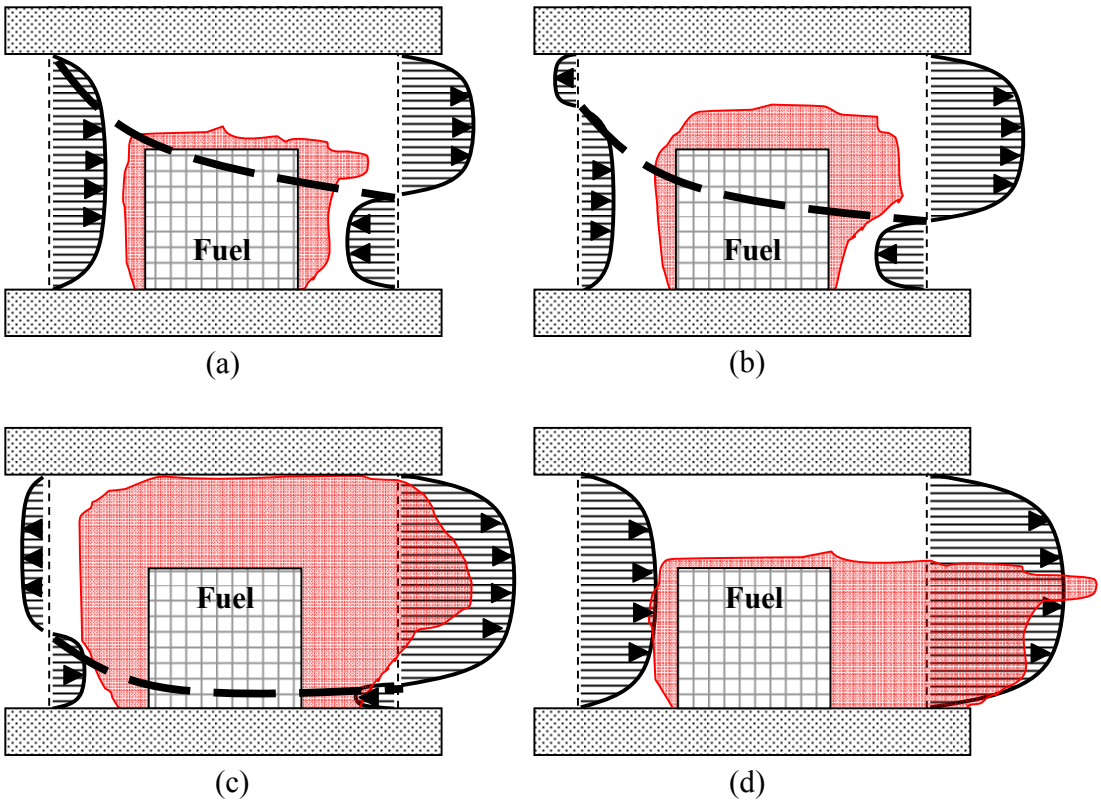

Figure 2. Conceptual diagram of each step in pulsation cycle; the velocity profiles near the fuel location, upstream and downstream, is given with the shaded area, which indicates the shape of the flame. Dashed line divides the flame into two parts – flame area where fresh oxygen entrainment is allowed (below the dashed line) and not allowed (above the dashed line). During pulsation, step (a) through (d) occurs repetitively.

As the fire size grows, the mass burning rate increases due to heat feedback from the flames and the boundaries such as the walls near the fuel. In a partially confined space with a forced air flow, as in the tunnel fire case with longitudinal ventilation, an increase in the released fuel vapor would encourage insufficient mixing between the vapor and air near the fuel location. Because flames can only propagate through a certain concentration range of flammable vapor mixture (a mixture of fuel vapor and air), between the Lower Flammable Limit (LFL) and Upper Flammable Limit (UFL), the insufficient mixing would cause the flames near the fuel location to reduce in size, for the volume with a concentration within the flammable limit decreases at that area. Though the flames die out, the mass burning rate is not affected significantly because the heated boundaries can supply enough heat energy for further vaporization of the solid fuel. Due to the decrease

in the fire size, the pressure around the fuel package would also decrease, allowing more oxygen to flow in to the area by increasing the upstream air flow velocity.

With the upstream air flow velocity increased, the flames now receive more oxygen and have better mixing in the gaseous phase between the fuel vapor and air near the fuel load. This affects the combustion process. The volume occupied with flammable vapor increases, and hence, allows the flame to become larger. However, the forced air flow velocity is high at this point to provide enough residence time for the combustion to fully occur. The flammable vapor have shorter period of time to react. The slightly increased heat release would cause the temperature and pressure in this region to increase. With the pressure increase at this area, the air inflow from the upstream of the fire would start to reduce. (See (a) in Figure 2.) The fire starts to entrain air from downstream of the fire as the reaction zone within the flame increases.

The decrease in the upstream air flow velocity provides longer residence time of the flammable vapor, which thickens the reaction zone within the flame. This encourages more combustion allowing an increase in the gas temperature and pressure near the fuel load. More combustion products are produced, while the upstream air inflow velocity decreases due to the pressure increase. The hot gases from the fire reaching the ceiling may flow in the opposite direction forming a ceiling jet depending on the air inflow velocity. (See (b) in Figure 2.) As this condition continues, the reaction zone increases to a point where the amount of entrained air can no longer support the flames. The increase in the reaction zone is similar to a flashover. (See (c) in Figure 2.) However, the flashover condition is quickly limited by the availability of oxygen within the reaction zone. This restraint allows the flame to reduce in size. However, in this stage, the fuel vapor is supplied continuously from the heat feedback to the solid fuel surfaces, which accelerates the oxygen limited condition in the near-fuel region. The pressure of this region starts to drop, and therefore, increases the upstream air inflow velocity. (See (d) in Figure 2.) The increase in the upstream flow velocity supplies more oxygen to the area close to the fuel location, but once again, the flow velocity is high that the residence time of the flammable vapor is short for an efficient combustion reaction. The flame length extends further downstream as the gases travel away from the near-fuel area because a significant amount of fuel-rich flammable vapor from the near-field region, which was accumulated

during the last stage, burns as it mixes with the air supply. The flame at the vicinity of the fuel package becomes smaller as the flammable gas mixture is blown away from this area. With this increase in the air supply, the fire receives more oxygen and has a chance of better mixing in the gas phase in the near-fuel region. Therefore, the flame starts to grow with more air entrainment near the floor. Now the process stage is back to (a) in Figure 2. The whole process repeats itself until the pulsation cycle is influenced by other effects such as a limitation in the fuel supply.

In the next sections, numerical analyses are conducted using two types of models: a simplified three zone model developed in this study and Fire Dynamics Simulator Version 4.0 developed by National Institute of Standards and Technology. There were two reasons why this series of numerical analyses were arranged. One was to test each model's capability of reproducing the given tunnel fire scenario, and the other was to understand further about the tunnel fire conditions, so that the explanation of pulsation given in this section could be verified to a certain degree.

4. SIMPLE ONE-DIMENSIONAL FLOW MODEL WITH ONE-ZONE COMPARTMENT MODEL

Simplified modeling of a fire in a tunnel with forced ventilation provides an understanding of the conditions within a tunnel under fire conditions. The tunnel was represented by three control volumes as shown in Figure 3: CV_{up}, CV_{down}, and CV_{fire}. The first two control volumes correspond, respectively, to the upstream and downstream portions of the tunnel, relative to the fire location. The third control volume represents the combustion zone near the original location of the fuel load, a "uniform property" modeling approach that was first introduced by Quintiere [30] is used to model compartment fire phenomena under vitiated conditions [7, 28]. This simplification offers insight into the fundamental characteristics of the tunnel fire properties.

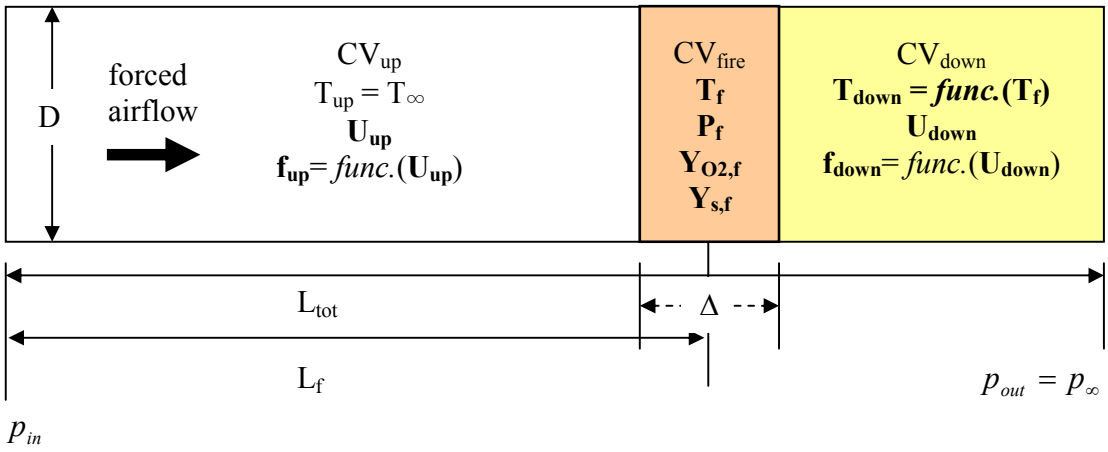

Figure 3. Simplified modeling of tunnel fires with forced longitudinal ventilation. The system is constructed with three control volumes; upstream tube, CV_{up}, downstream tube, CV_{down}, and fire area, CV_{fire}.

In this model, pressure changes in the fire control volume are generated by the energy input from combustion. These variances in pressure drive the velocity changes in the upstream and downstream tubes, varying the amount of air supplied into CV_{fire} and of gases leaving this control volume. Using the mass flow information in and out of CV_{fire}, the oxygen and fuel concentrations within CV_{fire} are found. The calculated species

concentrations of oxygen and fuel are directly related to the one-step combustion model, which determines the energy release in the fire control volume.

4.1. Flow modeling: CV_{up} and CV_{down}

For the gas flow calculations in the upstream and downstream control volumes, conservation of momentum is satisfied by Eq. (1), in which the shear stress term, τ_0, is expressed using the Darcy-Weisbach friction factor, f.

$$\frac{\partial \overline{U}}{\partial t} + \overline{U}\frac{\partial \overline{U}}{\partial x} = -\frac{1}{\rho}\frac{\partial p}{\partial x} - g\frac{dz}{dx} - \frac{4\tau_0}{\rho D} \qquad \text{Eq. (1)}$$

$$\text{where} \qquad \tau_0 = \frac{\rho f \overline{U}^2}{8}$$

The flow is assumed to be incompressible because the flow velocities found in tunnel fires with forced longitudinal ventilation have low Mach numbers. (Mach number is the ratio of fluid velocity over speed of sound.) For gas flow velocities with Mach numbers less than 0.3, the effects of gas density on flow pressure are negligible, such that the density is essentially constant under isothermal condition [**Error! Reference source not found.**]. The temperature in the upstream control volume is assumed to be its ambient value, T_∞ and that of the downstream control volume is found by conserving mass and allowing mass storage via temperature change in CV_{down}. (See Eq. (2).) The gases obey the ideal gas law and because the pressure changes within the control volumes are expected to be on the order of hundreds of Pascals, the pressure effect on density is considered to be minimal. (See Eq. (3).)

$$\frac{dm_d}{dt} = \left(\rho_f A X \overline{U}_d + \rho_{up} A(1-X)\overline{U}_{up}\right) - \rho_d A \overline{U}_d \qquad \text{Eq. (2)}$$

$$\text{where } X = \frac{A_{CV_{fire}}}{A_{tot}}$$

$$\left(\rho T\right)_\infty = \rho T = \frac{\overline{P}M}{R} = const \qquad \text{Eq. (3)}$$

The Darcy friction factor in the shear stress term is a function of surface roughness and Reynolds number. The friction factor is determined from Eq. (4) with an initial estimate from Eq. (5) that reduces the number of required iterations to find an appropriate f. The tube surface roughness was selected as that of the concrete.

$$\frac{1}{f^{0.5}} = -2.0\log\left(\frac{e/D}{3.7} + \frac{2.51}{\mathrm{Re}\, f^{0.5}}\right) \qquad \text{Eq. (4)}$$

$$f_0 = 0.25\left[\log\left(\frac{e/D}{3.7} + \frac{5.74}{\mathrm{Re}^{0.9}}\right)\right]^{-2} \qquad \text{Eq. (5)}$$

The initial velocities are prescribed, such that; $U_{up} = U_{down} = U_0$. The boundary conditions for each tube, which was given by the pressure information at one of each tube ends, were determined from the initial velocity value, U_0. The inlet pressure, P_{in} in the upstream tube was calculated using Eq. (6) and the outlet pressure, P_{out} in the downstream tube was assumed to be the same as the ambient, P_∞. They were kept constant throughout each calculation.

$$p_{in} = p_{atm} + \rho \frac{f}{D}\frac{L_{tot}}{2}\overline{U_0}^2 \qquad \text{Eq. (6)}$$

The final form of the equations used in the model, are as follows:

$$\frac{d\overline{U}_u}{dt} = -\frac{1}{\rho_{up}}\frac{\left(P_f(t) - P_{in}\right)}{L_f} - \frac{f_{up}}{D}\frac{\overline{U}_u{}^2}{2} \qquad \text{Eq. (7)}$$

$$\frac{d\overline{U}_d}{dt} = -\frac{1}{\rho_{down}}\frac{\left(P_\infty - P_f(t)\right)}{L_{tot} - L_f} - \frac{f_{down}}{D}\frac{\overline{U}_d{}^2}{2} \qquad \text{Eq. (8)}$$

$$\frac{dT_d}{dt} = -\frac{T_d{}^2}{(\rho T)_\infty V_d}\left(\left(\rho_f AX\overline{U}_d + \rho_{up}A(1-X)\overline{U}_{up}\right) - \rho_d A\overline{U}_d\right) \qquad \text{Eq. (9)}$$

4.2. One-zone compartment modeling for near-fire region: CV_{fire}

The near-fire region is modeled as one-zone compartment [7, 28, 30]. This region is considered to be a well-mixed system with uniform properties throughout. To find fluid properties within this control volume (e.g., gas temperature, pressure and species), conservation of mass, energy and species - oxygen and fuel - equations are required as follows:

$$\frac{dm_f}{dt} = \left(\rho_{up} A\overline{U}_{up} - \rho_d A\overline{U}_d\right) + \dot{m}_{s,fire} \qquad \text{Eq. (10)}$$

$$\frac{dE}{dt} = c_p A(\rho T)_\infty \left(\overline{U}_{up} - \overline{U}_d\right) + c_{p,s}\dot{m}_{s,fire} T_s + \dot{Q}_{actual} \qquad \text{Eq. (11)}$$

$$\frac{dm_{O_2,f}}{dt} = \dot{m}_{net\ inflow,O_2} - \frac{1}{r}\frac{\dot{Q}_{actual}}{\Delta H_{ch}} \qquad \text{Eq. (12)}$$

where

$$\dot{m}_{net\ inflow,O_2} = Y_{O_2,\infty}\rho_{up} AX\overline{U}_{up} - Y_{O_2,f}\rho_d AX\overline{U}_d \quad \left(\overline{U}_{up} \rangle 0, \overline{U}_d \rangle 0\right)$$

$$= Y_{O_2,f}\rho_{up} AX\overline{U}_{up} - Y_{O_2,f}\rho_d AX\overline{U}_d \quad \left(\overline{U}_{up} \langle 0, \overline{U}_d \rangle 0\right)$$

$$= Y_{O_2,\infty}\rho_{up} AX\overline{U}_{up} - Y_{O_2,\infty}\rho_d AX\overline{U}_d \quad \left(\overline{U}_{up} \rangle 0, \overline{U}_d \langle 0\right)$$

$$\frac{dm_{s,f}}{dt} = \dot{m}_{s,fire} + \dot{m}_{net\ inflow,s} - \frac{\dot{Q}_{actual}}{\Delta H_{ch}} \qquad \text{Eq. (13)}$$

where

$$\dot{m}_{net\ inflow,s} = -Y_{s,f}\rho_d A\overline{U}_d \quad \left(\overline{U}_{up} \rangle 0, \overline{U}_d \rangle 0\right)$$

$$= Y_{s,f}\left(\rho_{up} A\overline{U}_{up} - \rho_d A\overline{U}_d\right) \quad \left(\overline{U}_{up} \langle 0, \overline{U}_d \rangle 0\right)$$

$$= 0 \quad \left(\overline{U}_{up} \rangle 0, \overline{U}_d \langle 0\right)$$

The combustion reaction is assumed to be instantaneous. The reaction is limited by the amount of fuel and oxygen that exist in CV_{fire}. The amount of energy released, $\dot{Q}_{actual}$, is calculated using Eq. (14). This expression accounts for incomplete combustion due to limited ventilation. The amount of pyrolyzed fuel in the control volume, $\dot{m}_s$, is specified as a function of time; the unburned fuel stored in the control volume, $m_{s,f}$ is also available for combustion. The gases in this fire control volume are assumed to obey the ideal gas

law. The density is a function only of temperature only because the pressure changes within CV_{fire} during the fire is on the order of hundreds of Pascals, which is negligible compared to the atmosphere pressure. The combustion reaction is bounded when the control volume is vitiated. The limiting oxygen concentration for vitiation was assumed as less than 1 % of oxygen in volume.

$$\dot{Q}_{actual} = \dot{m}_s \Delta H_{ch} \frac{Y_{O_2,f}}{Y_{O_2,\infty}} \quad \text{Eq. (14)}$$

The initial conditions for the temperature, oxygen and fuel concentrations are found from the ambient conditions, $T_f = T_\infty$, $Yo_{2,f0} = Yo_{2,\infty} = 0.233$ kgO_2/kg air and $Ys,_{f0} = Ys,_\infty = 0$, and that of the pressure is calculated from the initial flow velocity as follows:

$$p_{f0} = p_\infty + \rho \frac{f_{up,0}}{D} \frac{\left(L_{tot} - L_f\right)}{2} U_0^2 \quad \text{Eq. (15)}$$

The equations for the model are as follows:

$$\frac{dT_f}{dt} = -\frac{T_f^{\,2}}{(\rho T)_\infty V_{CV}} \left(\left(\rho_{up} A \overline{U}_{up} - \rho_d A \overline{U}_d \right) + \dot{m}_{s,fire} \right) \quad \text{Eq. (16)}$$

$$\frac{dP_f}{dt} = \frac{\gamma - 1}{V_{CV}} \left(c_p A (\rho T)_\infty \left(\overline{U}_{up} - \overline{U}_d \right) + c_{p,s} \dot{m}_{s,fire} T_s + \dot{Q}_{actual} \right) \quad \text{Eq. (17)}$$

$$\frac{dY_{O_2,f}}{dt} = \frac{T_f}{(\rho T)_\infty V_{CV}} \left(\dot{m}_{net\ inflow,O_2} - \frac{1}{r} \frac{\dot{Q}_{actual}}{\Delta H_{ch}} \right) + \frac{Y_{O_2,f}}{T_f} \frac{dT_f}{dt} \quad \text{Eq. (18)}$$

$$\frac{dY_{s,f}}{dt} = \frac{T_f}{(\rho T)_\infty V_{CV}} \left(\dot{m}_{s,fire} + \dot{m}_{net\ inflow,s} - \frac{\dot{Q}_{actual}}{\Delta H_{ch}} \right) + \frac{Y_{s,f}}{T_f} \frac{dT_f}{dt} \quad \text{Eq. (19)}$$

4.3. Results and Discussion

The results from this modeling work are compared with the Runehamar tunnel fire test data [5, 6, 25]. An ordinary differential equation solver for stiff equations in MATLAB was used to perform the calculations. The fuel supply rate is specified using a t-square fire with an alpha value of 0.8 kW/s^2 to represent the fire growth in the Runehamar tunnel fire tests. The length of three control volumes is 1600 m, as in the experiments, with the

upstream and downstream control volumes 1000 m and 600 m in length, respectively. The diameter of the tube is 8 m and the initial flow velocity is 3 m/s.

The calculation results show that when the air flow into CV_{fire} is small enough, CV_{fire} becomes vitiated at a lower heat release rate. As the ratio, X, of cross-sectional area of CV_{fire} to that of the total area reduces, the control volume becomes vitiated earlier and at a lower actual heat release rate, $\dot{Q}_{actual}$. Because a t-square fire is used in the model, the specified heat release rate, $\dot{Q}_{specified}$, is likewise smaller. In Figure 4, modeling results with different values for X are shown. When X is 1.0 (i.e., 100 % of the air flow from the upstream tube enters CV_{fire}), the fire control volume became vitiated at t = 648 sec. at which the actual heat release rate was 183.5 MW. The fuel could have produced 336 MW fire if it was not limited by ventilation.

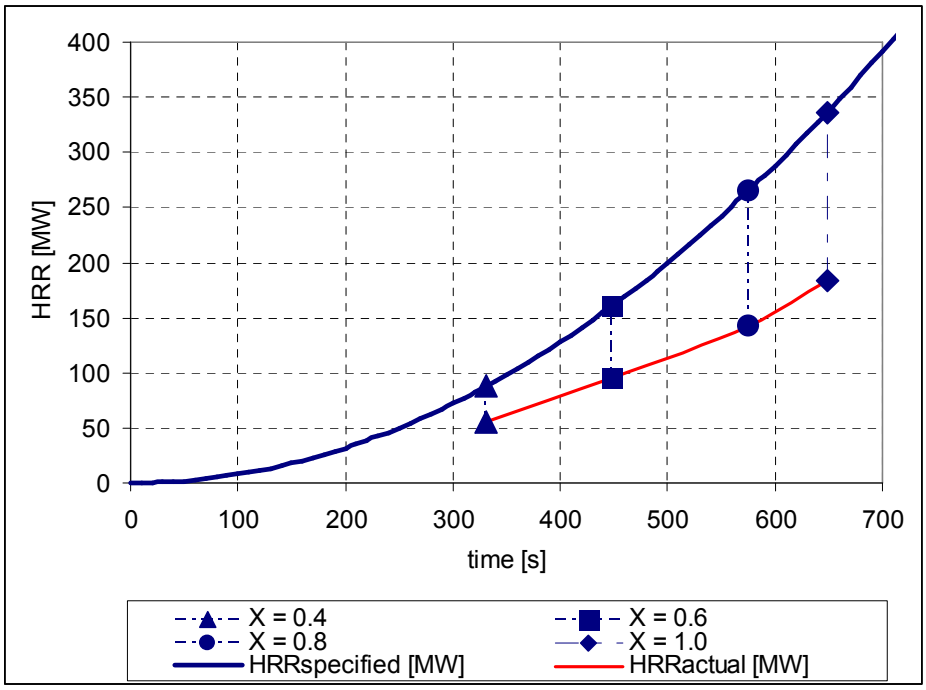

Figure 4. Model calculation results: It shows the relationship between the ratio, X, of CV_{fire} cross-sectional area to total cross-sectional area and CV_{fire} vitiation. t^2 fire with $\alpha = 0.8$, adiabatic condition, D = 8 m, Δ = 30 m, L_{tot} = 1600 m, L_f = 1000 m, T_{amb} = 283 K, U_0 = 3 m/s.

When the fire control volume is vitiated, flame is no longer supported due to lack of ventilation. The actual heat release rate, $\dot{Q}_{actual}$, becomes 0 at the time of vitiation and the pressure, P_f, drops accordingly due to less energy input to the CV_{fire}. This allows more air flow from the upstream tube, which increases the available oxygen. The increased

oxygen supply supports combustion once again. Shortly after the combustion resumes, CV_{fire} becomes vitiated as the oxygen within the control volume is quickly consumed. Therefore, the process forms a cycle as shown in Figure 5. Figure 5 shows the results from a case with 40 % of heat loss to the boundaries and 50 % of the air flow from the upstream tube entering the fire control volume. CV_{fire} is 30 m long. Vitiation occurs 457 seconds from ignition and the actual heat release rate at that time is 100 MW, which is 67 MW less than the maximum. The oscillation is observed in pressure and species – oxygen and fuel – concentrations of CV_{fire} and in the heat release rate. Although there were pressure fluctuations in CV_{fire}, the magnitude of its change was small to force the flows in the upstream and downstream tube to oscillate also, and hence, the gas flows were less affected from vitiation. This is shown in Figure 5 and Figure 6.

This simplified approach to a complex problem shows a qualitative agreement to the experimental data. The second test in the Runehamar tunnel fire experiment pulses when the fire size was larger than 125 ~ 135 MW; the modeling results shown in Figure 5 and Figure 6 reasonably match with the test data. Although the calculated pressure fluctuation in CV_{fire} was not sufficient to affect the flows in the upstream and downstream tubes, it is possible that the periodic changes in pressure at the fire location caused by vitiation resulted in standing pressure waves, amplified until the gas flow velocities in the tunnel was affected. The results from this simple model support the theory of a locally under-ventilated fire causing pulsation. The pulsation steps explained in the theoretical analysis part are consistent with the vitiated CV_{fire} from the model causing oscillations in pressure, species concentrations and heat release rate.

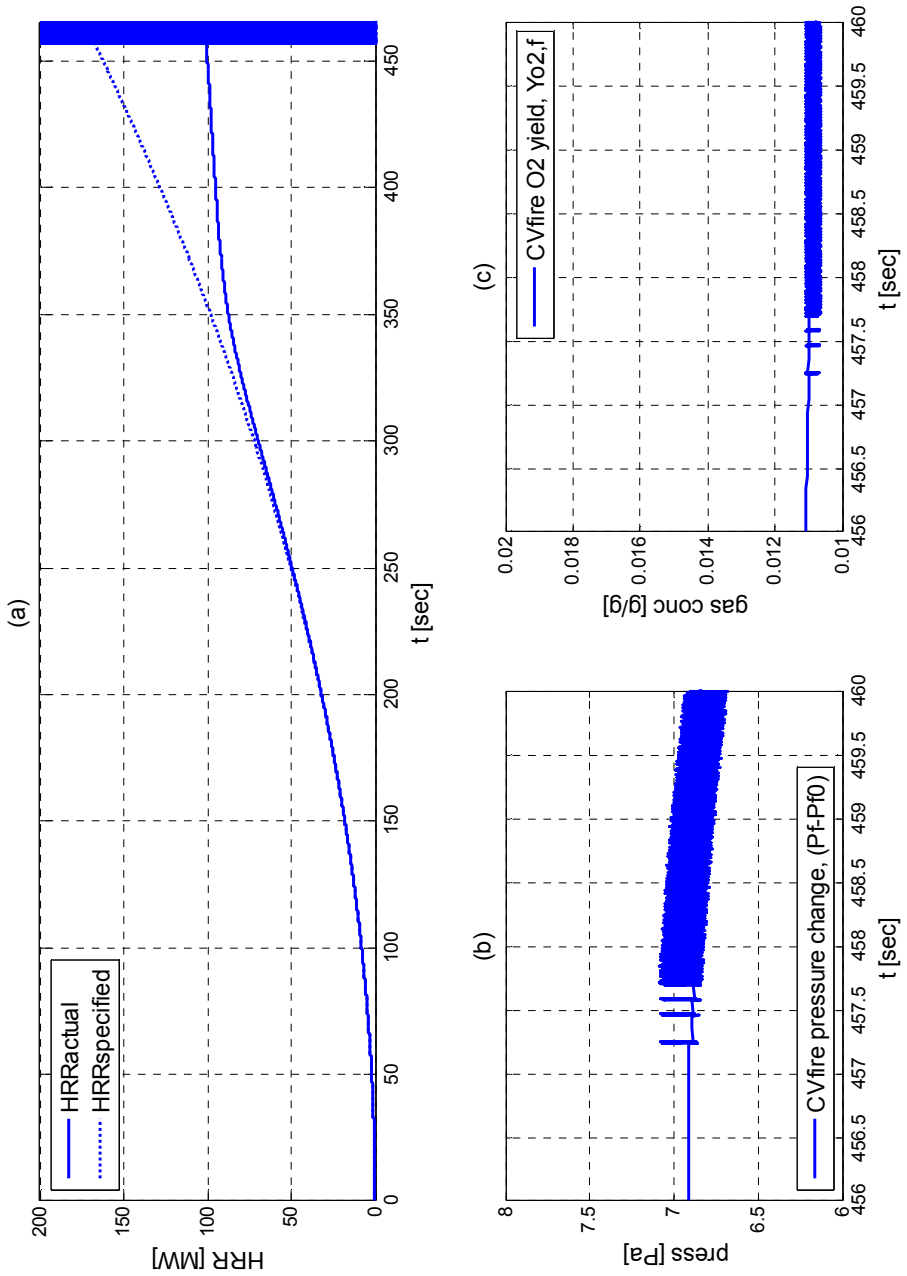

Figure 5. **A case run, which demonstrates the oscillation from t = 443 seconds: t^2 fire with α = 0.8, 40 % heat loss, X = 0.5, D = 8 m, Δ = 30 m, L_{tot} = 1600 m, L_f = 1000 m, T_{amb} = 283 K, U_0 = 3 m/s. (a) Heat release rates, HRR_{actual} and $HRR_{specified}$; (b) Pressure change in CV_{fire}; (c) Species concentration in CV_{fire}**

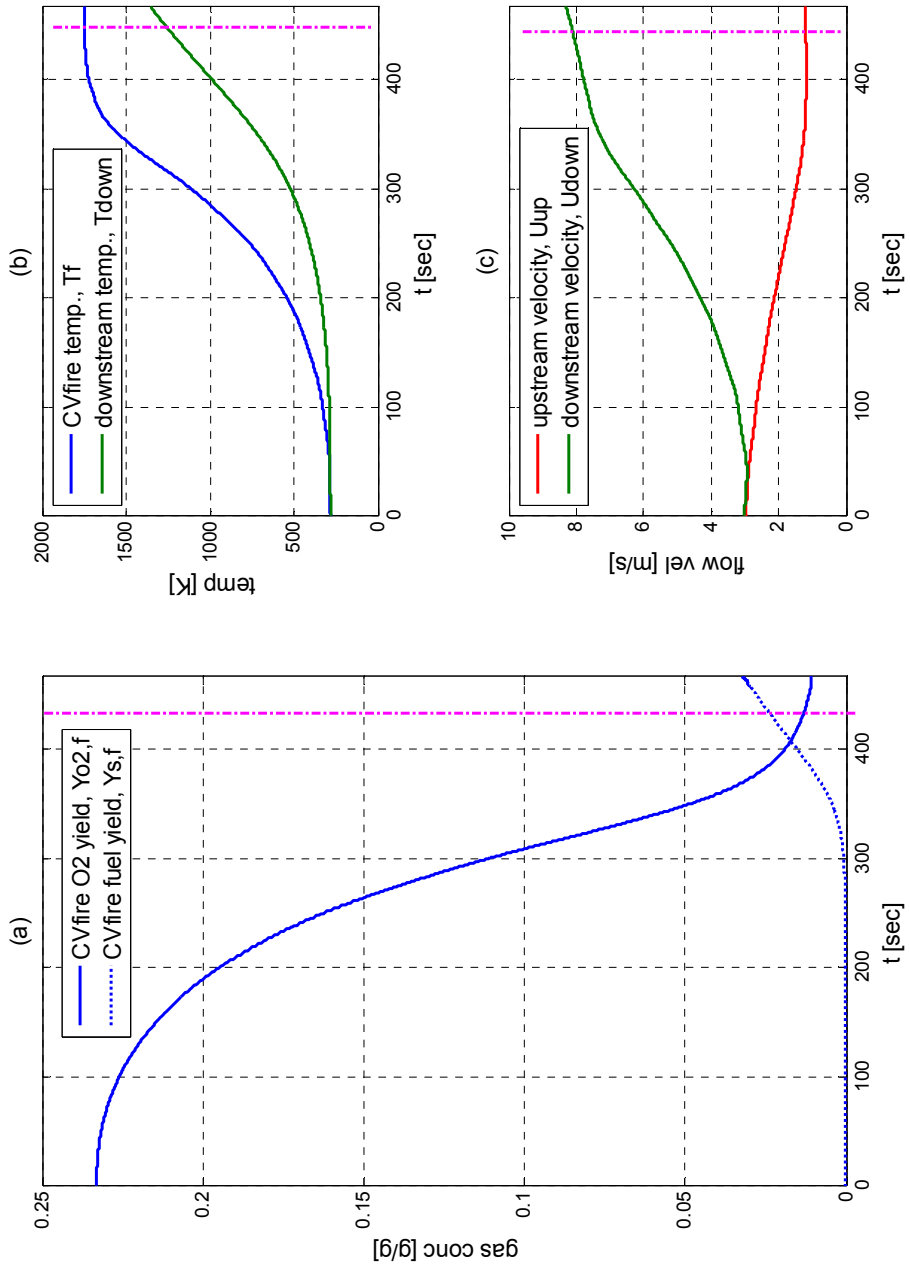

Figure 6. A case run, which shows the results with CV_{fire} vitiation from t = 480 seconds: t^2 fire with α = 0.8, 40 % heat loss, X = 0.5, D = 8 m, Δ = 30 m, L_{tot} = 1600 m, L_f = 1000 m, T_{amb} = 283 K, U_0 = 3 m/s, $(Y_{o2,s})_{lim}$ = 0.011. (a) Species concentration in CV_{fire}; (b) Gas temperatures in CV_{fire} and CV_{down}; (c) Flow velocities in CV_{up} and CV_{down}. The pink dashed line(-.-) indicates the time of initiation of vitiation.

5. EVALUATION OF FIRE DYNAMICS SIMULATOR VERSION 4.0FOR TUNNEL FIRE SCENARIOS WITH FORCED LONGITUDINAL VENTILATION

Esther Kim, John P. Woycheese and Nicholas A. Dembsey, Worcester Polytechnic Institute, Worcester, MA 01609 – 2280

Abstract

In this study, a series of sensitivity analyses were conducted to calibrate a computational fluid dynamic (CFD) model, Fire Dynamics Simulator (FDS) version 4.0, for tunnel fire simulations. A tunnel fire test with a fire size on the order of a 100 MW with forced, longitudinal ventilation was chosen from the Memorial Tunnel Ventilation Test Program (MTVTP) after considering recent tunnel fire accidents and the use of CFD models in practice. A careful study of grid size and parameters used in the Large Eddy Simulation (LES) turbulence model – turbulent Prandtl number, turbulent Schmidt number, and Smagorinsky constant – was conducted. More detailed analyses were performed to refine the smoke layer prediction of FDS, especially on backflow (i.e., a reversed smoke flow near the ceiling). Also, energy conservation was checked for this scenario in FDS. A simple guideline is given for smoke layer simulations using FDS for similar tunnel fire scenarios.

Keywords: tunnel fire, CFD, FDS, model calibration, longitudinal ventilation, backlayering, backflow

Nomenclature

D*: characteristic fire diameter
$\dot{Q}$: heat release rate
Δ: grid length scale
μ: viscosity
c_p: specific heat capacity
Cs: Smagorinsky constant
D: mass diffusivity
k: conductivity
Pr_{turb}: turbulent Prandtl number
Q*: characteristic fire size
Sc_{turb}: turbulent Schmidt number
T: temperature
u, v, w: flow velocities in x, y and z direction
ρ: density

Subscripts
∞: ambient
LES: for Large Eddy Simulation

5.1. Introduction

Over the past 10 years, several accidents in tunnels have demonstrated the serious consequences of uncontrolled fires in confined spaces [5-1]. The Mont Blanc (France/Italy) incident in 1999 involved multiple heavy goods vehicles (HGVs) and passenger cars and had an estimated peak heat release rate (HRR) of 300 to 380 MW, which is significantly higher than typical design fires for tunnel analyses [5-2, 5-3]. Over forty people were killed and the tunnel was significantly damaged. Two years later, a similar fire in the St. Gotthard (Switzerland) tunnel [5-4] resulted in 11 fatalities. In addition to the human cost, tunnel closures for structural repairs, as experienced from these past accidents, have significant economic impact over a wider region. The increasing frequency of these fire incidents has led to greater effort to identify and reduce the potential fire risks in tunnels.

One of the tools commonly used by engineers to study and design fire-safe tunnels is computational fluid dynamics (CFD) simulation, which is more cost-effective than conducting large-scale fire experiments. The model parameters must be carefully tuned for each scenario to ensure that appropriate results are developed. Simulations without this critical model calibration may give a false basis for engineering decisions.

As with any other types of models, CFD simulations have limitations in predicting the dynamics of the fluid, as determined by assumptions inherent in the model. As algorithms become more complex, it is harder to identify the limitations of the model. Hence, testing the model under known conditions and comparing the simulated results to data from a particular fire test is important before using the model to predict the results of a similar, untested scenario. This methodology identifies computational limitations of the CFD models.

In this study, Fire Dynamics Simulator (FDS) Version 4.0 [5-5, 5-6], which is a well-known CFD tool for the fire protection engineering field, was used. This model was developed by the National Institute of Standards and Technology (NIST). FDS was evaluated via sensitivity analyses of grid sizes and several parameters to determine its ability to resolve large fires, on the order of a 100 MW, in tunnels with forced,

longitudinal smoke ventilation. This study identifies limitations when using FDS for similar tunnel fires and provides guidelines for simulating these types of fire scenarios.

5.2. Background

In this section, background research on FDS Version 4.0 [5-5, 5-6], the Memorial tunnel fire test [5-7] 621A, and other FDS model calibration work [5-8, 5-9, 5-10] on tunnel fires are introduced. The research results for FDS and model calibration are included for general information about the model and past studies using FDS on tunnel fires. The Memorial tunnel fire test is discussed to provide general information about the experiment and to explain why Test 621A was of special interest to this study.

5.2.1. Fire Dynamics Simulator Version 4.0

FDS [5-5, 5-6] simulates thermally driven flows with relatively low speed compared to the speed of sound. The model assumes that the flow is weakly compressible, which allows larger time steps because acoustic pressure waves are not considered in the calculations.

In turbulent flows, there are wide ranges of length and time scales involved in the dynamics of the flow. For the turbulence calculations in the gas phase the user can apply either the Direct Numerical Simulation (DNS) or the Large Eddy Simulation (LES) model within FDS. For DNS, all fluctuations within the flow are solved directly, which can be extremely time-consuming. LES, which was used in this study, assumes that the large eddies in the turbulent flow dominate the transport of conserved properties of the gas phase [5-11]. This model approximates the sub-scale turbulence and directly calculates the swirls and fluctuations that have relatively large length scales compared to those used in DNS. The Smagorinsky model, which is used for the sub-scale calculation, is based on the eddy viscosity assumption. This approach assumes that the small scales are in equilibrium and, hence, the energy production and dissipation are in balance [5-12]. With a carefully chosen grid size, LES produces reasonable results; however, several weaknesses of the Smagorinsky model have been identified. For example, the Smagorinsky constant depends on the flow conditions; unfortunately, the near-wall flows are not resolved sufficiently by LES. Another drawback is that the Smagorinsky sub-grid model can only account for forward scatter, (i.e., energy dissipation from large to small

scale), which can cause significant error when there is energy flow in the other direction [5-13, 5-14].

Combined with the turbulence model, FDS [5-5, 5-6] uses the mixture fraction approach to model combustion. This approach traces the mixture fraction of fuel and oxygen to find the flame sheet location, where the reactants are consumed and combustion products with energy are released. The mixture fraction approach assumes that the combustion reaction depends on the mixing of fuel and oxygen. This assumption may not hold for cases where combustion does not take place, even with the proper mixing. One example is ventilation-limited conditions. FDS implements an empirical model for flame extinction to account for this phenomenon. The volume fraction of the oxygen and temperature of the volume near the fire is evaluated within the model to determine whether or not the flame is supported.

5.2.2. Memorial Tunnel Fire Test

The Memorial Tunnel Ventilation Test Program (MTVTP) was conducted in the early 1990s to study tunnel fires with various types of ventilation systems: full and partial transverse ventilation, natural ventilation, and longitudinal ventilation with jet fans. The fire sizes were varied from 10 MW to 100 MW while closely observing the ability of each ventilation system to extract smoke and reduce gas temperatures within the tunnel for fire emergencies. A total of 98 tests were included in this program.

Out of 98 tests, Test 621A, which had a fire size of 100 MW during the test and longitudinal ventilation system using jet fans placed along the ceiling, was selected for this study due to the following reasons: Similarity of fire size to the potential fire load in current tunnels and of the ventilation approach in methods used to determine the critical ventilation velocity. Assessing up-to-date tunnel fire accidents, engineers determined that in many cases the fires developed up to several 100 MWs [5-1, 5-15] without a tanker being involved in the fire. However, there has been less research conducted for tunnel fires with this fire size because they are far in excess of those used in current practice to represent the fire risk from vehicles in tunnels. According to the World Road Association (PIARC), Fire and Smoke Control in Road Tunnels (Tables 2.4.1 and 2.4.3, and Sections II.4.1 and II.4.3) [5-2], only a tanker fire was suggested to produce a heat

release rate around 100 MW. This information is also included in the National Fire Protection Association (NFPA) 502, Standard for Road Tunnels, Bridges, and Other Limited Access Highways, 2004 Edition [5-3], and is used fairly often in practice to find feasible protection measures for suggested design fires.

The ventilation system used in this test is frequently modeled by practitioners using CFD codes to find the sufficient ventilation velocity for preventing backlayering (i.e., critical ventilation velocity) [5-16, 5-17]. Backlayering, also known as backflow, refers to a condition where smoke flows in the opposite direction of the forced, longitudinal ventilation. When longitudinal ventilation is applied, hot gases from the fire are pushed towards one end of the tunnel, allowing a smoke-free path in the upstream of the fire for emergency escapes and fire brigades. (See Figure 5-1.) However, if the ventilation velocity is not high enough, backlayering occurs, which may result in high concentration of toxic smoke and high heat flux from the hot gas layer in the emergency route.

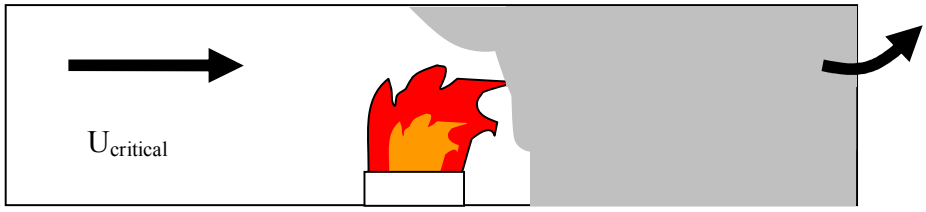

Figure 5-1. A diagram of a tunnel with forced longitudinal ventilation: the smoke produced from the fire is pushed towards the tunnel exit (downstream of the fire) due to the forced air flow from the upstream of the fire. The ventilation allows the upstream of the fire to be smoke-free for emergency evacuation and fire brigades.

5.2.3. Model Calibration on Tunnel Fires

There have been several attempts to calibrate FDS [5-8, 5-9, 5-10] for a given tunnel fire scenario. The results from these works may or may not be helpful in terms of understanding FDS's capability of simulating the tunnel fire scenario selected in this study – tunnel fire with a fire size ~ 100 MW and forced, longitudinal ventilation – because the outcomes of each model calibration work differ case by case.

McGrattan and Hamins [5-8] have conducted model calibration work using data from two tests from the Memorial Tunnel Ventilation Test Program (MTVTP) [5-7], which had fire sizes of 20 MW and 50 MW. Both tests were naturally ventilated. They compared the gas temperature data to the predicted ones from FDS calculations. The

measured maximum temperature above the fire near the ceiling was 300 °C and 800 °C for 20 MW and 50 MW fires, respectively, while the simulation results showed an agreement with the test data within 50 °C. Hwang and Edwards [5-9] used the data from the work of Hwang and Wargo (small scale) [5-18] and MTVTP (full scale) to verify FDS. Both test data were tunnel fires with forced, longitudinal ventilation. The HRRs of the fire in small and full scale experiments were around 3.3 kW and 50 MW, respectively. They compared the simulated backlayering thickness with the actual test results using the velocity profile and the shape of the gas temperature contour within the tunnel. For small scale tunnel fire, backlayering was under-predicted by FDS while in the other case, it was over-predicted. It was noted by the authors that this was observed may be due to the difference in the tunnel ceiling shape used in the experiment and in the FDS simulation. Another set of numerical studies using FDS was conducted by Lee and Ryou [5-10]. They compared the small scale tunnel fire experiment data, which had a fire size from 2.47 to 12.30 kW, to the FDS simulation results. They concluded that FDS had simulated the backlayering quite well in terms of predicting the gas temperature and velocity.

5.3. FDS Set-up

Figure 5-2 shows a partial diagram of the Memorial tunnel. In the figure, the fire location is placed at 0 m while the upstream and downstream of the fire is found at the negative and positive side of the fire. This notation was defined for consistency in indicating the axial locations within the Memorial tunnel throughout this study.

The geometry of Memorial tunnel is 8.8 m wide, 7.9 m high, and 853.7 m long with a 3.2 % uphill grade and a semi-circular ceiling. For test 621A, the tunnel entrance was located -615.5 m upstream of the fire (approximately 72 % of the tunnel length). Fuel Oil No. 2, also known as diesel fuel, was used to generate a pool fire that resulted in a fire size approximately 100 MW. Forced, longitudinal ventilation was supplied by jet fans placed along the ceiling. The tunnel had a concrete wall and the ambient temperature was approximately 10 °C.

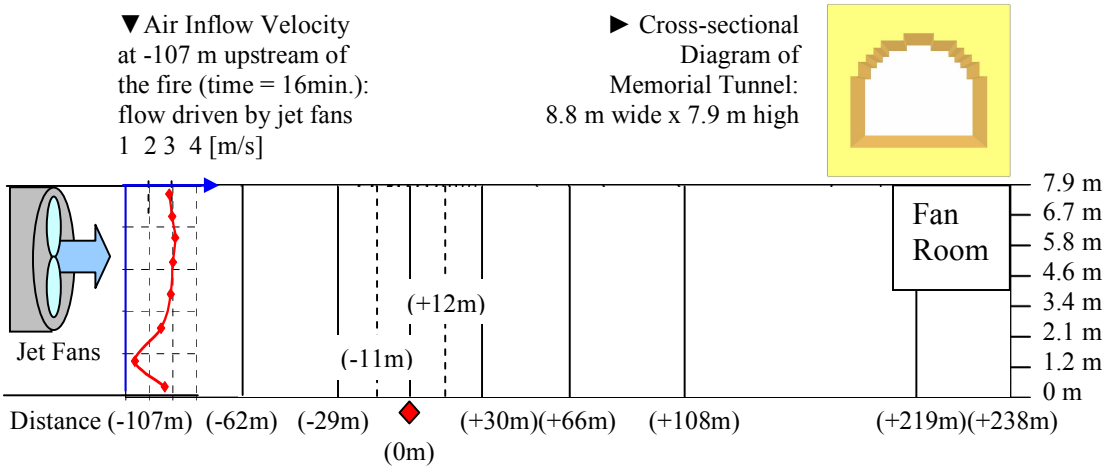

Figure 5-2. Memorial Tunnel Test 621A: Forced longitudinal ventilation was supplied by multiple jet fans placed upstream of the location -107 m upstream of the fire. Fire location is indicated with a red diamond (♦).The airflow velocity profile is plotted in red at the left side of the figure, which was used as an input velocity in FDS.

For FDS simulations, the Memorial tunnel geometry was simplified (See Figure 5-2). First, only 40 % of the tunnel was simulated: from -107 m upstream of the fire to the tunnel exit (+238 m downstream of the fire). The two reasons for these simplifications are related to the number of grid cells and jet fan simulation. If the whole tunnel was simulated, the number of grid cells in the simulation would be in excess of the maximum number of grid cells for the project personal computer (CPU of 3.4 GHz and a RAM of 3.25 GB) to manage. With the finest grid for the grid sensitivity analysis, 3.32×10^6 cells would be required to model the entire tunnel, from the tunnel entrance to the exit. This simulation would need a computer with a RAM memory greater than 3.25 GB. In addition, the reduced tunnel length avoids difficulties in simulating the jet fans installed along the ceiling, from the tunnel entrance (-615.5 m upstream of the fire) to approximately -100 m upstream of the fire. Downstream of -107 m location, which is shown in Figure 5-2, the forced air flow was influenced only by the fire and tunnel walls. Second, the uphill grade was ignored. Third, the semi-circular ceiling was constructed using rectangular obstructions as shown in Figure 5-2 (tunnel cross-section). This method is known as the stair-stepping. In the later part of this study, the effect of having a stair-stepped ceiling on the simulation results were checked by using a feature in FDS called

SAWTOOTH. The SAWTOOTH feature eliminates the small eddies generated by the stair-stepping near the ceiling.

The fire is simulated using a propane burner. The fuel base area was measure to be approximately 46 m^2, and therefore, a 4.7 m by 4.7 m burner surface was modeled with a Heat Release Rate Per Unit Area, HRRPUA = 2180 kW/m^2. The heat release rate curve from the test report was used to account for the changes in the fire size during the simulation.

The forced, longitudinal ventilation was simulated using the velocity profile obtained from the actual test (Test 621A) measured at -107 m upstream of the fire. The velocity profile from this location, which was varying in time, was used as the air inflow boundary condition for FDS simulations. The other end of the tunnel, the exit, was opened to atmosphere assuming that the pressure was kept at its ambient value.

Table 5-1. A summary of FDS simulation set-up: shows how the tunnel geometry, fire, and ventilation from the actual test were reproduced in FDS environment.

	Actual Tunnel Test	**FDS Simulation**
Tunnel Geometry		
Tunnel Length	-615.5m < X < +238m	-107m < X < +238m
Tunnel Slope	3.2% uphill	neglected
Tunnel Ceiling	semi-circular	stair-stepping w/ or w/o SAWTOOTH
Fire		
Fuel Type	No.2 Fuel	propane
Fire Type	pool fire	gas burner fire
Fire History	heat release rate curve from the actual test	
Ventilation		
Ventilation Type	forced, longitudinal	
Ventilation Apparatus	jet fans placed along the tunnel ceiling	velocity profile measured from the actual test at -107m upstream of the fire was used as a forced inflow velocity

The initial and ambient air temperature was 10 °C. The tunnel walls were assumed as concrete with its backing insulated. The VBC parameter, which decides the near-wall slip conditions, was varied from its default value of 0.5 in the later part of the study. The VBC value can vary from -1 (no-slip condition) to 1 (free-slip). Additional grid cells were generated outside of the tunnel exit for more reliable CFD results.

The simulation results of gas temperature and velocity were compared with the test data. The simulated temperatures and velocities were recorded using point measurements (THCP) placed along the centerline of the tunnel as shown in Figure 5-2.

5.4. Results and Discussion

5.4.1. Grid sensitivity analysis

Finding a suitable grid size is one of the difficulties in using FDS. Fine resolution may produce more detailed and reliable simulation results but, at the same time, will significantly increase the simulation time, which can be unsuitable for practical use. Therefore, it is important to select an appropriate grid size: using a grid size that balances simulation time with accuracy. One methodology requires that the characteristic fire diameter, D* (see Eq. 5-1) span at least ten grid cells within D* [5-19]. This value may not be the same as the actual fire diameter. The expression comes from the characteristic fire size, Q* which is a dimensionless heat release rate that accounts for the fire size and length [5-20]. For the Memorial Tunnel Test 621A, $\dot{Q}$ = 100 MW, the D* value is approximately 6.05 m. For the grid sensitivity analysis, grid sizes of 5%, 8%, and 10% of D* (0.3 m, 0.48 m, and 0.6 m, respectively) were evaluated.

$$D^* = \left(\frac{\dot{Q}}{\rho_\infty c_p T_\infty \sqrt{g}} \right)^{\frac{2}{5}} \approx 6.05m \qquad \text{Eq. 5-1}$$

The grid sensitivity analysis shows that grid sizes of 5% to 10% of the characteristic fire diameter, D*, provide similar results for temperature and the velocity profiles within the tunnel. The discrepancies in the simulated maximum temperature near the fire area as comparable to test data were in the range of 21% (finest grid) ~ 36% (coarse grid).

A typical comparison between the simulated gas temperature and the experiment data at 12 m downstream of the fire is shown in Figure 5-3. In the downstream area, simulated temperatures from three FDS runs (simulations with grid sizes of 5%, 8% and 10% of the D* value) were very similar to each other. All three cases had gas temperatures that were approximately 100 ºC lower than those from the test data.

The velocity profiles from three FDS simulations show backlayering (i.e., hot gases from the fire traveling upstream against forced longitudinal ventilation), which did not occur in the tests. Apart from the near ceiling region where backlayering had occurred, the differences between the velocity outputs from these three simulations and the measured data were approximately ± 2 m/s.

The computational time for each simulation was approximately 0.6, 1.5 and 7.5 days for a case with grid sizes of 10%, 8% and 5% of the D* value, respectively. For these simulations, a computer that has a CPU of 3.4 GHz and a RAM of 3.25 GB was used. Therefore, considering the computational expenses (i.e., simulation time necessary for each FDS run) and the quality of the simulations, a grid size of 8 % of D* was used in the remainder of this study.

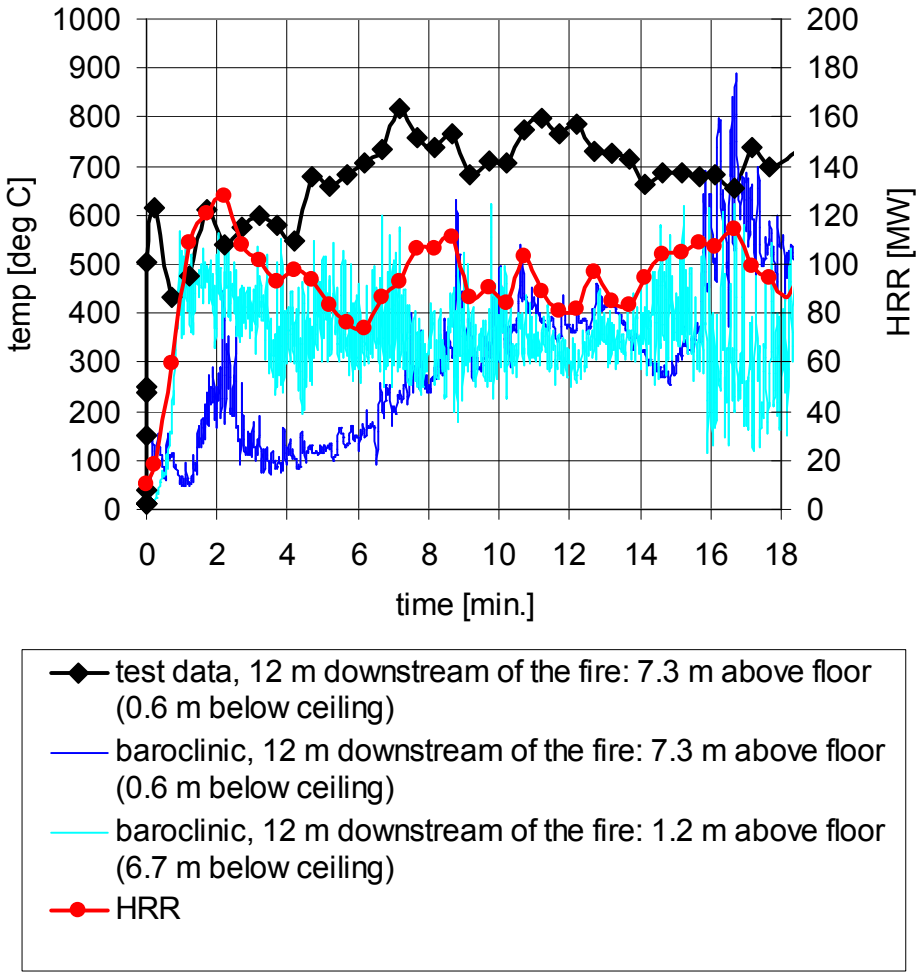

Figure 5-3. Gas temperatures near the ceiling at 12 m downstream of the fire with heat release rate (HRR) data using 8% of the D* for grid cell size: Temperature comparison between the simulation results with the consideration of baroclinic torque, and the test data. The simulated temperatures trace the given heat release rate.

5.4.2. Conservation of energy in FDS

The simulation results were analyzed to verify that the model conserves energy. To quantify the energy loss in the calculations, a steady 100MW fire in a tunnel is simulated with a constant longitudinal ventilation velocity of 3.0 m/s (top flow) and 2.5 m/s (bottom flow) at the tunnel entrance. The inflow velocity was kept at a constant value particularly for this simulation because a steady-state in FDS (in terms of energy balance) was desired to check the conservation of energy for this model. Other conditions are identical to the

Memorial Tunnel Test 621A simulations performed in the sensitivity analysis section. Using the method introduced in the user's guide [5-5] of FDS, the CONV and COND column in the hrr file were added and compared to the total heat release rate column, HRR, when the solid boundaries reached its steady state. The loss term is on the order of 2%, which is negligible.

5.4.3. Parameter sensitivity analysis related to the LES turbulence model

The next sensitivity analysis involved a series of user-specified parameters for the LES turbulence model in FDS [5-6]: the Smagorinsky constant, turbulent Prandtl number, and turbulent Schmidt number. These parameters were selected because they are directly related to the forced flow field and combustion calculations in the tunnel. The accuracy of the turbulent model determines the fire environment of the tunnel. Therefore, the values used for three user-specified parameters in the turbulence model were evaluated to understand how much they affect this tunnel simulation results. The default values of these parameters are 0.2, 0.5, and 0.5, respectively, for the Smagorinsky constant, turbulent Prandtl number, and turbulent Schmidt number.

Smagorinsky constant

The Smagorinsky constant is a parameter in FDS for modeling the flow turbulence. This parameter is used in the Smagorinsky sub-grid model in LES (see Eq. 5-2). The simulation length scale used in LES models is not sufficient to capture the details of eddies generated by the flow turbulence, so the dynamic flow viscosity is modeled assuming that the turbulent energy for length scales smaller than the grid is dispersed within the grid. This only allows energy flow from large to small scale.

$$\mu_{LES} = \rho(C_s\Delta)^2|S| \qquad \text{Eq. 5-2}$$

S is a function of velocity, as shown below:

$$|S|^2 = 2\left[\left(\frac{\partial u}{\partial x}\right)^2 + \left(\frac{\partial v}{\partial y}\right)^2 + \left(\frac{\partial w}{\partial z}\right)^2\right] + \qquad \text{Eq. 5-3}$$

$$\left(\frac{\partial u}{\partial y}+\frac{\partial v}{\partial x}\right)^2+\left(\frac{\partial u}{\partial z}+\frac{\partial w}{\partial x}\right)^2+\left(\frac{\partial v}{\partial z}+\frac{\partial w}{\partial y}\right)^2-\frac{2}{3}\left(\nabla\cdot\vec{u}\right)^2$$

For constant grid length scale, Δ, increasing or decreasing the Smagorinsky constant, C_s, increases or decreases the dynamic viscosity, μ_{LES} of the flow. Also, because the dynamic viscosity, μ_{LES}, is used in turbulent Prandtl number, Pr_{turb}, and Schmidt number, Sc_{turb}, changing the Smagorinsky constant, C_s, affects thermal conductivity, k_{LES}, and mass diffusivity within the flow, $(\rho D)_{LES}$, leading to changes in the temperature distribution and the flame location.

This constant can only be determined empirically because the dynamic viscosity is a function of the turbulent motions of the flow. Studies on the Smagorinsky constant [5-21, 5-22] have shown that there is no universal constant that satisfies every type of turbulent flows. For example, $C_s = 0.23$ is appropriate for simulations of decaying turbulence. For mixing layer flows, a Smagorinsky constant between 0.12 and 0.14 produces the most suitable results and 0.1 is required for turbulent channel flow [5-21]. For fire and smoke related flows in a standard fire room test model, 0.18 is appropriate for certain grid resolutions [5-14].

For this parameter sensitivity analysis, Smagorinsky constants of 25% smaller (0.15) and 25%, 50%, and 100% larger values (0.25, 0.30, and 0.40, respectively) than the default setting of 0.2 are used. The first two values are selected from the Smagorinsky constants introduced above that were successful in simulating different types of flow turbulences. The remaining values are tested to understand how the increase in the dynamic viscosity affects the near-wall condition predictions in FDS.

The results show that no single value models the entire gas phase flow throughout the tunnel. A relatively large Smagorinsky constant (compared to the default value) is needed to reduce the backflow in the simulation results that does not exist in the test data. Because a larger value of the Smagorinsky constant adds artificial viscosity to the flow, the hot gases from the fire travel less upstream (See Figure 5-4.). On the other hand, using a value greater than 0.2 causes the fire to lose small-scale dynamics. This means

that less vorticities and fluctuations are formed at the flame sheets. For the downstream region, where the hot gases from the upper layer continuously mix with the cold lower gas layer, a Smagorinsky constant of less than 0.2 is required (See Figure 5-5.). Note that FDS does not allow multiple Cs to be selected for a given simulation; therefore, optimizing for backflow adversely affects the downstream results and vice versa.

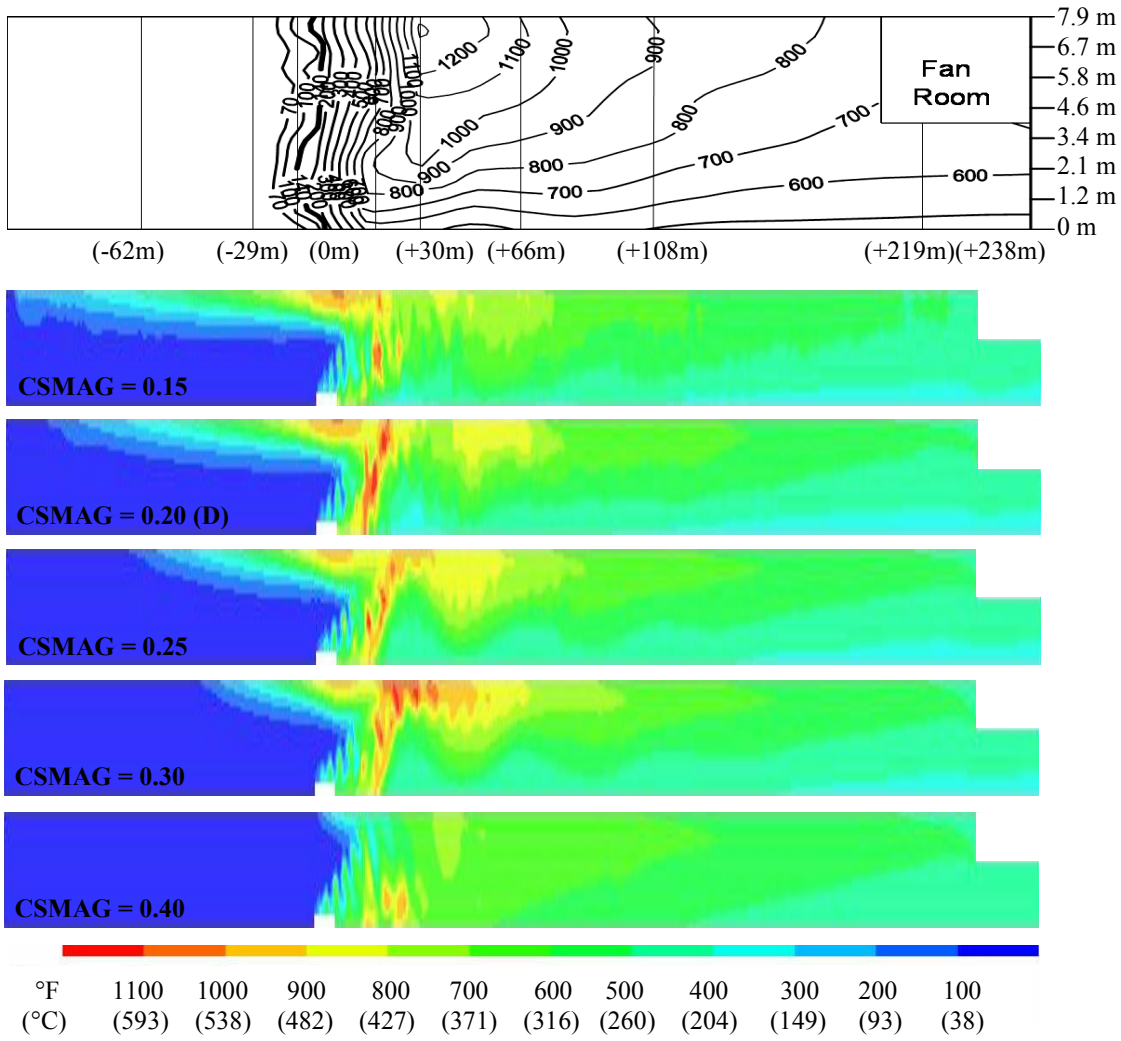

Figure 5-4. Temperature profiles from -107 m upstream of the fire to tunnel exit (238 m downstream of the fire) at time = 16 min. From the top, the CSMAG are 0.15, 0.20(D), 0.25, 0.30 and 0.40 respectively. As the CSMAG increases, backlayering and heat transfer downstream reduces. Also, the dynamics of the flame such as flame sheet fluctuations and vorticities disappears.

As shown in this analysis, a universal constant that can produce good calculation results for this tunnel fire is not available; however, considering that the fire region is the driving force that alters the forced fluid flow within the tunnel, simulating this region in a good

degree is selected as a priority for tunnel fire simulations. Therefore, the default value of 0.2 is suggested to be appropriate for this fire scenario.

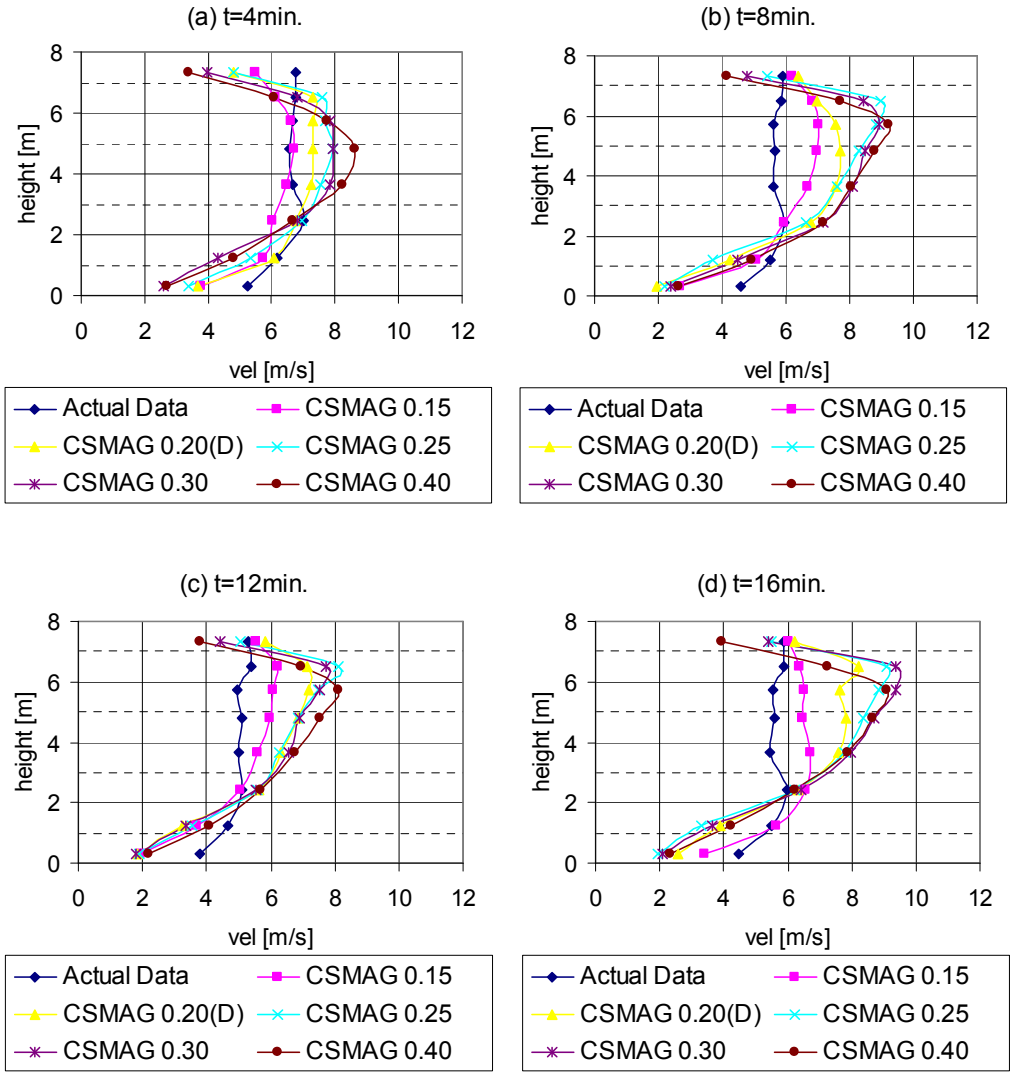

Figure 5-5. Velocity comparisons at 108 m downstream of the fire between the actual test data and simulated results: At each time, (a) through (d) (t = 4, 8, 12, 16 min. after ignition), simulated velocity output with Smagorinsky constant = 0.15 shows the best match with the experiment data.

Turbulent Prandtl and Schmidt number

In FDS, turbulent Prandtl and Schmidt numbers determine the thermal conductivity, k_{LES}, of the flow and the diffusivity of the species, $(\rho D)_{LES}$, within the flow (see Eq. 5-4). These properties account for the effects of both macroscopic motion from turbulence and

microscopic molecular motion during energy and mass transfer. It is difficult to solve the turbulence of the flow analytically, even for a simple case; therefore, empirically determined values, turbulent Prandtl number and Schmidt number, are used to model the turbulence effect in the transport phenomena.

$$k_{LES} = \frac{c_p \mu_{LES}}{\mathrm{Pr}_{turb}}, \qquad (\rho D)_{LES} = \frac{\mu_{LES}}{Sc_{turb}} \qquad \text{Eq. 5-4}$$

For air at atmospheric pressure, the Pr ranges from 0.536 to 0.786 depending on the air temperature ranging from 100 K to 3000 K. In the temperature range which the tunnel fires are involved in, the Pr number stays within 0.7 ± 0.05 [5-23]. However, the turbulent Prandtl number must be found based on the comparison between the simulation results and the test data. Only two values were proposed based on a theoretical assumption about the flow characteristic: for fully developed turbulent flow, unity (1.0) and for laminar flows, the molecular Prandtl number, Pr [5-24]. Much of the research conducted for the turbulent Prandtl number in the computational fluid dynamics field used a value between 0.2 and 0.9 [5-14]. For fire related problems using FDS, using a value of 0.5, which is the current default setting, was found to be reasonable [5-26].

To perform a sensitivity analysis on turbulent Prandtl number, values 40% (0.7) and 100% (1.0) greater than the default setting of 0.5 were selected for the Memorial tunnel test 621A simulations. A turbulent Prandtl number equal to 0.7 is similar to the molecular Prandtl number in the temperature range within 300 K to 2000 K, while 1.0 represents fully developed turbulent flows.

The simulation results show that varying the Pr_{turb} value did affect the temperature distribution without influencing the velocity profile. As shown in Figure 5-6, increasing the value from its default setting of 0.5 reduced the heat transfer within the gas phase. The effect is identified by the changes in the temperature distribution throughout the tunnel – hot gas regions (temperature greater than 427 °C (800 °F)) become less as the Pr_{turb} value increases. The isothermal lines of 427 °C (800 °F) in simulated results with turbulent Prandtl number of 0.7 and 1.0 shifted approximately 15 m and 20 m upstream compared to the default case with $Pr_{turb} = 0.5$. As shown in the results, the changes in the simulated gas temperature with varying the turbulent Prandtl number are less than the

uncertainty of the model; hence, it is suggested that using the default value of 0.5 is reasonable for this fire scenario.

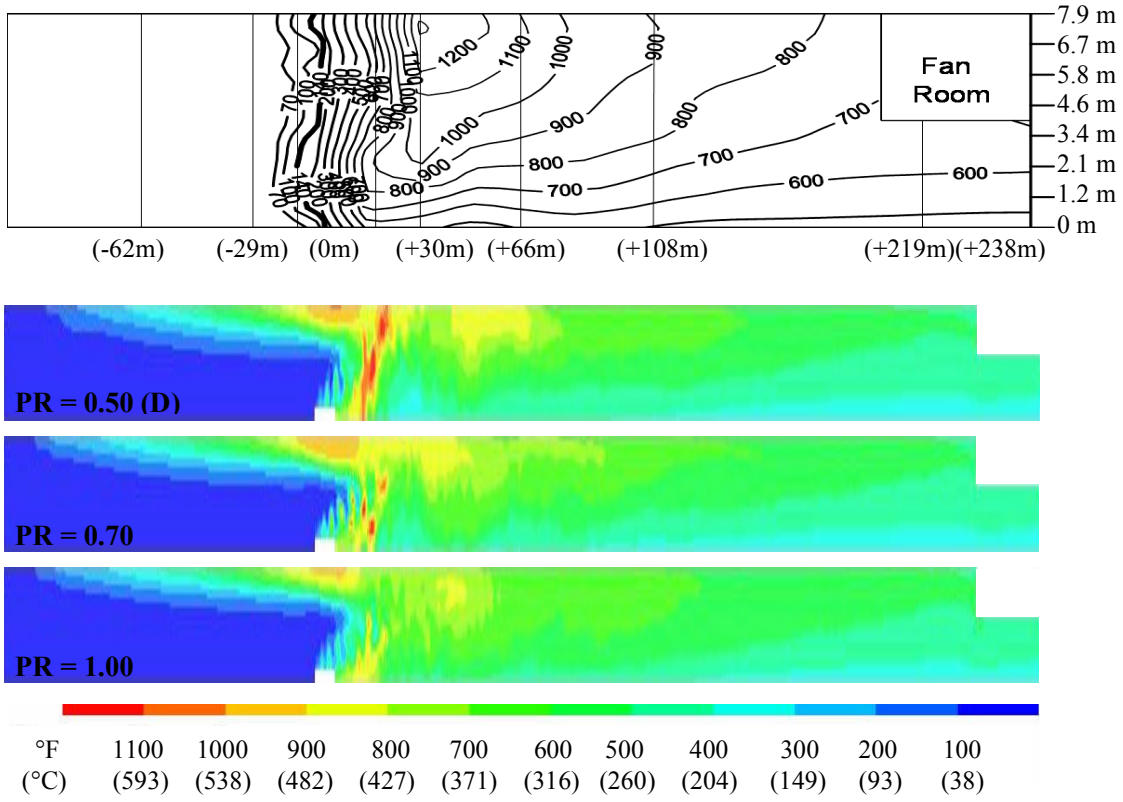

Figure 5-6. Temperature profiles from -107 m upstream of the fire to tunnel exit (238 m downstream of the fire) at time = 16 min. From the top, the Pr_{turb} are 0.50(D), 0.70 and 1.00, respectively. As the Pr_{turb} increases, the gas temperatures around and downstream of the fire decrease.

For the turbulent Schmidt number sensitivity analysis, values that were 20% smaller (0.4), 40 % (0.7) and 100% (1.0) greater than the default setting of 0.5 are evaluated. The values used in these analyses were found from previous research related to turbulent Schmidt number [5-26, 5-27].

The results demonstrated that the Schmidt number affects the length of the flame and alters the temperature distribution near the fire area. There is negligible effect on flow temperature and velocity in the downstream area. Calculation of the actual flame lengths for comparison to simulation results follows the approach taken by Lönnermark [5-28], in which the flame tip temperature in a tunnel fire is assumed to be 600 °C. Because the gas temperatures within the tunnel were generally low in the FDS simulations, comparison

between the simulated and measured flame tip location via gas temperatures was not possible. Instead, the flame tip location was identified using the Heat Release Rate Per Unit Volume (HRRPUV) results from FDS as shown in Figure 5-7.

The length of the flame from FDS was found to be proportional to the turbulent Schmidt number (see Figure 5-7). However, the differences in the flame lengths between the test data and the simulations were less than 10 m for each case. In the Memorial Tunnel Test 621A, the flame tip is located between 12 m and 30 m downstream of the fire. However, the turbulent Schmidt number that best represents the real flame length was not determined because the existing experiment data were insufficient to make the distinction. Therefore, it is suggested that using the default value of 0.5 is reasonable for this fire scenario.

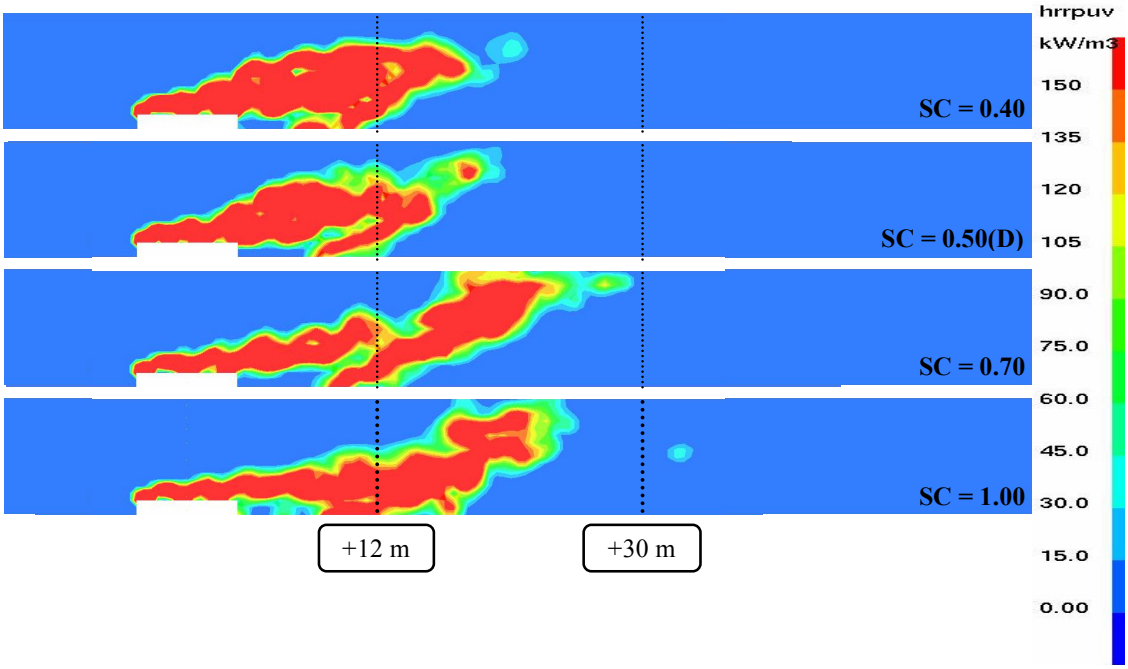

Figure 5-7. Heat release rate per unit volume comparison: From the top, the Sc_{turb} are 0.40, 0.50 (D), 0.70 and 1.00, respectively. As the Sc_{turb} increases, the flame length within the tunnel increases. Assuming 600 °C as the flame tip, the test data shows that the flame tip was approximately 30m downstream from the fire.

5.4.4. Calibration of FDS

Based on the results from the grid and parameter analyses conducted above, FDS was calibrated. From the grid sensitivity analysis, it was found that the 8% of the

characteristic length, D* was considered to be appropriate for a practical simulation of this tunnel fire scenario. To find the uncertainty of FDS in simulating gas temperatures and flow velocities, the measurements from the experiment and FDS simulation in the downstream region were compared.

The reason for considering only the downstream region in calculating the uncertainty of FDS was because FDS had simulated backlayers, which were not significantly present in the actual tunnel test. The simulated FDS results showed that the upstream region has two distinct layers: forced ventilation flow that blows towards the fire and the backflow that travels in the opposite direction. However, the downstream region has one mixing layer of products from the combustion reaction and air from forced ventilation. This made the simulated gas temperatures and velocities in the downstream region more comparable to the experimental data. With the experimental data, standard deviations of FDS predictions for temperature and velocity predictions were calculated: 100 °C and +2 m/s, respectively.

With these uncertainties of FDS in mind, the results from the parameter sensitivity analyses were compared with the actual test data. The results indicated that 0.2, 0.5 and 0.5 were appropriate for the Smagorinsky constant, turbulent Prandtl number and turbulent Schmidt number, respectively, for this tunnel fire scenario.

5.4.5. Backlayering

During the actual experiment, the fresh air inflow velocity was controlled by the number of jet fans that was used in the test. Because one of the purposes of the test was to find the critical ventilation velocity, the tunnel inflow velocity was slowly reduced until time of 13 min. after ignition. Around this time, flow measurements near the ceiling upstream of the fire identified backlayering. From this point, two more jet fans were turned back on, which caused the backlayering to disappear (see Figure 5-8).

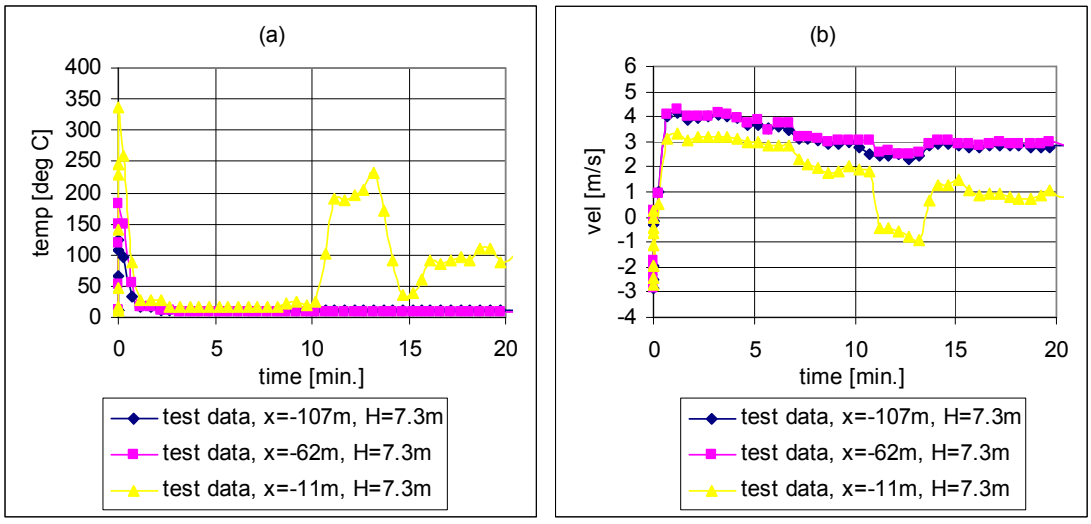

Figure 5-8. The temperature (a) and velocity (b) profiles from test data: there are three measurement locations in these graphs, which are -107 m, -62 m, and -11 m upstream from the fire and 7.3 m from the tunnel floor. Backlayering from the test is observed in 11 min. < t < 14 min.

When this was simulated using FDS, under default settings (C_s = 0.2, Sc_{turb} = 0.5 and Pr_{turb} = 0.5), the backlayering occurred approximately 6 min. earlier ($t \approx 5$ min. in Figure 5-9) at location 11 m upstream of the fire and 0.60 m below the ceiling. At the same location, the magnitude of velocity drop due to backlayering in FDS simulations was double the size of the measured values as shown as in Figure 5-9 at 11 min. < t < 13 min. The hot gases from the fire traveled in the opposite direction of the longitudinal ventilation, creating a ceiling jet. This continued until the hot gases reached the computational boundary at 107 m upstream of the fire. Even after the input velocity was increased around 14 min. after ignition, the backlayering stayed the same in the FDS results. Increased inflow velocity at 107 m upstream of the fire was not able to push the hot gases towards the downstream of the fire. Rather, the backlayering stayed the same with the relatively cold air (compared to the backlayer) flowing faster under the backlayer. In other words, smoke from backlayering was not effectively clearing out from the upstream of the fire, though the inflow velocity was increased. Considering that the slope of the tunnel was ignored in the computations, which may help the backlayering to propagate even further upstream, this backlayering simulation was a problem. A comparison of the velocity profile at location 11 m upstream of the fire from the actual

experiment and FDS simulation are made in Figure 5-9. The backlayering is also identified from the temperature results shown in the middle case in Figure 5-10**.**

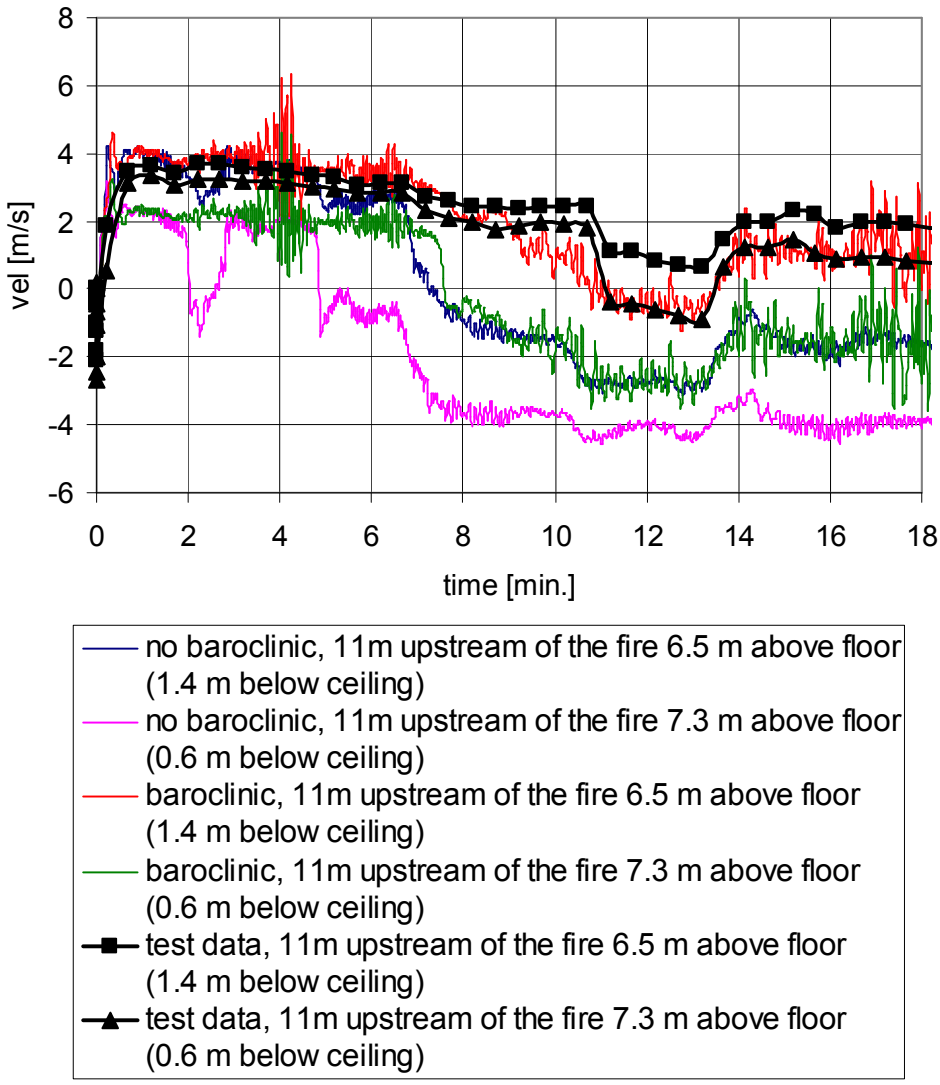

Figure 5-9. Velocity near the ceiling (7.3 m (0.6 m from ceiling) and 6.5 m (1.4 m from ceiling) above the tunnel floor) at approximately 13 m upstream from the fire using 8% of the D* for grid size: Comparison between the simulation results, one with default setting (no baroclinic) and the other with consideration of baroclinic torque (baroclinic), and the test data.

The following computational experiments using different features in FDS are conducted. These tests were performed to understand more about the poor smoke layer simulation results that FDS generates and to find means to improve the quality of FDS predictions, if possible.

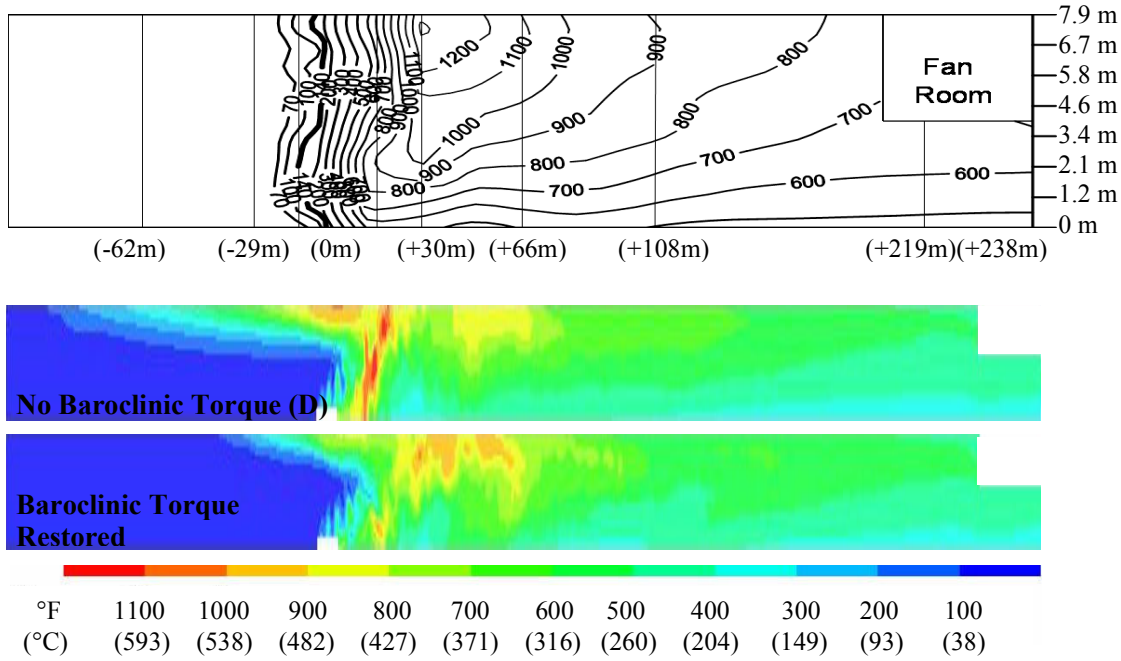

Figure 5-10. FDS simulation results comparison at t = 16 min. between the test data (top), default case (middle) and case with the baroclinic torque restored (bottom). The simulation with baroclinic torque restored better matches the test data (temperature distribution) than the default case run.

In the first set of computational experiments, the air inflow velocity near the ceiling was increased to eliminate the backflow. Three methods are used to increase the air flow velocity below the ceiling: (1) Placing additional obstructions near 30 m upstream of the fire near the side walls to block the cross-section (the velocity at this location will increase proportionally to the blockage ratio). It was found from the test report that around this location, there were many test instruments placed near the walls interfering the air flow [5-7]. (2) Using SAWTOOTH feature for the semi-circular ceiling (using this feature allows FDS to eliminate the extra voritices generated around the rectangular obstructions, which are used to create curved geometry, i.e., a "stair-stepping"). (3) Changing the VBC factor for the ceiling (a factor that decides the flow condition – no slip to free slip – near the walls). The first method had a small degree of positive effect, while the other two cases resulted in a more extended backflow.

Additional simulations were conducted with the baroclinic torque restored in the FDS calculations. Baroclinic torque, which is one of the sources for vorticity, is due to misalignment between the pressure and density gradients. This term is neglected by default in FDS to simplify the numerical calculations when the LES is used. The approach is a valid assumption when buoyancy-driven vorticity is the dominant source of vorticity generation, as in large-scale fire simulations in which significant density differences near the flames are not well-resolved [5-6].

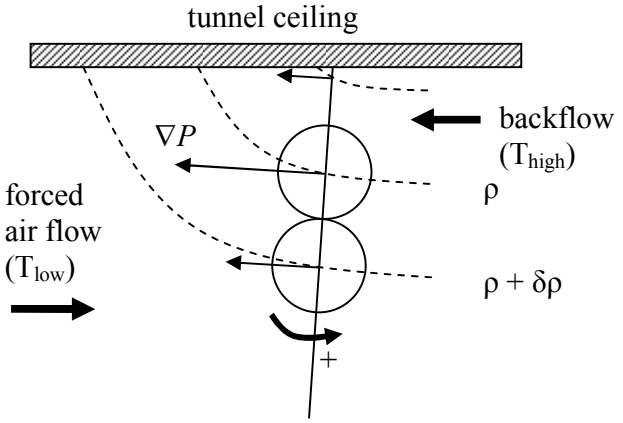

Figure 5-11. A schematic drawing of backflow reduction due to vorticity generation from baroclinic torque: The baroclinic torque driven vorticities are produced when the pressure gradient (generated due to velocity) in the horizontal direction and the density gradient (formed due to temperature difference) in the vertical direction are misaligned. This assists the vertical mixing and the backlayering is reduced.

Although this Memorial tunnel fire simulation does not have a high grid resolution, restoring baroclinic torque reduces the backflow as shown in Figure 5-9 and Figure 5-10**.** Because the gas density is treated as proportional to the inverse of temperature in FDS, a density gradient exists vertically in the backflow. The hot gas layer below the ceiling has lower density while the cold layer, the forced air inflow, has a higher density. Meanwhile, a pressure gradient is generated by the velocity field (flow from right to left in Figure 5-11) in the backflow in the horizontal direction. However, this pressure gradient is not aligned with that of density, and hence, vorticity is generated due to baroclinic torque in the direction that encourages the mixing of the hot backflow with cold air from the forced longitudinal ventilation. This effect reduces the unwanted backflow from propagating further upstream as shown in Figure 5-9 and Figure 5-10.

Restoring the baroclinic torque in FDS allowed the backflow to reduce – 50 ~ 60 % decrease in backlayering propagation length (from fire location to the tip of the backflow in the horizontal direction); however, the over-prediction of backflow by FDS still remains. Examining closely to the characteristics of the backflow generated in the above simulations, and considering that no other features available in FDS allows the decrease of the backflow, one may find that the unwanted backflows occur in the FDS calculations due to the known limitations of the model.

First, the boundary layers near the ceiling are not adequately resolved for FDS to simulate the smoke flow in forced, longitudinally ventilated tunnel fires. The grid sizes used in LES calculations are too large to capture the flow characteristics near the solid boundaries. Also, the simple wall function that FDS uses for near-wall calculations, is not sophisticated enough to simulate complex phenomena such as the changes in the backlayer.

Second, the earliest version of the Smagorinsky sub-grid scale model in FDS calculations with LES, only accounts for the forward scatter [5-13]. This means that the turbulent energy is only transferred from the large scale to the small scale. However for

transient flows, such as the near-wall flows, studies have shown that turbulent energy transfer from small to large scale exists, allowing less sub-grid-scale dissipation.

Third, LES model used with the original version of the Smagorinsky sub-grid scale model has been known to show decays of perturbations even when the flow needed to be unstable [5-21]. This limitation is applied at the interface region where backflow and forced air inflow meets. The model may calculate the initial growth rate of the perturbations to be small due to excessive damping. Therefore, less mixing is occurring at the interface region, allowing a rather stratified backflow layer propagating upstream quickly without mixing with the forced air flow.

It was known from the beginning that FDS has a weakness in simulating near-wall calculations. The computational experiments conducted in this research provided insight on how the model limitations on near-wall flow predictions affect an actual tunnel fire simulation with forced longitudinal ventilation. The results from this study shows that this weakness makes dynamic backlayering simulation more challenging for FDS.

5.5. Conclusions

Sensitivity analyses are conducted to evaluate the impact of grid size using the computational fluid dynamics model, Fire Dynamic Simulator (FDS) version 4.0 [5-5, 5-6]. This study is for tunnel fires that have fire sizes on the order of 100 MW with forced, longitudinal ventilation. An effort is made to quantify energy conservation discrepancies in FDS. Additional sensitivity analyses for turbulence parameters used in FDS were conducted to investigate their influences in the simulation results. Other features in FDS are used to improve the smoke layer predictions.

The grid sizes are based on a characteristic diameter, D*, which is a function of heat release rate and ambient conditions. For this study, the use of a grid length was evaluated at 5%, 8%, and 10% of the D* value. The simulation results from each case are compared with the velocity and temperature data at different locations within the Memorial tunnel. FDS predicted gas temperatures from the three cases that are 20 ~ 40% lower than the test data. However, the flow velocities show an agreement with the experimental data within ± 2 m/s, with the exception of the backlayering that occurred at the upstream of the fire in the simulations. This backlayering phenomenon was not observed in the

experiment. Considering simulation time and the quality of the calculated results, a grid size that is 8% of the D* value is recommended for this tunnel scenario.

In addition, the energy conservation within FDS is evaluated. The energy discrepancy in this tunnel fire simulation is approximately 2%, which is negligible. Hence, it is concluded that FDS conserves energy for this tunnel fire simulation.

The sensitivity analyses included an evaluation of three parameters related to the turbulence model: turbulent Prandtl number, Schmidt number and Smagorinsky constant. The results show that the first two parameters affect the temperature distribution within the tunnel (427 °C (800 °F) isothermal lines in the simulated results with turbulent Prandtl number 0.7 and 1.0 shifted approximately 15 m and 20 m upstream compared to the default case with Pr_{turb} = 0.5, respectively) and the flame lengths (changes within 10 m), respectively, which were considered to be minimal. On the other hand, the Smagorinsky constant significantly impacts simulation results in terms of altering the flow velocity, temperature and flame response within the tunnel. To model a tunnel fire with forced longitudinal ventilation, different values of the Smagorinsky constant would be necessary for the upstream, fire, and downstream regions (>0.2, 0.2, and <0.2, respectively) to address various phenomenological concerns. Unfortunately, only one value for the constant can be selected for a given FDS simulation. Thus, 0.2 is considered to be most appropriate, as the fire region is the driving force for the changes in the forced flow conditions within the tunnel.

Further investigation into FDS smoke layer prediction exposes concerns about extensive backflow in the FDS results, which occur when the inflow velocity at the boundary is slightly reduced. The resulting flow constriction causes the simulated tunnel fire conditions to deviate from those of the actual test. Several methods were used to reduce the backflow: increasing the forced ventilation velocity near the ceiling, removing unwanted eddies near the stair-stepped ceiling, changing the flow slip condition near the ceiling, and restoring the baroclinic torque. The results showed that, except for the last case, all three efforts were unsuccessful. Restoring the baroclinic torque reduces the simulated backflow propagation length up to 50 ~ 60 %; however, the simulation results still differ from the test data. Based on these computational experiments, it is concluded

that the backflow results from the known limitations of FDS. A weakness in near-wall calculations, the forward scattering limitation of turbulent energy transfer, and excessive damping of flow perturbations are the main stimuli for the unwanted backflow.

Based on this study, general guidelines for more accurate FDS simulations on tunnel fires with forced longitudinal ventilation can be developed. The simulations should include baroclinic torque. This will help the mixing of the backlayer and forced ventilation flow, allowing less backflow propagation. A constant inflow velocity at the boundary is also effective. By doing so, there will be minimum changes in the upstream smoke layer. This makes the simulation condition less challenging for FDS, which is known to have difficulties in calculating the changes in the flows at near-wall regions.

As shown from this study, FDS produces predictions that are in an agreement with the actual fire phenomena: simulated temperatures and flow velocities showing 30 ~ 40 % discrepancies from those of the experimental measurements. However, FDS have limitations, which affect the smoke layer prediction at the upstream region of the fire. Therefore, the practitioners or researchers should carefully consider these limitations when using this model to study tunnel fires or to make engineering judgments based on the model calculations to find appropriate protection means for tunnel fires.

Reference

5-1. Ingason, H., Fire Development in Catastrophic Tunnel Fires (CTF), In *Proceedings of the International Symposium on Catastrophic Tunnel Fires*, SP Swedish National Testing and Research Institute, SP Report 2004:05, Borås, Sweden, 20-21 November (2003) 31-47

5-2. Fire and smoke control in road tunnels, PIARC, 05, 05B-1999, ISBN : 2-84060-064-1, 1999

5-3. NFPA 502. Standard for Road Tunnels, Bridges, and Other Limited Access Highways, National Fire Protection Association, 2004 Edition

5-4. Bettelini, M., Neuenschwander, H., Henke, A., Gagliardi, M. and Steiner, W., The Fire in the St Gotthard Tunnel of October 24, 2001, In *Proceedings of the International Symposium on Catastrophic Tunnel Fires*, SP Swedish National Testing and Research Institute, SP Report 2004:05, Borås, Sweden, 20-21 November (2003) 49-68

5-5. McGrattan, K., Fire Dynamics Simulator (Version 4), User's Guide, NIST Special Publication 1019, National Institute of Standards and Technology, Gaithersburg, MD, September (2005)

5-6. McGrattan, K., Fire Dynamics Simulator (Version 4), Technical Reference Guide, NIST Special Publication 1018, National Institute of Standards and Technology, Gaithersburg, MD, September (2005)
5-7. Memorial Tunnel Fire Test 621 A, Memorial tunnel fire ventilation test program, produced for the Massachusetts Highway Department Central Artery/Tunnel Project, Federal Highway Administration, Parsons Brinckerhoff 4D Imaging, Denver, Colo. ©1996
5-8. McGrattan, K.B., Hamins, A., Numerical Simulation of the Howard Street Tunnel Fire, Baltimore, Maryland, July 2001, NISTIR 6902, NUREG/CR-6793, NRC Job Code J5414, National Institute of Standards and Technology, Gaithersburg, MD, January (2003) 42
5-9. Hwang, C.C., Edwards, J.C., The critical ventilation velocity in tunnel fires – a computer simulation, Fire Safety Journal 40 (2005) 213-244
5-10. Lee, S.R., Ryou, H.S., A numerical study on smoke movement in longitudinal ventilation tunnel fires for different aspect ratio, Building and Environment 41(6) (2006) 719-725
5-11. Ferziger, J.H., Subgrid-Scale Modeling, Part One: Fundamentals of Large Eddy Simulation, Large Eddy Simulation of Complex Engineering and Geophysical Flows, Cambridge Univ. Press, New York, NY ©1993
5-12. Germano M., Piomelli, U., Moin P., Cabot, W.H., A dynamic subgrid-scale eddy viscosity model, Phys. Fluids A 3(7), July (1991), 1760-1765
5-13. Piomelli, U., Zang, T.A., Speziale, C.G., Hussaini, M.Y., On the large-eddy simulation of transitional wall-bounded flows, Phys. Fluids A 2(2), February (1990), 257-265
5-14. Zhang, W., Hamer, A., Klassen, M., Carpenter, D., Roby, R., Turbulence statistics in a fire room model by large eddy simulation, Fire Safety Journal 37(8), November (2002), 721-752
5-15. Ingason, H., Lönnermark, A., Heat release rates from heavy goods vehicle trailer fires in tunnels, Fire Safety Journal 40 (2005) 646-668
5-16. Hwang, C.C., Edwards, J.C., CFD Modeling of Smoke Reversal, Proc International Conference on Engineered Fire Protection Design (Jun 11-15, 2001; San Francisco, CA), Bethesda, MD: Society of Fire Protection Engineers, Inc.: 376-387
5-17. Yunlong Liu, et al, CFD-Aided Tenability Assessment of Railway Tunnel Train Fire Scenarios, *International Journal of Ventilation,* V5, N2 (2006) 205-218
5-18. Hwang, C.C., Wargo, J.D., Experimental study of thermally generated reverse stratified layers in a fire tunnel, Combust. Flame 66 (1986), 171-80
5-19. McGrattan, K., Large eddy simulations of smoke movement, Fire Safety Journal 30(2) (1998) 161-178
5-20. Drysdale, D., An Introduction to Fire Dynamics, 2nd edition, John Wiley & Sons, ©1998
5-21. Yoshizawa, A., Eddy-viscosity-type subgrid-scale model with a variable Smagorinsky coefficient and its relationship with the one-equation model in large eddy simulation, Phys. Fluids A 3(8), August (1991), 2007-2009
5-22. Piomelli, U., Cabot, W.H., Moin, P., Lee, S., Subgrid-scale backscatter in turbulent and transitional flows, Phys. Fluids A 3 (7), July (1991), 1766-1771

5-23. The SFPE Handbook of Fire Protection Engineering, 3rd ed., National Fire Protection Association, Quincy, MA, ©2002
5-24. Welty, J.R., Wicks, C.E., Wilson, R.E., Rorrer, G., Fundamentals of Momentum, Heat, and Mass Transfer, 4th ed., John Wiley & Sons, Inc., New York, NY, ©2001
5-25. W. Zhang, N. Ryder, R.J. Roby, and D. Carpenter. Modeling of the Combustion in Compartment Fires Using Large Eddy Simulation Approach. In *Proceedings of the 2001 Fall Technical Meeting, Eastern States Section*. Combustion Institute, Pittsburgh, Pennsylvania, December (2001)
5-26. H. Pitsch, H. Steiner, Large-eddy simulation of a turbulent piloted methane/air diffusion flame (Sandia flame D), Physic of Fluids, Volume 12, Number 10, October (2000)
5-27. N. Branley, W.P. Jones, Large Eddy simulation of a turbulent non-premixed flame, Combustion and Flame 127 (1-2) (2001) 1914-1934
5-28. Lönnermark, A., Ingason, H., Fire Spread and Flame Length in Large-Scale Tunnel Fires, Fire Technology, In Press

6. RUNEHAMAR TUNNEL FIRE TEST SIMULATIONS

With optimum model parameters from the prior section, two Runehamar tunnel fire tests have been simulated using FDS [14, 15]. Both fires have peak heat release rate in excess of 100 MW. The two tests had similar peak heat release rates, but one exhibited pulsation (T2) and the other (T3) did not.

6.1. Computational experiment system set-up for Runehamar tunnel fire tests

The Runehamar tunnel [5] was simplified for the FDS simulations. The slope of the tunnel was ignored and a rectangular object was created to simulate fans placed at the entrance of the tunnel. One side of the oject that faces the tunnel blows air into the tunnel while the back surface entrains air from outside of the tunnel, similar to a real fan. This approach allows any pressure increase at the fire location to affect the flow within the tunnel. The protection boards that were placed near the fuel area in the actual tests are assumed to create adiabatic conditions with insulated backing. Other surfaces are assumed to be concrete. Although the fuel package was a mock-up of a semi-heavy goods vehicle, it is approximated using a propane gas burner in the simulations. A propane burner with a specified heat release rate was used to simulate the given fire scenario in a simplified manner, eliminating other factors, such as flame spread on solid fuel, affecting the combustion. The grid sizes were 8% of the characteristic length, as determined in the sensitivity analysis (Chapter 5). The results from the sensitivity analysis using the Memorial tunnel test data was considered to be appropriate because the Runnehamar tunnel test conditions were similar to that of the Memorial tunnel test in terms of the fire size, geometry and ventilation type. All parameters are their default values. Additional grid cells are generated outside of the tunnel exit for more reliable CFD calculation results.

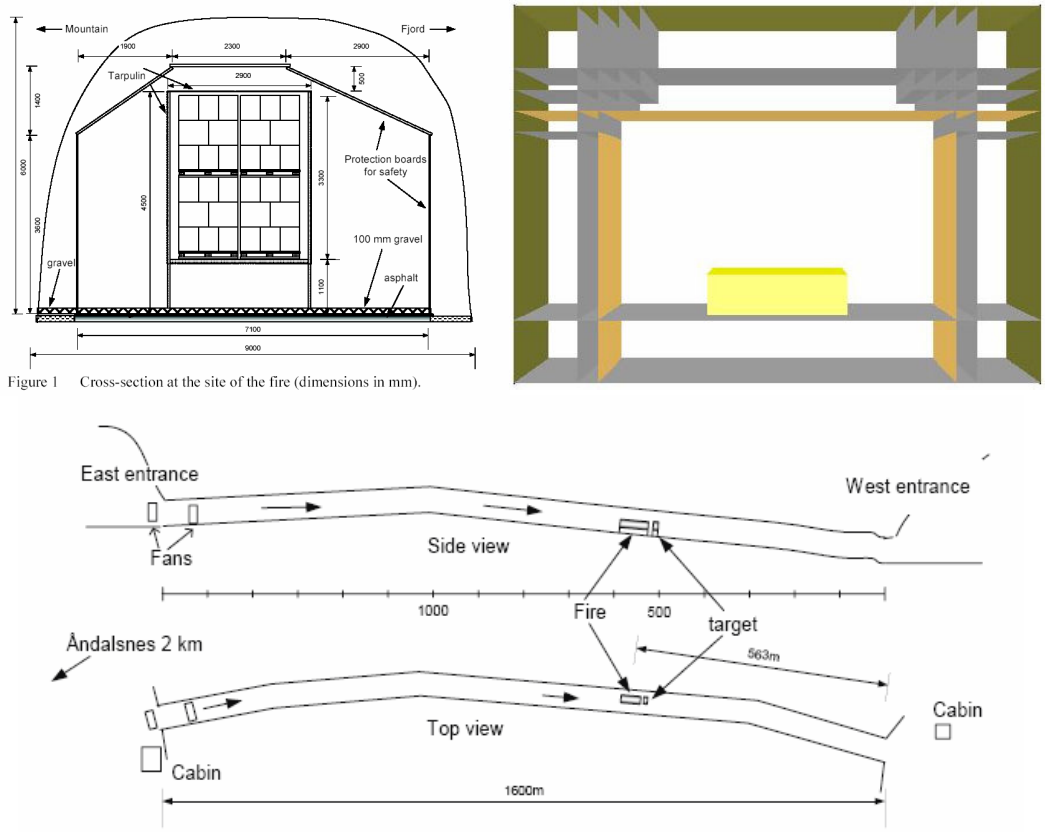

Figure 1 Cross-section at the site of the fire (dimensions in mm).

Figure 7. Comparison between the cross-sectional area of the real Runehamar tunnel (left) and that of the simulation using FDS (right) with a longitudinal diagram of the Runnehamar tunnel. The surface of the simulated protection boards are placed on the tunnel walls and ceiling as in the test.

6.2. Runehamar tunnel fire test simulation results

The simulation results are compared to the limited amount of test data available [5, 6, 13, 23, 25]: heat release rate (HRR), gas temperature of the downstream flow, velocity upstream and downstream of the fire, radiative heat fluxes on solid boundaries near the fire, and species concentrations sampled at the measuring station.

As discussed earlier, the heat release rate in each test is prescribed. However, the output of the FDS calculated heat release rates are checked to see how dynamic were the fire. From Figure 8, in both tests, as the fire size grew above 80 to 100 MW range, the fluctuations in heat release rate are more seen. This indicates that the fire was more changing in size depending on the mixing between the fuel vapor and air when large fuel supply was given.

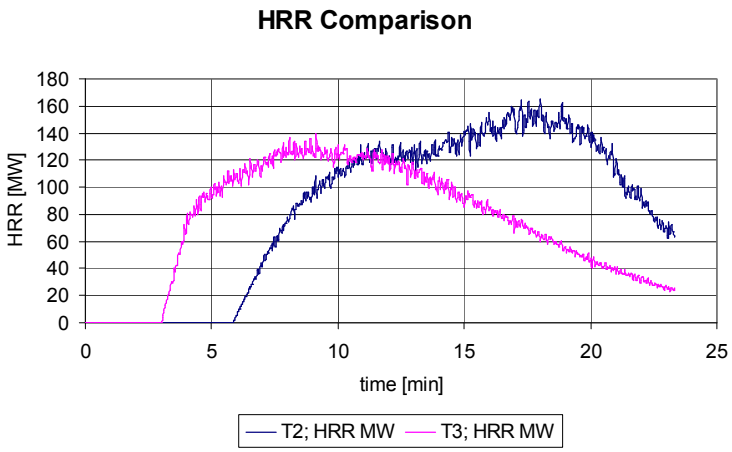

Figure 8. Heat release rate comparison of Runehamar tunnel fire tests, T2 and T3. With the given input of the heat release rate data, FDS inserts fuel into the computational domain. The above results are given by FDS where heat release rate is given by the combustion model.

The predicted gas temperatures show qualitative agreement with the test data. For example, in the T2 results (see T2(a) in Figure 9) the temperature +100 m from the fire shows an increase around 15 min. after the prescribed heat release rate increases, similar to the experimental data. In T3 (shown in T3 (a) in Figure 9), the temperature measurements taken +70 or +100 m downstream of the fire increase until 10 to 12 min. after ignition and a decrease that drops the temperatures to about half of its maximum. These trends are also shown in the test data. However, compared to the test data, the maximum temperatures were lower and the region of high gas temperature was located about 30 to 60 m further downstream from the fuel area. For T2, the measured gas temperature at +10 m was an average of 1150 ºC, while FDS show a maximum of around 900 ºC, +40 to +70 m downstream. The results are similar for the T3 scenario. The maximum temperature measured during T3 was around 1100 ºC near + 10 m while the simulated temperature is 900 ºC, +40 to +70 m downstream. A possible reason behind these differences in the FDS predictions and test data will be addressed in the discussion section.

Similar to the gas temperature FDS predictions, the velocity profiles within the tunnel for T2 and T3 are reproduced, qualitatively. Using the default VBC value, which determines the flow slip condition near solid boundaries, results in a large discrepancy between the velocity near the ceiling (2.0 m/s) and that in the center of the tunnel cross-section (4.5 m/s). The VBC value is not adjusted owing to the effect on backflow, as

described in the previous section. Instead, a mean flow velocity of 2.5 m/s to 3.0 m/s, equal to the bulk volume flow divided by the cross-sectional area of the tunnel, is used to simulate the Runehamar tunnel fire test flow conditions before ignition. This provides a similar amount of fresh air inflow to the combustion zone as in the real test. In both FDS cases, T2 and T3, the flow velocity increases as the fire starts in the downstream part of the tunnel, while it decreases in the tunnel upstream of the fire. (See T2 (b) and T3 (b) in Figure 9.) These results are consistent with the trend of the test data.

Generally, heat flux predictions in FDS for T2 and T3 poorly match the test data. For T2, the heat flux gauge located 5 m upstream from the fuel package and facing the fire measured a peak value of 35 kW/m^2 at the starting phase of the test (around 10 min. after ignition) and leveled out around 10 kW/m^2 in the experiment. The gauge on the floor facing the ceiling at 12 m downstream of the fire followed the heat release rate curve, increasing up to 200 kW/m^2 and gradually asymptoting to approximately 10 kW/m^2 over the next 10 min. The heat flux gauge 25 m upstream of the fire center facing the fire also followed the heat release rate curve, peaking at 3 kW/m^2 and then leveling out around 1.5 kW/m^2 for about 5 min. after a steep decrease. The radiative heat flux decreased to zero when pulsation occurred and increased again to 0.5 kW/m^2 when pulsation ceased. The trends are similar in T3 with smaller maximum heat flux values than that of T2: maxima of 20 kW/m^2 (5 m upstream from the fuel package, facing the fire), 75 kW/m^2 (12 m downstream of the fire, facing the ceiling) and 2 kW/m^2 (25 m upstream of the fire center facing the fire), respectively. However, FDS results does not show a sharp increase followed by a decrease in the heat flux measurements. (See T2(c) and T3 (c) in Figure 9.) Rather, there are no changes in the heat fluxes once the fire starts. Also, as summarized in Table 1, FDS predicts maximum heat fluxes for each location that are lower than the test data. The discrepancies in the results of FDS and experiment are more significant for the T2 case than that of T3. The FDS heat flux results for the gauges placed upstream of the fire might have been affected by the fuel configuration because they both face the fuel. In the actual tests, the solid fuel package was stacked up to the ceiling height, where the gauges see the flames on the fuel surface better. In the simulations, however, a propane burner was used instead and, hence, the flame leans more towards the floor as the forced ventilation pushes the flames downstream. This probably made the calculated heat flux

values at the upstream of the fire to be smaller than that of the experiment. A sensible explanation for the differences in measurements and FDS predictions for the third gauge will be made in the discussion section.

Table 1. Heat flux measurements comparison. The gauges for floor2, floor3 and floor4 were placed near the fire, -5 m, +7 m and -20 m from the fuel package, respectively.

Max. Heat Flux [kW/m^2]	T2		T3	
	Test Data	FDS	Test Data	FDS
5 m upstream	35	10	20	10
7 m downstream	200	70	75	60
20 m upstream	3	1.2	2	1.4

The predicted species concentration at the measuring station, which was located approximately 450 m downstream of the fuel location, are compared to the test data. Because propane is used in FDS for both test simulations, the species concentration for carbon monoxide and carbon dioxide are not expected to match the test data; however, they are listed in Table 2 to provide some means of comparison between T2 and T3. Both concentrations are greater in the former than in the latter. The propane reaction used in the simulations precludes a direct comparison of simulated carbon monoxide and dioxide concentration to the experiment values; however, the simulated temperature and oxygen concentration should be similar to the test data because the amount of oxygen consumed in fire can be related directly to the heat release rate, independent of fuel. This assumption is used in oxygen consumption calorimetry that to calculate heat release rate calculations. For simulations T2 and T3, the calculated maximum temperatures and oxygen concentrations are greater than the test data as summarized in Table 2. The temperatures found in FDS results are approximately twice as large and the oxygen concentrations are 14 to 17 % greater than those in the experiments.

Table 2. Maximum temperature and species concentrations, oxygen, carbon monoxide and carbon dioxide, at the measuring station are compared with the experimental data.

	T2		T3	
	Test Data	FDS	Test Data	FDS
T_{max} [ºC]	97	195	79	174
$O_{2,min}$ [%]	8.6	10.1	11.7	13.3
CO_{max} [ppm]	2430	136	491	105
$CO_{2,max}$ [%]	9.2	5.3	6.7	4.1

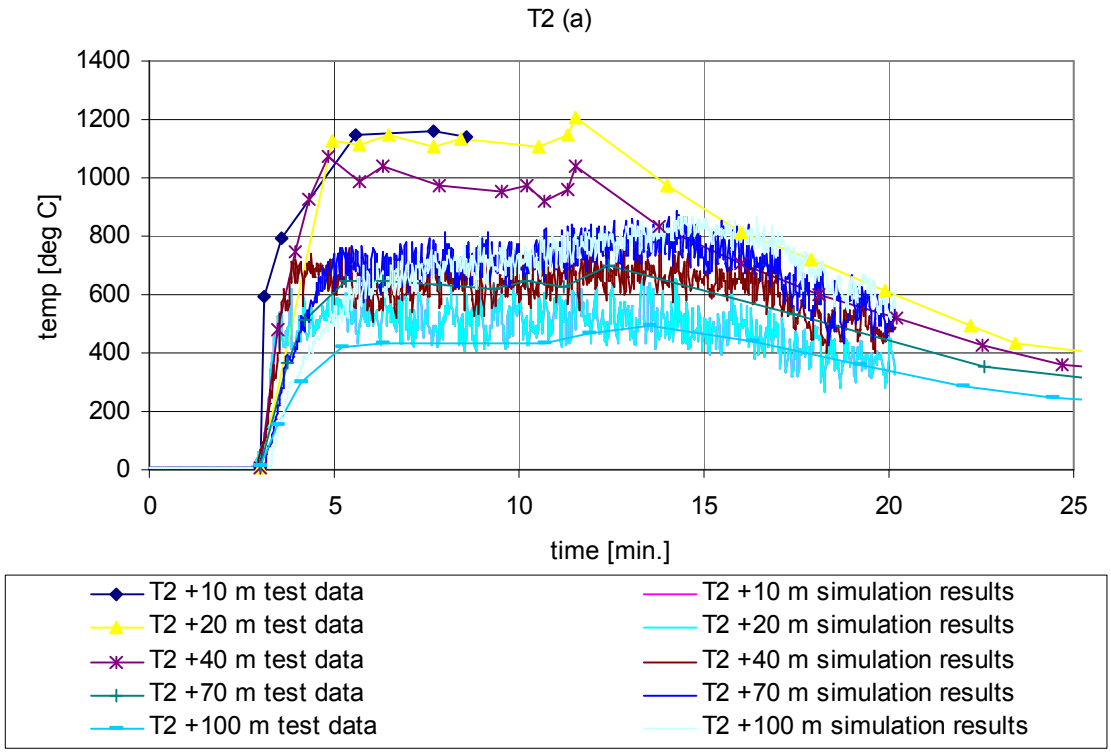
T2 (a)
temp [deg C]
time [min.]
T2 +10 m test data
T2 +20 m test data
T2 +40 m test data
T2 +70 m test data
T2 +100 m test data
T2 +10 m simulation results
T2 +20 m simulation results
T2 +40 m simulation results
T2 +70 m simulation results
T2 +100 m simulation results

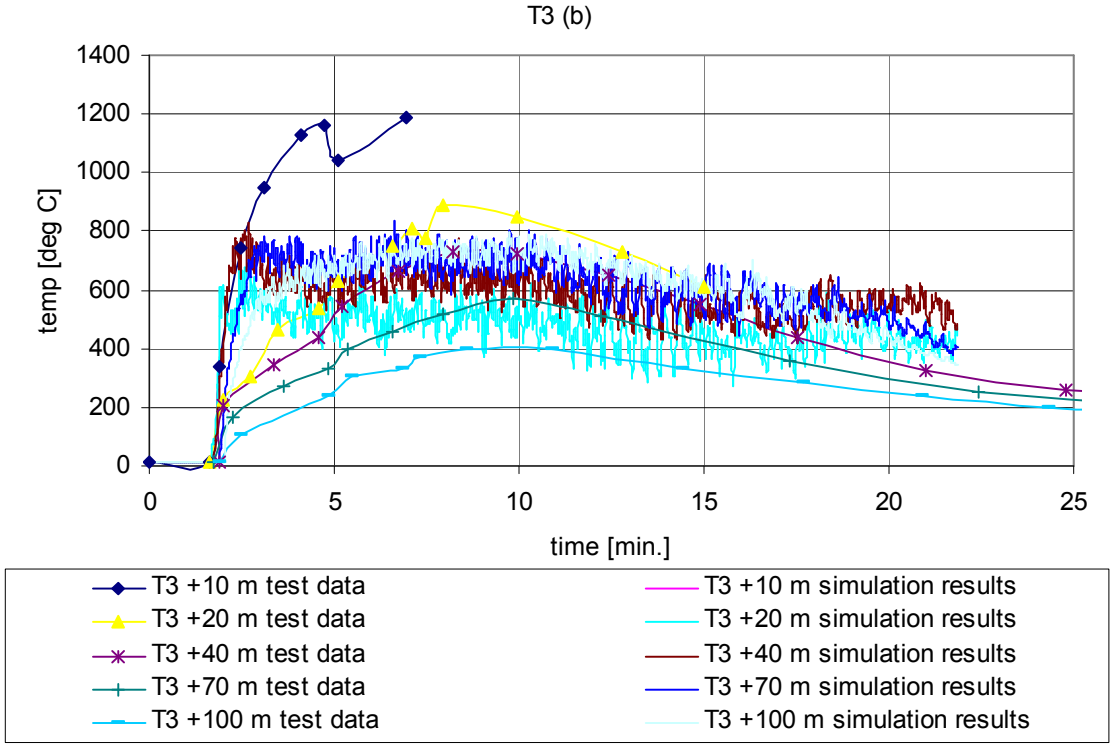
T3 (b)
temp [deg C]
time [min.]
T3 +10 m test data
T3 +20 m test data
T3 +40 m test data
T3 +70 m test data
T3 +100 m test data
T3 +10 m simulation results
T3 +20 m simulation results
T3 +40 m simulation results
T3 +70 m simulation results
T3 +100 m simulation results

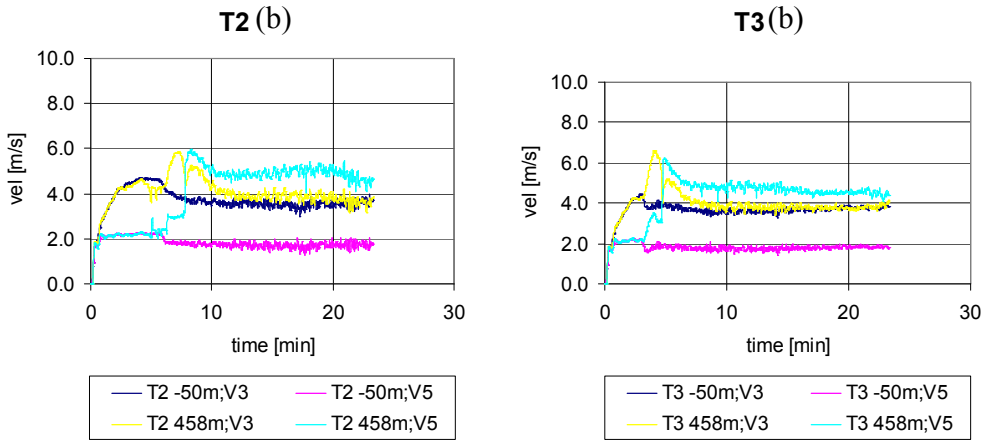
T2 (b)
T3 (b)
vel [m/s]
time [min]
T2 -50m;V3
T2 -50m;V5
T2 458m;V3
T2 458m;V5
T3 -50m;V3
T3 -50m;V5
T3 458m;V3
T3 458m;V5

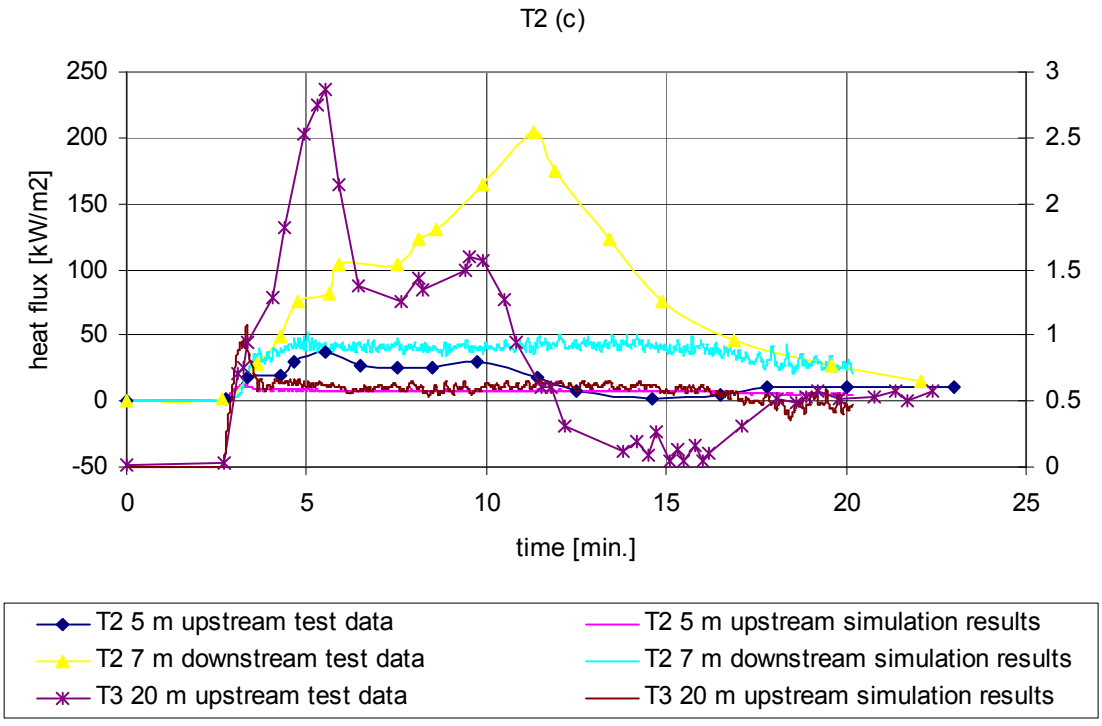
T2 (c)
heat flux [kW/m2]
time [min.]
T2 5 m upstream test data
T2 5 m upstream simulation results
T2 7 m downstream test data
T2 7 m downstream simulation results
T3 20 m upstream test data
T3 20 m upstream simulation results

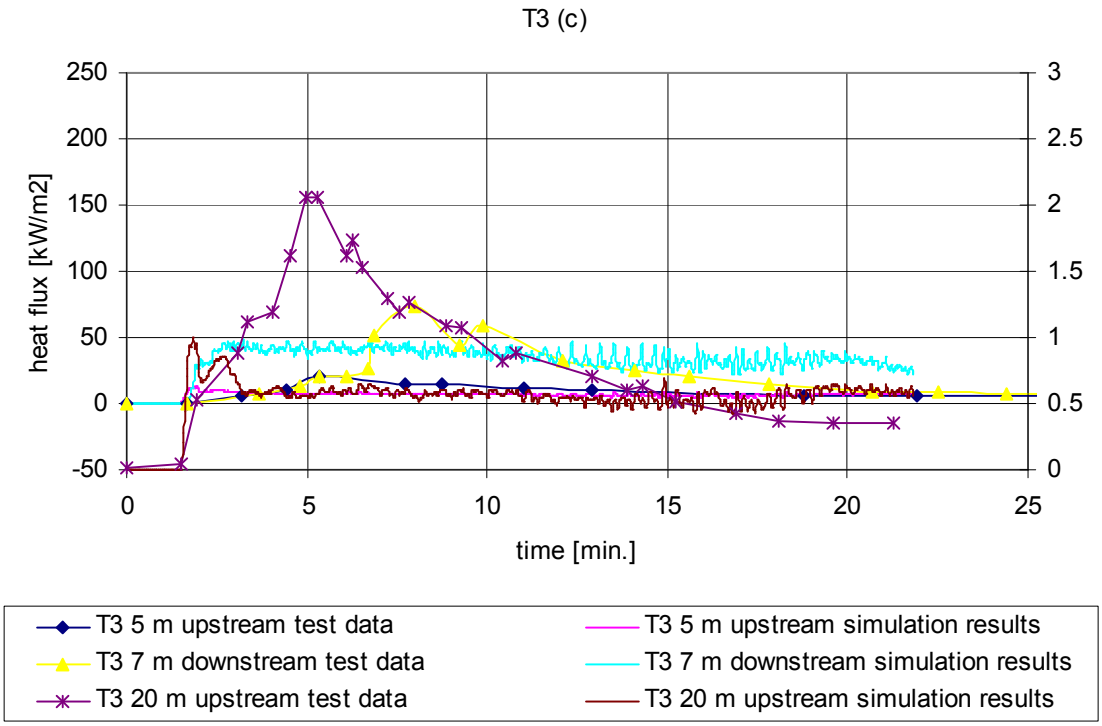

Figure 9. FDS simulation results of Runehamar tunnel fire tests, Test 2 (shown pulsation when the fire size grew above 130 MW) and Test 3 (no pulsation was observed). From the top, (a) temperature, (b) velocity, (c) heat flux, respectively.

6.3. Discussion

The results from modeling Runehamar tunnel fire tests, T2 and T3, were compared with the limited amount of experimental data that were available in this section and relatively they showed good agreement in terms of predicting the trend of change. However, there were few FDS results that presented poor agreement to the test data. After identifying and assessing the differences in the simulated results and the ones from the actual tests, the reason for this discrepancy was found. They are addressed below.

The problem of having a low gas temperature in the combustion zone, which was already discussed in the model validation (quantified as 30 to 40 % reduction) work, gave an early switch on to the flame extinction sub-model in FDS [14]. This sub-model was implemented to account for vitiated conditions that may occur in fire situations. Figure 10 indicates the flame extinction criteria that are a function of gas temperature and oxygen concentration. When this sub-model is turned on, the flame becomes intermittent. Figure

11 illustrates two distinct regions where the flames are continuous, and where the flame extinction model is turned on and off (after +20 m from the fire and near the ceiling above the fuel package). This figure is a slice file output from T2 simulation at t = 2 min. 54 sec. At this time, the temperatures, +20 m and +100 m from the fuel load, are fluctuating around 500 °C and 800 °C, respectively. (See T2 (a) in Figure 9.) Because the limiting oxygen concentration is between 6.5 % and 10 % (volume fraction) from +20 m to +100 m away from the fuel, the model activates the flame extinction model depending on the gas temperature and the availability of oxygen. As shown in the figure, with this model turned on, the flame length extends downstream until the unburned fuel is completely consumed by combustion. T2 simulation shows a good example of this. As the flame extinction continued, the flames were observed at the tunnel exit, where abundant oxygen was found. The extended flame length caused the downstream gas temperatures to be generally higher than the experiment values. In addition to its influence on flame length and downstream gas temperatures, the flame extinction sub-model affected the radiative heat flux predictions at 7 m downstream from the fuel package. It did not allow the heat flux to peak in both T2 and T3 cases, but rather present a steady heat flux throughout the simulations. Therefore, although FDS was trying to capture the flame extinction phenomena under vitiated conditions, the low gas temperatures near the fire, which was from FDS simulations, increased the limiting oxygen concentration level (see Figure 10 – as the temperature decreases, the oxygen concentration where vitiation occurs increases). Then the flame extinction sub-model activates, resulting in a lower temperature within the combustion zone with extended flame length downstream.

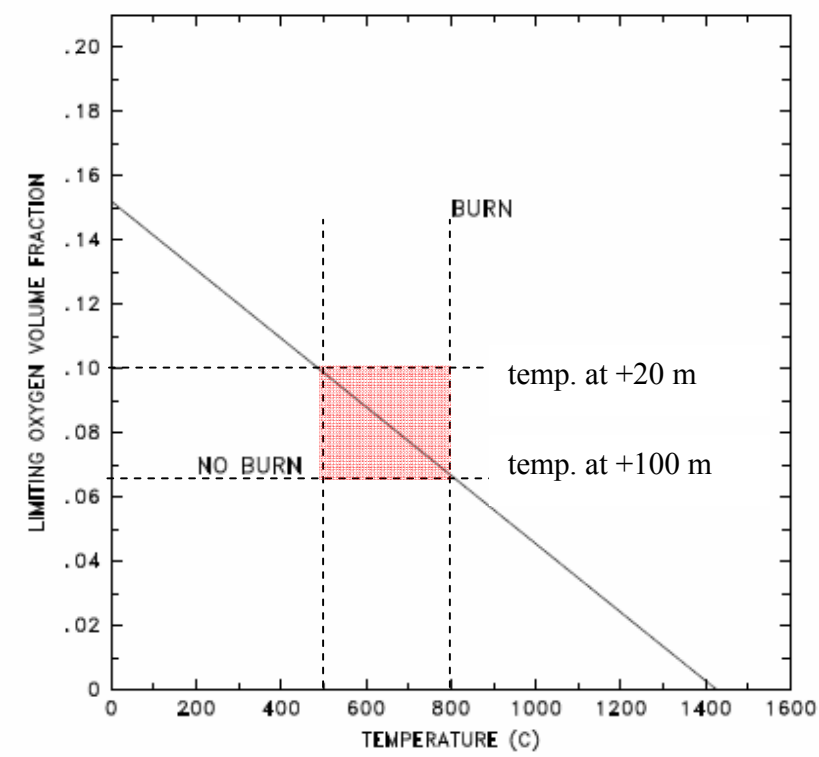

Figure 3.2: Oxygen-temperature phase space showing where combustion is allowed and not allowed to take place.

Figure 10. Flame extinction criteria for fires under vitiated conditions. The graph is reproduced from FDS technical guide [14].

As discussed above, FDS had limitations in modeling the flame extinction in vitiated fire condition; however, the results from this model support the suggested theory about pulsation. The simulation results from FDS showed that a locally vitiated region in the combustion zone may exist due to poor gaseous mixing between the supplied fuel vapor and air in the near-field when fuel supply rate increases while the flow velocities remains approximately the same. This fire condition, which was used as an assumption in the theoretical approach, supports the pulsation theory by identifying the possibility of having a locally under-ventilated condition due to insufficient gas phase mixing in the near-field.

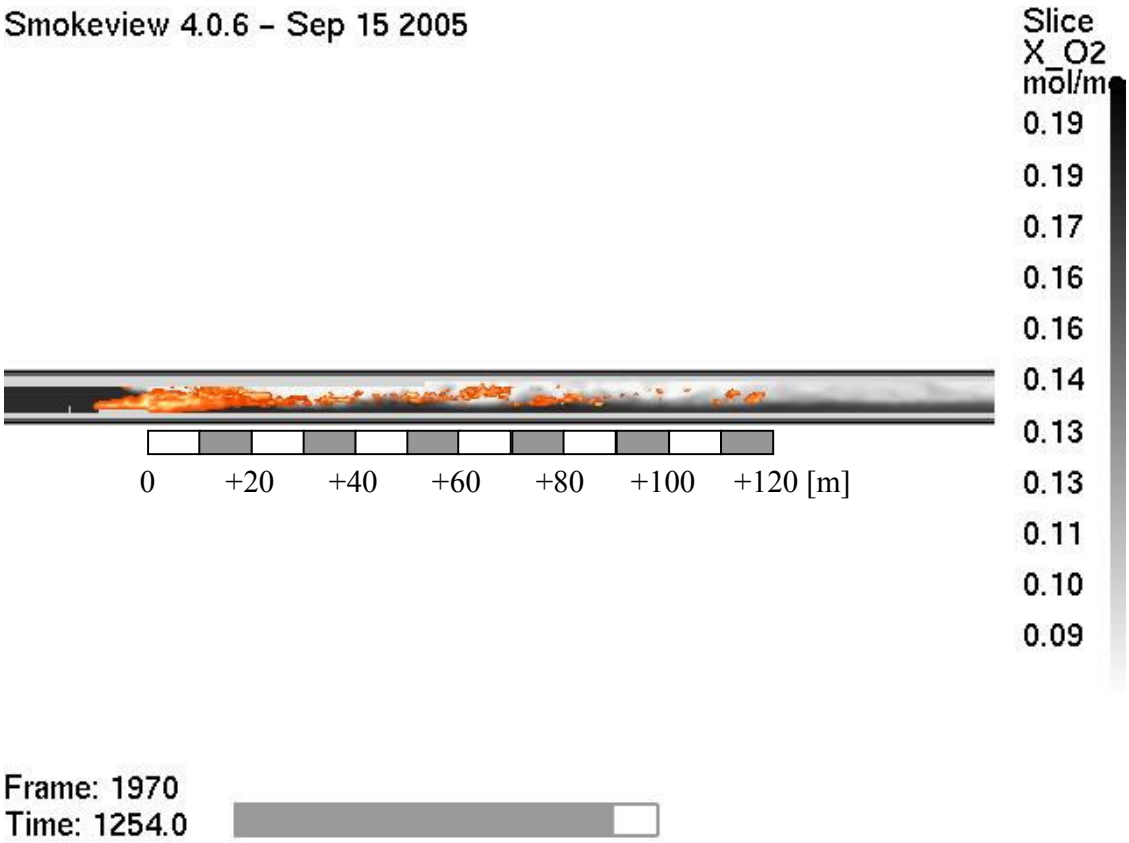

Figure 11. Slice file of the oxygen concentration across the centerline of the tunnel with heat release rate per unit volume indicating the flame location. This snap shot was at t = 20 min. 54 sec. after ignition for Runehamar tunnel fire test T2 simulation.

7. CONCLUSIONS

This study was conducted to understand pulsation phenomena, which was observed during the first two tests, T1 and T2 in the Runehamar tunnel fire tests [6, 13, 25]. The work started with background research, which led to an "oscillating flame" found in vitiated compartment fires and a "pressure oscillation" that exists in resonant combustion systems. This pressure oscillation is also known as the thermo-acoustic instability. These were both considered to have a relevance to pulsation phenomena due to the similarities in their characteristics with oscillations found in pulsation.

According to the frequency analyses done by SP [13], the pulsation periods found from the Runehamar tunnel fire tests, T1 and T2, are close to the resonance of the tunnel, and therefore, it is reasonable to believe that the thermo-acoustic instability was involved in pulsation. However, to have sustained thermo-acoustic instability, energy, which allows the amplitude of the oscillations to grow, must be fed into the system. In other words, the system must satisfy the Rayleigh criterion [9]. When this criterion is met, the acoustic waves are amplified, initiating instability in the system.

Among various factors that might have caused the initiation of the thermo-acoustic instability, a locally under-ventilated condition in the near-field of the fire was suggested as the most reasonable explanation due to the following reasons. First, even in a globally well ventilated fire condition, there is a possibility of having an insufficient mixing between the fuel vapor and air due to characteristics of the flow near the fire and system configuration. Second, the low carbon monoxide, CO concentration data from T1 and T2 [13] cannot be used as a reliable indication of under-ventilated fire because the high temperature in the near-field may have caused further oxidation of CO and the distant gas sampling port from the fire zone under turbulent flow conditions may have caused the combustion products to mix well with the air stream that was not involved in the combustion process. Third, in both tests, T1 and T2, the pulsation occurred when the heat release rate (HRR) of the fire exceeded 125 ~ 135 MW [6, 13]. This is when sufficient fuel vapor was supplied while the flow stayed the same, and therefore, it is highly possible that a localized under-ventilation condition occurred due to lack of mixing in the

near-field. Last, the flame response during pulsation was similar to that of the oscillating flames observed in the vitiated compartment fires [7, 8].

Based on the assumption of having a locally under-ventilated condition near the fuel location in the time range where pulsation occurred, a theoretical explanation of pulsation phenomena was proposed. This theoretical approach was constructed by considering the velocity field near the locally under-ventilated region within the combustion zone, the time necessary for proper mixing between the fuel and air supplied from forced ventilation, i.e. the residence time, and the boundary conditions of the surrounding near this region. In short, the theory suggests that pulsation may occur when there is enough fuel load and the solid boundaries near the fuel have hot surface temperatures to encourage pyrolisis even with a small flame. There is a limitation in the amount of oxygen supply and residence time. Both the oxygen supply and the residence time are determined by the flow field near the fuel, which is a function of pressure change driven by the energy input due to combustion. The constant changes in the pressure produced by localized under-ventilated conditions in the area near the fuel location, drives the pulsation cycle.

For further analysis, a simple model was developed to understand the characteristics of the fire conditions in a tunnel. Also, more sophisticated modeling work was conducted using Fire Dynamics Simulator (FDS) Version 4.0 [14, 15].

The results show that the model predictions, both from the simple model and FDS, give a qualitative agreement with the test data in terms of simulating the temperature and the velocity field, and species concentrations within the tunnel. In addition to the qualitative predictions, the results from the simple model and FDS also support the proposed theoretical explanation of pulsations.

The results from the simple model showed an oscillation when the oxygen concentration within the fire control volume reached a limit of vitiation (oxygen volume concentration less than 1%). Due to the vitiation limiting the combustion reaction, the pressure drops allowing more storage of oxygen and fuel in the fire control volume. When the oxygen concentration increased above the limitation for vitiation, combustion resulted in a decrease in the oxygen concentration once again. Therefore, cycling

oscillations in heat release rate, pressure and species concentrations were produced. The FDS simulation results demonstrated that the gaseous mixing between the supplied fuel vapor and air in the near-field becomes less effective in the near-fuel supply area as the specified fuel vapor supply rate increases while the flow velocities approximately stay the same. The findings indicate that the fire characteristics found in these modeling results were similar to the ones used in the theoretical approach, and hence, it provides stronger evidence that pulsations were possibly due to a locally under-ventilated condition in the near-field.

The research performed in this work – background research, theoretical studies, and mathematical modeling using a simple approach and FDS – suggests that there is a high possibility that the pulsation, which occurred during the Runehamar tunnel fire tests [6, 13, 25], was due to a locally under-ventilated condition near the fuel location. However, more experimental work related to tunnel fires with longitudinal ventilation is necessary for further verification of the pulsation theory.

As a future work, a practical means for eliminating pulsation in tunnel fires with forced, longitudinal ventilation should be found – either by limiting the potential fuel load within the tunnel to eliminate the locally under-ventilated condition or by increasing the ventilation velocity. The existing pulsation affects the efficiency of smoke ventilation. Also, pulsation enhances the mixing between the smoke from the fire and the fresh air stream supplied by the ventilation in the region where smoke-free condition is desired for safety evacuation and fire brigade.

8. REFERENCE

1. Ingason, H., Fire Development in Catastrophic Tunnel Fires (CTF), Proceedings of the International Symposium on Catastrophic Tunnel Fires, 20-21 November 2003
2. Bettelini, M., Neuenschwander, H., Henke, A., Gagliardi, M. and Steiner, W., The Fire in the St Gotthard Tunnel of October 24, 2001, In *Proceedings of the International Symposium on Catastrophic Tunnel Fires*, SP Swedish National Testing and Research Institute, SP Report 2004:05, Borås, Sweden, 20-21 November (2003) 49-68
3. Fire and smoke control in road tunnels, PIARC, 05, 05B-1999, 1999
4. NFPA 502. Standard for Road Tunnels, Bridges, and Other Limited Access Highways, 2004 Edition
5. Ingason, H., Lönnermark, A., Heat release rates from heavy goods vehicle trailer fires in tunnels, Fire Safety Journal 40 (2005) 646-668
6. Lönnermark, A., Persson, B., Ingason, H., Pulsation during large-scale fire tests in the Runehamar tunnel, Fire Safety Journal, In Press, Corrected Proof, Available online 17 April 2006
7. Utiskul, Y., Quintiere, J.G., Rangwala, A.S., Ringwelski, B.A., Wakatsuki, K., Naruse, T., Compartment fire phenomena under limited ventilation, Fire Safety Journal 40 (2005) 367-390
8. Kim, K.I., Ohtani, H., Uehara, Y., Experimental study on oscillating behaviour in a small-scale compartment fire, Fire Safety Journal, Volume 20, Issue 4, 1993, 377-384
9. Rayleigh, J.W.S., The Theory of Sound: Vol. II, Dover, New York, 1945
10. P. L. Rijke, Philosophical Magazine, **17**, (1859) 419-422.
11. Marble, F.E., Candel, S.M., An analytical study of the non-steady behavior of large combustors, 17th Symposium (International) on Combustion Organized by The Combustion Institute, 1978
12. Flandro, G.A., Majdalani, J., Aeroacoustic Instability in Rockets, AIAA 2001-3868, 2001
13. Lönnermark, A., Ingason, H., Acoustic Considerations Regarding Pulsations during Large-scale Fire Tests in a Tunnel, Eighth international symposium on fire safety science, Beijing, China; 18-23 September, 2005
14. McGrattan, K., Fire Dynamics Simulator (Version 4), Technical Reference Guide, NIST Special Publication 1018
15. McGrattan, K., Fire Dynamics Simulator (Version 4), User's Guide, NIST Special Publication 1019
16. Fox, R.W., McDonald, A.T., Introduction to Fluid Mechanics, 5th ed., John Wiley & Sons, Inc.
17. Ferziger, J.H., Subgrid-Scale Modeling, Part One: Fundamentals of Large Eddy Simulation, Large Eddy Simulation of Complex Engineering and Geophysical Flows, Cambridge Univ. Press, New York, NY ©1993
18. Germano M., Piomelli, U., Moin P., Cabot, W.H., A dynamic subgrid-scale eddy viscosity model, Phys. Fluids A 3(7), July (1991), 1760-1765

19. Piomelli, U., Zang, T.A., Speziale, C.G., Hussaini, M.Y., On the large-eddy simulation of transitional wall-bounded flows, Phys. Fluids A 2(2), February (1990), 257-265
20. Zhang, W., Hamer, A., Klassen, M., Carpenter, D., Roby, R., Turbulence statistics in a fire room model by large eddy simulation, Fire Safety Journal 37(8), November (2002), 721-752
21. Memorial tunnel fire ventilation test program, produced for the Massachusetts Highway Department Central Artery/Tunnel Project, Federal Highway Administration, 1996
22. McGrattan, K., Large eddy simulations of smoke movement, Fire Safety Journal 30(2), 161-178, 1998
23. Lönnermark, A., Ingason, H., Fire Spread and Flame Length in Large-Scale Tunnel Fires, Fire Technology, In Press
24. Yoshizawa, A., Eddy-viscosity-type subgrid-scale model with a variable Smagorinsky coefficient and its relationship with the one-equation model in large eddy simulation, Phys. Fluids A 3(8), August (1991), 2007-2009
25. Lönnermark, A., On the Characteristics of Fires in Tunnels, Doctoral Thesis, Department of Fire Safety Engineering, Lund Institute of Technology, Lund University, 2005
26. Blomqvist, P., Lönnermark, A., Characterization of the Combustion Products in Large-scale Fire Tests: Comparison of Three Experimental Configurations, Fire and Materials, Fire Mater. 25, 71 – 81 (2001)
27. Gottuk, D.T., Roby, R.J. and Beyler, C.L., The Rold of Temperature on Carbon Monoxide Production in Compartment Fires, Fire Safety Journal 24 (1995) 315-331, ©1995
28. Rangwala, A.S., Mathematical Modeling of Low Ventilation Small-scale Compartment Fires, Master Thesis, Department off Fire Protection Engineering, University of Maryland, 2002
29. Drysdale, D., An Introduction to Fire Dynamics, 2nd edition, John Wiley & Sons, ©1998
30. Quintiere, J.G., Fundamentals of Enclosure Fire "Zone" Models, Journal of Fire Protection Engineering, 1 (3), 1989, 99-119
31. Kanury, A.M., Ignition of Liquid Fuels, Chapter 8, Section 2, The SFPE Handbook of Fire Protection Engineering, 3rd ed., 2002

APPENDIX

A.1. A SIMPLIFIED TUNNEL MODEL

A.1.1. Unsteady flow in a tube

A flow within the tube can be calculated using the Newton's Second Law, i.e., momentum equation. The momentum equation can be set up using the average velocity, $\overline{U}(x,t)$ and the Darcy-Weisbach friction factor, f instead of the velocity, u(x,r,t) and the shear stress, τ.

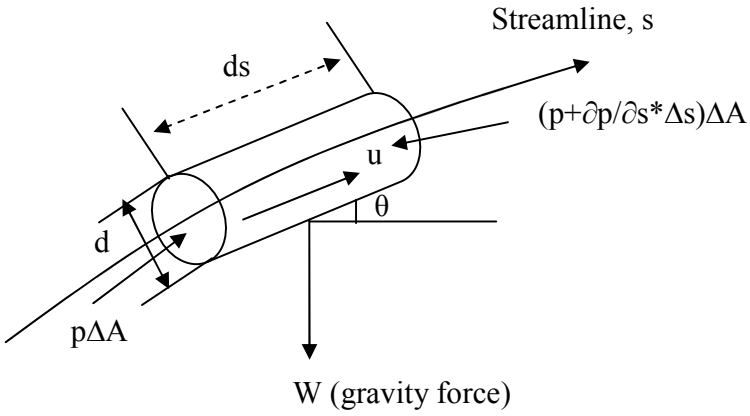

Figure A. 1. 1. A diagram of the local rate of momentum increase within the control volume in a given streamline.

The summation of the force acting on the fluid is equal to its local rate of momentum increase within the control volume and the net rate of efflux of momentum across the surface of the control volume. (See Figure A. 1. 1.) The s in the diagram signifies the streamline direction.

$$\sum F_s = \frac{\partial(mu)}{\partial t} + \frac{\partial(umu)}{\partial x} = \frac{\partial(\rho \Delta V\, u)}{\partial t} + \frac{\partial(u\,\rho \Delta V u)}{\partial x} \qquad \text{Eq. A.1.1}$$

Left hand side (LHS) of the above equation can be written in detail.

$$\frac{\partial(\rho \Delta V\, u)}{\partial t} + \frac{\partial(u\,\rho \Delta V u)}{\partial x} = \sum F_s \qquad \text{Eq. A.1.2}$$

$$= p\Delta A - \left(p + \frac{\partial p}{\partial s}\Delta s \right) \Delta A - W \sin\theta - \tau\, \Delta s\, \pi d$$

Using the following equations, the momentum equation above can be re-written in a one dimensional Euler equation form.

$$W = \rho \Delta V g = \rho(\Delta s \Delta A)\, g \qquad \text{Eq. A.1.3}$$

$$\Delta A = \frac{\pi d^2}{4} \qquad \text{Eq. A.1.4}$$

$$\frac{\Delta s\, \Delta A}{W} = \frac{\Delta V}{\rho \Delta V g} = \frac{1}{\rho\, g} = \frac{1}{\gamma} \qquad \text{Eq. A.1.5}$$

$$\sin\theta = \frac{\partial z}{\partial s} \qquad \text{Eq. A.1.6}$$

Therefore, the one-dimensional Euler equation form of the momentum equation is as follows;

$$\frac{\partial(\rho u)}{\partial t} + \frac{\partial(u \rho u)}{\partial x} = -\frac{\partial p}{\partial s} - \rho g \frac{\partial z}{\partial s} - \tau \frac{\Delta s\, \pi d}{\Delta s \Delta A} \qquad \text{Eq. A.1.7}$$

$$\frac{1}{\gamma}\left(\frac{\partial(\rho u)}{\partial t} + \frac{\partial(u \rho u)}{\partial x} \right) = -\frac{1}{\gamma}\frac{\partial p}{\partial s} - \frac{\partial z}{\partial s} - \frac{4\tau}{\gamma d} \qquad \text{Eq. A.1.8}$$

Introducing the average velocity, $\overline{U}(x,t)$ this equation can be re-written to the following equation.

$$\frac{1}{\gamma}\left(\frac{\partial(\rho \overline{U})}{\partial t} + \frac{\partial(\overline{U} \rho \overline{U})}{\partial x} \right) = -\frac{1}{\gamma}\frac{\partial p}{\partial s} - \frac{\partial z}{\partial s} - \frac{4\tau_0}{\gamma D} \qquad \text{Eq. A.1.9}$$

Using the conservation of mass law, the momentum equation can be reduced further more.

$$\frac{1}{\gamma}\left(\rho \frac{\partial \overline{U}}{\partial t} + \left(\rho \overline{U}\right)\frac{\partial \overline{U}}{\partial x} \right) = -\frac{1}{\gamma}\frac{\partial p}{\partial s} - \frac{\partial z}{\partial s} - \frac{4\tau_0}{\gamma D} \qquad \text{Eq. A.1.10}$$

$$\frac{\partial \overline{U}}{\partial t} + \overline{U}\frac{\partial \overline{U}}{\partial x} = -\frac{1}{\rho}\frac{\partial p}{\partial s} - g\frac{\partial z}{\partial s} - \frac{4\tau_0}{\rho D} \qquad \text{Eq. A.1.11}$$

Since z is a function only of s, partial differential term can be changed.

$$\frac{\partial \overline{U}}{\partial t} + \overline{U}\frac{\partial \overline{U}}{\partial x} = -\frac{1}{\rho}\frac{\partial p}{\partial s} - g\frac{dz}{ds} - \frac{4\tau_0}{\rho D} \qquad \text{Eq. A.1.12}$$

Shear stress, τ_0 can be expressed in a more practical way using the Darcy-Weisbach friction factor, f. The final equation can be applied to a compressible or an incompressible flow.

$$\tau_0 = \frac{\rho f \overline{U}^2}{8} \qquad \text{Eq. A.1.13}$$

$$\frac{\partial \overline{U}}{\partial t} + \overline{U}\frac{\partial \overline{U}}{\partial x} = -\frac{1}{\rho}\frac{\partial p}{\partial s} - g\frac{dz}{ds} - \frac{f\overline{U}^2}{2D} \qquad \text{Eq. A.1.14}$$

If there are no gradient in the tube and the flow of the fluid is assumed as incompressible, equation is more simplified. This equation was used in the upstream and downstream gas flow modeling in the simplified tunnel model.

$$\frac{\partial \overline{U}}{\partial t} = -\frac{1}{\rho}\frac{\partial p}{\partial x} - \frac{f\overline{U}^2}{2D} \qquad \text{Eq. A.1.15}$$

For downstream tube, a conservation of mass law was used to calculate the density change within the control volume.

$$\frac{dm_d}{dt} = \left(\rho_f A X \overline{U}_d + \rho_{up} A(1-X)\overline{U}_{up}\right) - \rho_d A \overline{U}_d \qquad \text{Eq. A.1.16}$$

$$\text{where } X = \frac{A_{CV_{fire}}}{A_{tot}}$$

A.1.2. One-zone model for near-field region in a tunnel fire with forced longitudinal ventilation

The one-zone model uses an assumption that the near-fire field region in a tunnel with longitudinal ventilation has uniform properties: temperature, pressure and species concentrations (oxygen and fuel). Based on this approach, a pseudo-compartment model is driven. The combustion reaction depends on the availability of oxygen and fuel (The

amount of fuel supplied in the control volume, $\dot{m}_s$ depends on the specified fuel source supply and the unburned fuel left in the control volume, $Y_{s,f.}$), and is assumed to be instantaneous. The gases obey ideal gas law. The density change due to pressure change within the control volume is assumed to be negligible.

Combustion model

$$\dot{Q}_{actual} = \dot{m}_s \Delta H_{ch} \frac{Y_{O_2,f}}{Y_{O_2,\infty}} \quad \left(V_{O_2,f} \geq 1\, Vol\%\ of\ ambient, 21\%\right)$$

$$= 0 \quad \left(V_{O_2,f} < 1\, Vol\%\ of\ ambient, 21\%\right)$$

where $\dot{m}_s = \dot{m}_{s,storage} + \dot{m}_{s,fire}$

$$= \frac{m_f Y_{s,f}}{\Delta t} + \dot{m}_{s,fire}$$

$$= \frac{\left(\rho_f V_{CV}\right) Y_{s,f}}{\Delta t} + \dot{m}_{s,fire}$$

Conservation of Mass

$$\frac{dm_f}{dt} = \frac{d}{dt}\left(\rho_f V_{CV}\right) = \frac{d}{dt}\left(\frac{(\rho T)_\infty}{T_f} V_{CV}\right) = \left(\dot{m}_{net\ in,CV}\right) + \dot{m}_{s,fire}$$

$$\frac{dT_f}{dt} = -\frac{{T_f}^2}{(\rho T)_\infty V_{CV}}\left(\left(\dot{m}_{net\ in,CV}\right) + \dot{m}_{s,fire}\right)$$

where $\dot{m}_{net\ in,CV} = \rho_{up} A\overline{U}_{up} - \rho_d A\overline{U}_d$

$$\rho_f = \frac{(\rho T)_\infty}{T_f}$$

Conservation of Energy

$$\frac{d}{dt}\left(c_v n T_f\right) = \frac{d}{dt}\left(\frac{nRT_f}{\gamma - 1}\right) = \frac{V_{CV}}{\gamma - 1}\frac{dP_f}{dt}$$

$$= c_p A(\rho T)_\infty \left(\overline{U}_{up} - \overline{U}_d\right) + c_{p,s}\dot{m}_{s,fire}T_s + \dot{Q}_{actual}$$

$$\frac{dP_f}{dt} = \frac{\gamma - 1}{V_{CV}}\left(c_p A(\rho T)_\infty \left(\overline{U}_{up} - \overline{U}_d\right) + c_{p,s}\dot{m}_{s,fire}T_s + \dot{Q}_{actual}\right)$$

where $\dot{Q}_{actual} = \left(\underline{\underline{\frac{m_{s,f}}{\Delta t}}} + \dot{m}_{s,fire}\right)\Delta H_{ch}\frac{Y_{O_2,f}}{Y_{O_2,\infty}} \quad \left(Y_{O_2,f} \rangle 0, m_{O_2,available} \rangle m_{O_2,needed}\right)$

$$\left(\frac{m_{s,f}}{\Delta t} = \frac{m_f Y_{s,f}}{\Delta t} = \frac{(\rho_f V_{CV})Y_{s,f}}{\Delta t} = \left(\left(\frac{(\rho T)_\infty}{T_f}\right)V_{CV}\right)\frac{Y_{s,f}}{\Delta t}\right)$$

$$= \left(\underline{\underline{\frac{m_{O_2,f}}{\Delta t}}} + \dot{m}_{net\ inflow,O_2}\right)\left(r\,\Delta H_{ch}\right) \quad \left(Y_{O_2,f} \rangle 0, m_{O_2,available} \langle m_{O_2,needed}\right)$$

$$\left(\frac{m_{O_2,f}}{\Delta t} = \frac{m_f Y_{O_2,f}}{\Delta t} = \frac{(\rho_f V_{CV})Y_{O_2,f}}{\Delta t} = \left(\left(\frac{(\rho T)_\infty}{T_f}\right)V_{CV}\right)\frac{Y_{O_2,f}}{\Delta t}\right)$$

$$= \left(\underline{\underline{\frac{m_{s,f}}{\Delta t}}} + \dot{m}_{s,fire}\right)\Delta H_{ch} \quad \left(Y_{O_2,f} = 0, m_{O_2,available} \rangle m_{O_2,needed}\right)$$

$$= \dot{m}_{net\ inflow,O_2}\left(r\,\Delta H_{ch}\right) \quad \left(Y_{O_2,f} = 0, m_{O_2,available} \langle m_{O_2,needed}\right)$$

where $\dot{m}_{net\ inflow,O_2} = Y_{O_2,\infty}\rho_{up}A\overline{U}_{up} - Y_{O_2,f}\rho_d A\overline{U}_d \quad \left(\overline{U}_{up} \rangle 0, \overline{U}_d \rangle 0\right)$

$$= Y_{O_2,f}\rho_{up}A\overline{U}_{up} - Y_{O_2,f}\rho_d A\overline{U}_d \quad \left(\overline{U}_{up} \langle 0, \overline{U}_d \rangle 0\right)$$

$$= Y_{O_2,\infty}\rho_{up}A\overline{U}_{up} - Y_{O_2,\infty}\rho_d A\overline{U}_d \quad \left(\overline{U}_{up} \rangle 0, \overline{U}_d \langle 0\right)$$

Conservation of Species, Oxygen

$$\frac{dm_{O_2,f}}{dt} = \frac{d}{dt}\left(m_f Y_{O_2,f}\right) = \frac{d}{dt}\left(\frac{(\rho T)_\infty}{T_f}V_{CV}Y_{O_2,f}\right)$$

$$= (\rho T)_\infty V_{CV} \frac{d}{dt}\left(\frac{Y_{O_2,f}}{T_f}\right) = (\rho T)_\infty V_{CV}\left(\frac{1}{T_f}\frac{dY_{O_2,f}}{dt} - \frac{Y_{O_2,f}}{{T_f}^2}\frac{dT_f}{dt}\right)$$

$$= \frac{(\rho T)_\infty V_{CV}}{T_f}\left(\frac{dY_{O_2,f}}{dt} - \frac{Y_{O_2,f}}{T_f}\frac{dT_f}{dt}\right) = \dot{m}_{net\ inflow,O_2} - \frac{1}{r}\frac{\dot{Q}_{actual}}{\Delta H_{ch}}$$

$$\frac{dY_{O_2,f}}{dt} = \frac{T_f}{(\rho T)_\infty V_{CV}}\left(\dot{m}_{net\ inflow,O_2} - \frac{1}{r}\frac{\dot{Q}_{actual}}{\Delta H_{ch}}\right) + \frac{Y_{O_2,f}}{T_f}\frac{dT_f}{dt}$$

where r is from the stoichiometric reaction,

$$f \cdot Fuel + o \cdot Oxygen \rightarrow p \cdot Product$$

$$r = \frac{f}{o}\left[\frac{kg\ fuel}{kg\ O_2}\right]$$

Conservation of Species, Fuel

$$\frac{dm_{s,f}}{dt} = \frac{d}{dt}\left(m_f Y_{s,f}\right) = \frac{d}{dt}\left(\frac{(\rho T)_\infty}{T_f} V_{CV} Y_{s,f}\right)$$

$$= (\rho T)_\infty V_{CV} \frac{d}{dt}\left(\frac{Y_{s,f}}{T_f}\right) = (\rho T)_\infty V_{CV}\left(\frac{1}{T_f}\frac{dY_{s,f}}{dt} - \frac{Y_{s,f}}{{T_f}^2}\frac{dT_f}{dt}\right)$$

$$= \dot{m}_{s,fire} + \dot{m}_{net\ inflow,s} - \frac{\dot{Q}_{actual}}{\Delta H_{ch}}$$

$$\frac{dY_{s,f}}{dt} = \frac{T_f}{(\rho T)_\infty V_{CV}}\left(\dot{m}_{s,fire} + \dot{m}_{net\ inflow,s} - \frac{\dot{Q}_{actual}}{\Delta H_{ch}}\right) + \frac{Y_{s,f}}{T_f}\frac{dT_f}{dt}$$

where $\dot{m}_{net\ inflow,s} = -Y_{s,f}\rho_d A\overline{U}_d \quad \left(\overline{U}_{up} \rangle 0, \overline{U}_d \rangle 0\right)$

$$= Y_{s,f}\left(\rho_{up} A\overline{U}_{up} - \rho_d A\overline{U}_d\right) \quad \left(\overline{U}_{up} \langle 0, \overline{U}_d \rangle 0\right)$$

$$= 0 \quad \left(\overline{U}_{up} \rangle 0, \overline{U}_d \langle 0\right)$$

A.2. SENSITIVITY ANALYSIS FOR TUNNEL FIRES USING FDS V4

A.2.1. Grid Sensitivity Analysis

Finding a suitable grid size is one of the difficulties in using FDS. The use of fine resolutions for the computational grid may produce more detailed and reliable simulation results, but at the same time it may extremely increase the simulation time, which can be unsuitable for practical use. Therefore, finding an appropriate grid size that produces calculation results, which reasonably well-represent the actual fire conditions, and also consumes a feasible simulation time, is important. One of the suggestions made by the developers of FDS was to span at least ten grid cells within the characteristic fire diameter, D* (see Eq. A.2.1) [34] D* is not essentially the same as the actual fire diameter. The expression comes from the characteristic fire size, Q*[2]. For the Memorial Tunnel Test 621A the D* value becomes approximately 6.05m. Hence, any grid size greater than 10% of the D* value, 6.05m was discarded from the study. Including the 10% of D* case, 5% and 8% cases were simulated for the grid sensitivity analysis (See Figure A.2.1, Figure A.2.2).

$$D^* = \left(\frac{\dot{Q}}{\rho_\infty c_p T_\infty \sqrt{g}} \right)^{\frac{2}{5}} \qquad \text{Eq. A.2.1}$$

$$= \left(\frac{100 \times 10^3 kJ/s}{1.2 kg/m^3 \times 1.01 kJ/kg \cdot K \times 293 K \times \sqrt{9.8 m/s^2}} \right)^{\frac{2}{5}} \approx 6.05 m$$

A.2.1.1 Upstream region

Comparing the results from the FDS simulations, the backflow of the hot gases from the fire had occurred extensively in all three cases. The difference between the three cases is that the coarsest grid, 10% D* case had a thicker in depth, and shorter in terms of the backflow length traveling upstream. The 5% D* case resulted in a thinner, but more lengthy backflow. Due to the backflows, the temperature distribution and the velocity profile of the simulation runs at the upstream area was much higher near the ceiling comparing to the actual test data. However, the temperature and velocity results from the simulations did not show a significant difference by changing the grid sizes.

A.2.1.2 Near-fire region

In order to check whether FDS was burning the total amount of the fuel prescribed in the input file, the total heat release rate for each case run were compared with the heat release rate curve given. Although the total heat release rate curve from the simulations showed oscillations, the average heat release rates from each case run were close to the input information. The 8% D* case had the most significant oscillations, in the order of ±10 MW while others were in the range of ±5 MW.

The test data shows that the maximum temperature within the tunnel locates near the ceiling at Loop 303 throughout the test and its peak of 1502 ºF exists around 430 seconds after ignition. The 10% D* case shows the similar condition, though with 36% reduction in the maximum temperature in the time interval of 430 ± 100 seconds. The 8% D* case had resulted in placing the maximum temperature around the center of the tunnel. The flames from the tunnel floor to the ceiling were the hottest area. Also, the hot gases traveled upstream leading to an increase in the temperature readings above the fire base. The maximum temperature had reduced 35% compared to the test data. The results from the 5%D* case were similar to the 8%D* case run. However the maximum temperature was closer to the actual test data than other two cases. The maximum temperature was 21% less than that of the test data with its location around the center of the tunnel not the ceiling.

The velocity profiles of the three case runs were similar. The discrepancies between three cases were less than 1m/s.

A.2.1.3 Downstream region

Generally, the temperatures were low compared to the test data throughout the downstream area. The average difference between the simulation results and the test data were around 200ºF. However, the shapes of the temperature distribution of three cases were similar. As the distance from the fire increases further down to the tunnel exit, the gases became cooler from the floor area leaving relatively low temperatures around the tunnel exit.

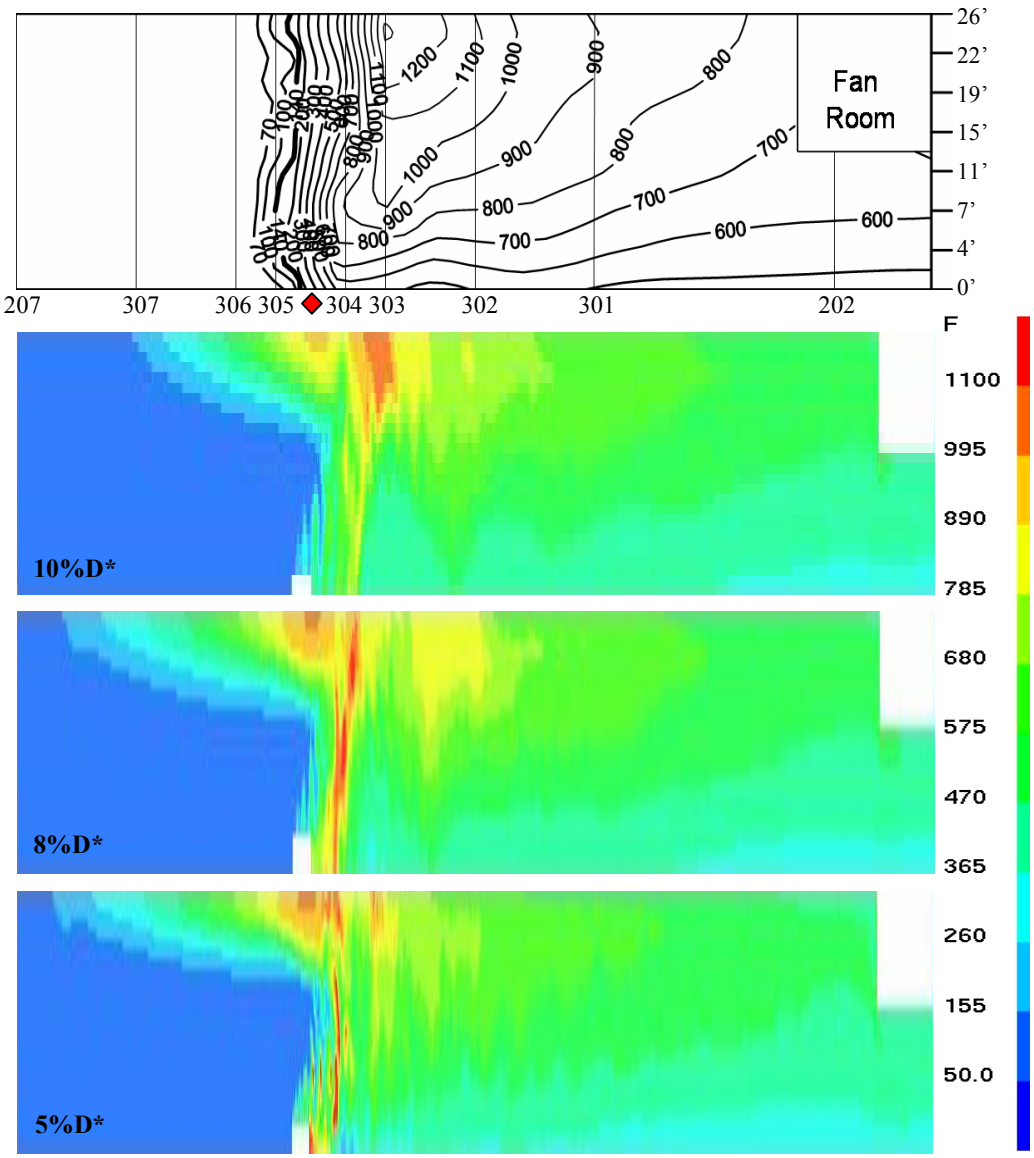

Figure A.2.1. Temperature Profile at time = 16min. of Memorial Tunnel Test 621A; From the top, actual test data, 10%D* grid, 8%D* grid and 5%D* case. There are not much of a difference in the temperature distribution throughout the tunnel between the 8%D* and 5%D* case.

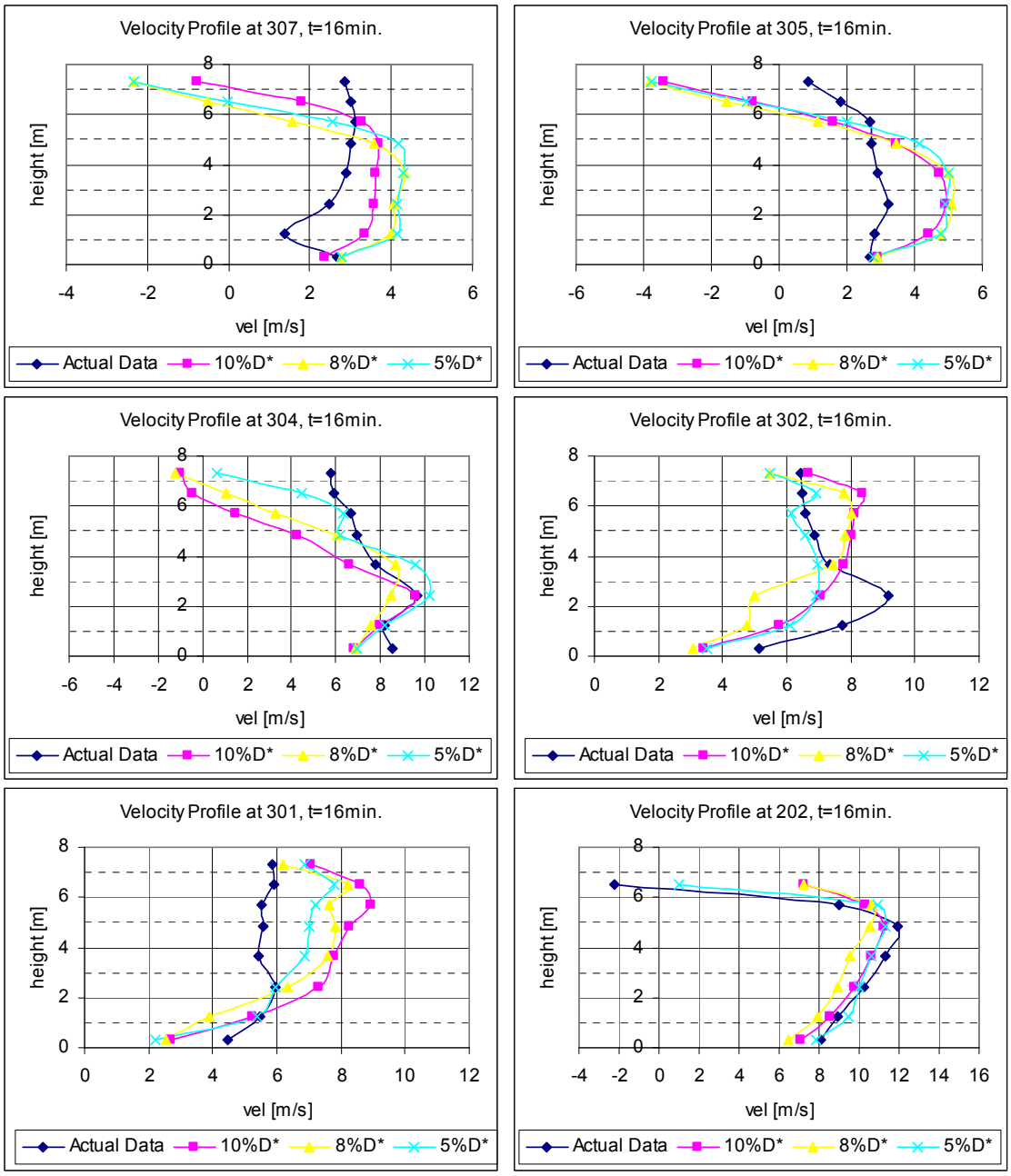

Figure A.2.2. Velocity Profile using different grid sizes at time = 16min. of Memorial Tunnel Test 621A; From the top left, velocity at Loop 307, 305, 304, 302, 301 and 202. The difference between the velocity outputs from 10%D*, 8%D* and 5%D* cases are insignificant.

Though the velocity profile of the 5%D* case was the closest to the actual test data, the results from 8%D* and 10%D* were also similar to the finest grid case presenting an average deviation of ±1m/s. The difference shown in the velocity reading at Loop 202 between the 5%D* case and the other two cases were due to the height of the fan room located around the tunnel exit. Solid obstructions generated in FDS must align with the

grid. Hence inevitably the distance between the measurement location of the top probe, and the ceiling, which is the bottom of the fan room, were closer for the 5%D* case reducing the flow than the others.

The grid sensitivity analysis above had demonstrated that using the finest grid of the three, the 5%D* case would give the best simulation results in terms of reproducing the conditions of fire and its surroundings. However, the results also show that applying a grid size in the range of 5 to 10% of the characteristic fire diameter, D* does not generate a significant change in the simulation outputs such as the temperature and the velocity profile within the tunnel. Therefore, the grid size found in the 8%D* case was used for further studies considering both the computational expenses and the quality of the simulations. 6 to 7 days of an additional computational time was required to run the same partial Memorial Tunnel Test 621A when 5% of the D* was used as a grid length compared to the 8%, to produce simulation results, which were not critically different from the ones from the 8%D* case as shown above.

A.2.2. Parameter Sensitivity Analysis

Among the user specified parameters that are used in FDS, the main focus will lie on the ones that are directly related to the LES turbulence model; Turbulent Pr number, PR, turbulent Sc number, SC, and Smagorinsky constant, CSMAG. There default values are 0.5, 0.5 and 0.2, respectively.

A.2.2.1 Turbulent Prandtl number, PR

For turbulent flows, two different kinds of momentum transfer needs to be considered; momentum transfer due to the random motions of molecules and due to the large scale fluctuations which exists in the turbulence. However, unlike the molecular exchange of momentum the analytical explanation of turbulence has not been developed. The phenomenon is far too complicated to be solved analytically even for the simplest cases. Therefore, former scientists and engineers have found a way to account for the effect of the turbulence by treating the macroscopic exchange of momentum in turbulent flow as one of the shear stresses instead of directly calculating the fluctuations. The turbulent

shear stress also known as the Reynolds stress is significantly greater than the molecular contribution with an exception near the solid boundaries. The total shear stress may be expressed as below where the ε_M is the eddy diffusivity of momentum;

$$\left(\tau_{yx}\right)_{total} = \left(\tau_{yx}\right) + \left(\tau_{yx}\right)_{turb} = \rho\left(\nu + \varepsilon_M\right)\frac{d\overline{v_x}}{dy} \qquad \text{Eq. A.2.2}$$

By analogy, the turbulence effect can be considered for the energy transfer. Both the microscopic molecular motions and the macroscopic turbulences must be counted for in the analyses. Hence, the total energy flux can be expressed using the same mathematical form above but with the use of the eddy diffusivity of heat, ε_H instead of the eddy diffusivity of momentum, ε_M;

$$\left(\frac{q_y}{A}\right)_{total} = \left(\frac{q_y}{A}\right) + \left(\frac{q_y}{A}\right)_{turb} = -\rho c_p\left(\alpha + \varepsilon_H\right)\frac{d\overline{T}}{dy} \qquad \text{Eq. A.2.3}$$

Where the flow is fully turbulent, the molecular heat diffusivity is far smaller than the eddy diffusivity for all fluids except for liquid metals; $\alpha << \varepsilon_H$.

Using these two expressions, the turbulent Prandtl number used in FDS can be introduced as below. Both in the eddy viscosity term, μ_{LES} and the thermal conductivity term, k_{LES} includes the molecular viscosity or the conductivity which is from the property of the fluid and the eddy diffusivity of momentum or heat which is determined by the

$$\mathrm{Pr}_{turb} = \frac{\nu + \varepsilon_M}{\alpha + \varepsilon_H} = \frac{\frac{\mu}{\rho} + \varepsilon_M}{\frac{k}{\rho c_p} + \varepsilon_H} = \frac{\frac{1}{\rho}\left(\mu + \rho\varepsilon_M\right)}{\frac{1}{\rho c_p}\left(k + \rho c_p \varepsilon_H\right)} = \frac{c_p \mu_{LES}}{k_{LES}} \qquad \text{Eq. A.2.4}$$

$$k_{LES} = \frac{c_p \mu_{LES}}{\mathrm{Pr}_{turb}} \qquad \text{Eq. A.2. 5}$$

turbulent motions of the flow. During the FDS simulations, the Pr_{turb} value decides the thermal conductivity of the fluid, k_{LES} and therefore changing the Pr_{turb} value would affect the gas phase temperature distribution throughout the tunnel. In order to find the proper value used for Pr_{turb} in the simulations the information from the fluid properties

and the characteristics of the flow should be considered at the same time and hence the number can only be determined empirically due to the difficulties in analytically solving the turbulence of the flow.

However, two theoretical turbulent Prandtl numbers can be found by applying assumptions about the flow characteristics. As mentioned earlier, in the turbulent region the molecular diffusivity of momentum and heat are insignificant compared to the eddy diffusivities but for laminar flows the eddy diffusivities are insignificant. Therefore, the turbulent Prandtl number for the fully developed turbulent flow is unity and for laminar flows is the original Prandtl number, Pr which is the ratio of the molecular diffusivity of momentum and heat [3]. For air at atmospheric pressure, the Pr ranges from 0.536 to 0.786 depending on the air temperature ranging from 100K to 3000K. In the temperature range which the tunnel fires are involved in, the Pr number stays within 0.7 ± 0.05. [**Error! Reference source not found.**] Other than these two extreme cases where the flow is either fully turbulent or laminar, the turbulent Prandtl number must be found based on the comparison between the simulation results and the test data. Many of the work done for the turbulent Prandtl number used in the computational fluid dynamics field used a value between 0.2 and 0.9 [4]. For fire related problems using FDS, using a value of 0.5 which is the current default setting was found to be reasonable [**Error! Reference source not found.**]. In order to calibrate the use of the default value and to demonstrate the effects of changing the parameter, a sensitivity analysis has been performed in the following section. The simulations were done with values 40% and 100% greater than the default setting and the calculation results were compared with the actual test data and the default case run.

$$\mathrm{Pr}_{turb}\big|_{fully\ turb} = \frac{\nu + \varepsilon_M}{\alpha + \varepsilon_H} = \frac{\varepsilon_M}{\varepsilon_H} \to 1 \quad \left(\nu << \varepsilon_M, \alpha << \varepsilon_H\right) \qquad \text{Eq. A.2.6}$$

$$\mathrm{Pr}_{turb}\big|_{lam} = \frac{\nu + \varepsilon_M}{\alpha + \varepsilon_H} = \frac{\nu}{\alpha} \to \mathrm{Pr} \quad \left(\nu >> \varepsilon_M, \alpha >> \varepsilon_H\right) \qquad \text{Eq. A.2.7}$$

A.2.2.1.1 Upstream region

Similar to the above results in the grid and CSMAG sensitivity analyses, backflow had occurred extremely in all three cases, PR = 0.5, 0.7 and 1.0 compared to the test data. The backflow caused the temperatures and the velocities of the gas phase to be higher than the actual test data near the ceiling. As demonstrated in Figure A.2.3, changing the turbulent Prandtl number in FDS does not help in decreasing the backflow length. However, it shows that the thickness of the backflow is somewhat reduced as the value had increased from 0.5 to 1.0. The differences in the velocity profiles in the upstream region for the three case runs (see Figure A.2.4) were negligible.

A.2.2.1.2 Near-fire region

The total heat release rates in the hrr file were checked to make sure FDS was consuming the full amount of the heat release rate prescribed in the input file. Although the total heat release rate curve from the simulations showed oscillations, the average heat release rates from each case run were close to the input information. The oscillations in the total heat release rate were all in the order of ±10MW.

The test data shows that the maximum temperature within the tunnel locates near the ceiling at Loop 303 throughout the test and its peak of 1502˚F exists around 430 seconds after ignition. The results from PR = 0.5(default) case had placed its maximum temperature around the center of the tunnel cross section area rather than near the ceiling. The flames from the tunnel floor to the ceiling were the hottest area. Additionally due to the backflow, the hot gases traveled upstream leading to an increase in the temperature readings right above the fire base (see Figure A.2.3). The maximum temperature had reduced 35% compared to the test data. The PR = 0.7 and 1.0 case results were similar to the PR = 0.5 (default) case but with reduced backflow thickness and heat transfer downstream. The 600ºF lines in Figure A.2.3 propagate less downstream as the turbulent Prandtl number increases. The maximum temperatures in the time interval of 430 ± 100 seconds for PR = 0.7 and 1.0 cases were approximately 24% and 32% lower than the reported value respectively. These temperatures were found closer to the ceiling than that of the default case.

The velocity profiles at Loop 305, 304 and 302 (see Figure A.2.4) are almost identical for all three case runs. The discrepancies between the actual test data and the simulated ones are within the range of ±6m/s for near-wall regions while ±2m/s for the flows located in the center of the tunnel.

A.2.2.1.3 Downstream region

Even though there were no significant changes by using different Pr_{turb} values, the heat transfer downstream reduced as the Pr_{turb} value used in FDS calculations increased as mentioned in the previous section. It may be found by following the temperature lines in Figure A.2.3 which indicate the temperature of 500˚F. The line remains closer to the fire location as the Pr_{turb} value increases. Also, the temperature results from the three cases were low in general compared to the test data throughout the downstream area. The average difference between the simulation results and the test data were around 200ºF. However, the overall shapes of the temperature distribution of three case runs were similar with each other and to the actual test data. As the distance from the fire increases further down to the tunnel exit, the gases became cooler from the floor area leaving relatively low temperatures around the tunnel exit.

The velocity profile at Loop 301 and 202 demonstrated that changing the Pr_{turb} value nearly affects the FDS calculations for velocities. The difference between the actual test data and the simulation results were around ±2m/s for all three cases.

The turbulent Prandtl number sensitivity analyses verified that changing the constant has less impact over the FDS simulation results compared to the Smagorinsky constant, which will be discussed later. However, varying the Pr_{turb} value did slightly affect the temperature distribution with influencing the velocity profile to its least amount.

Increasing the value from its default setting reduced the heat transfer within the gas phase. The effect is shown by the changes occurred in the thickness of the backflow and the temperature profile at the downstream region. Comparing the results from these three case runs to the actual data, using the default setting of 0.5 seems to be the most reasonable decision to make considering the sensitivity of the Pr_{turb} value in the simulation results and the temperature profile within the tunnel.

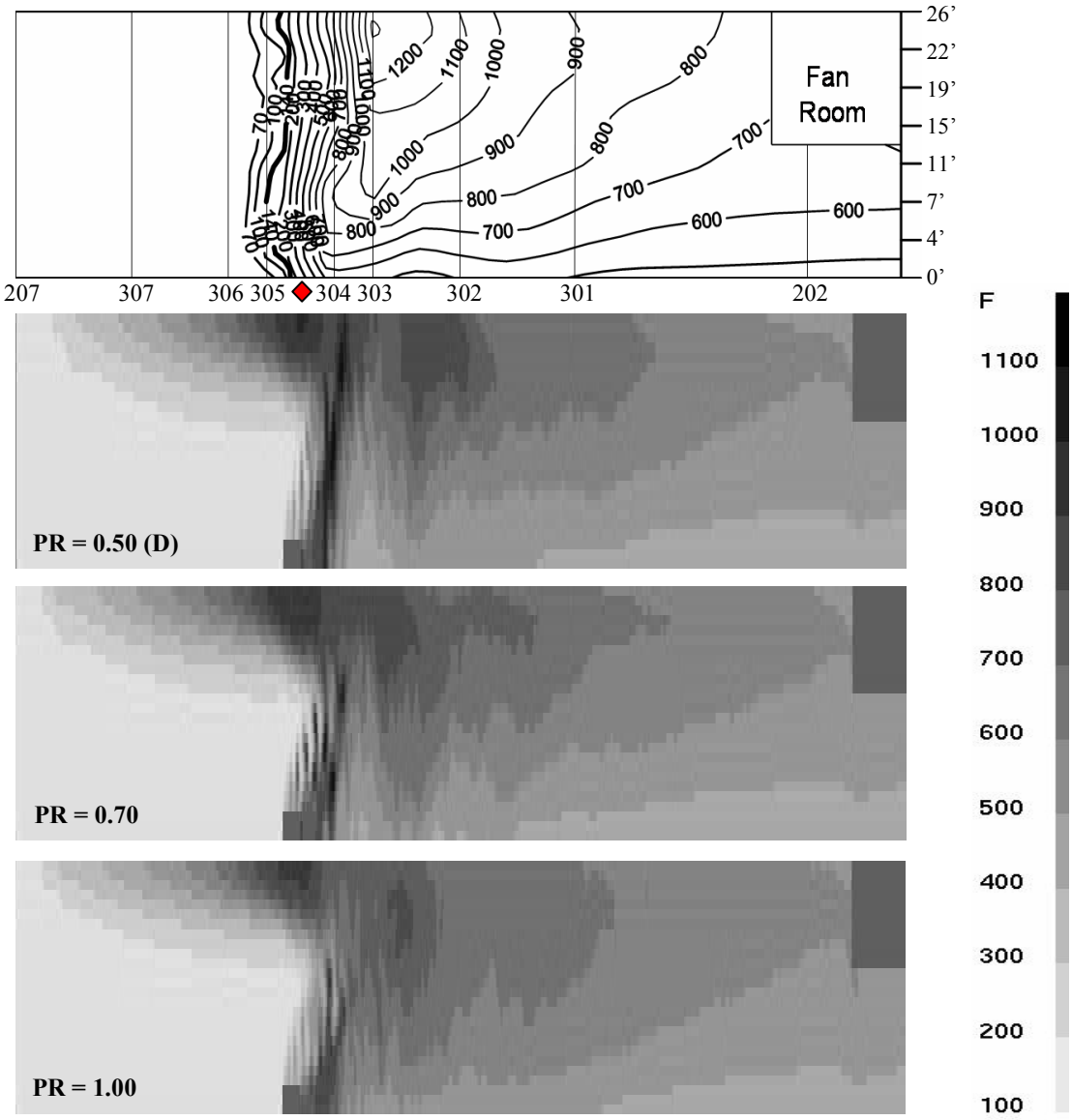

Figure A.2.3. Temperature Profile at time = 16min. of Memorial Tunnel Test 621A; From the top, actual test data, PR of 0.50 (default value), 0.70 and 1.00. The gas phase temperature reduces as PR increases.

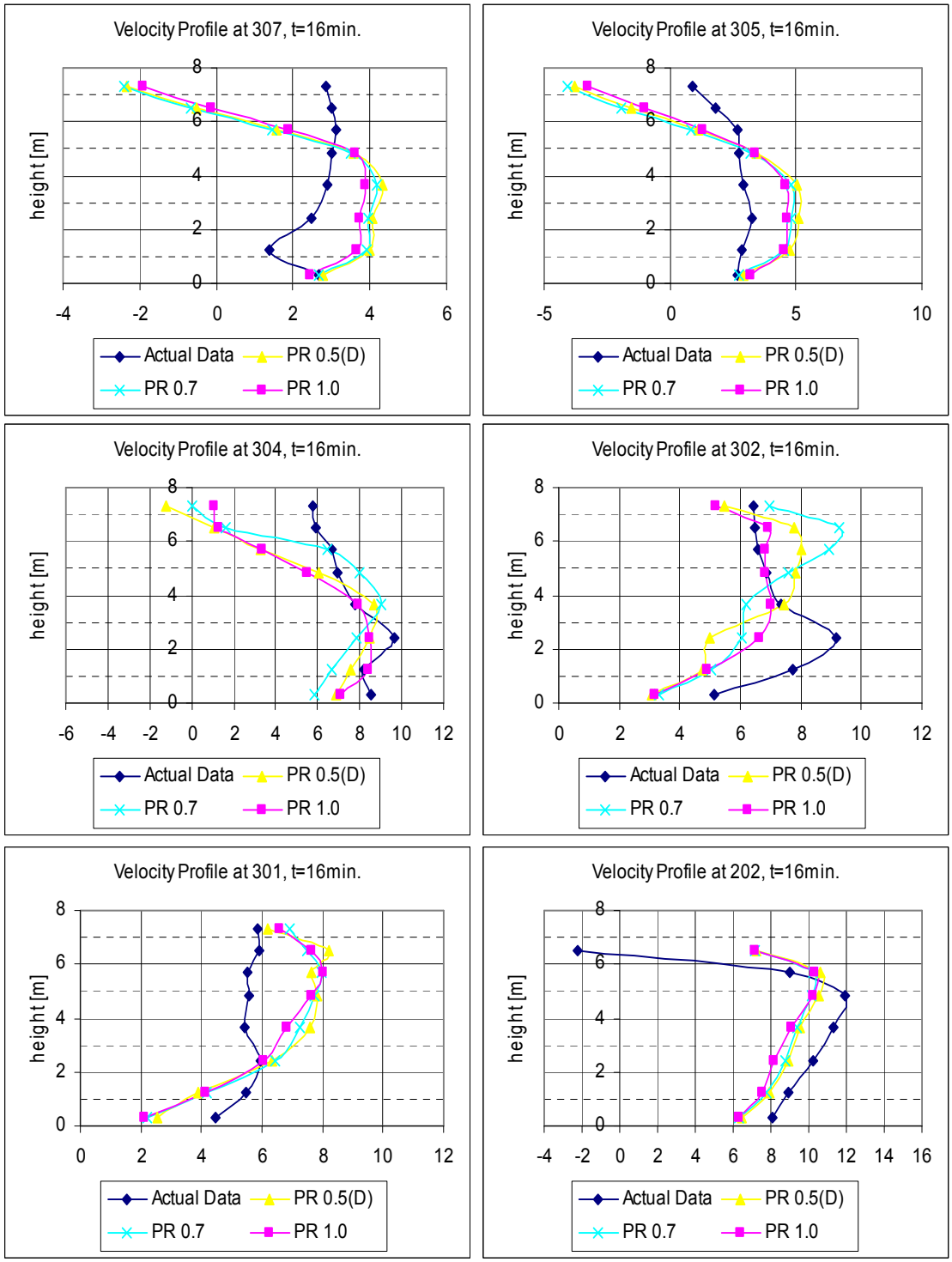

Figure A.2.4. **Velocity Profiles using different PR values at time = 16min. of Memorial Tunnel Test 621A; From the top left, velocity at Loop 307, 305, 304, 302, 301 and 202. There are no significant differences in the velocity outputs between the three cases; PR = 0.5(default), 0.7 and 1.0.**

A.2.2.2 Turbulent Schmidt number, SC

An analogous to the eddy diffusivity of momentum and heat mentioned earlier in the turbulent Prandtl number section, the turbulent effect can be considered for the mass transfer also. Two parts of the mass diffusivity must be included in the analyses; the microscopic molecular motions and the macroscopic turbulence effects. The total energy flux can be expressed using the same mathematical form above but with the use of the eddy diffusivity of mass, ε_D instead of the eddy diffusivity of heat, ε_H;

$$\left(N_{A,y}\right)_{total} = \left(N_{A,y}\right) + \left(N_{A,y}\right)_{turb} = -\left(D_{AB} + \varepsilon_D\right)\frac{d\overline{c_A}}{dy} \qquad \text{Eq. A.2.8}$$

Where the flow is fully turbulent, the magnitude of the molecular heat diffusivity is much less than that of the eddy diffusivity; $\alpha << \varepsilon_D$.

Using the expressions for the total diffusivities of momentum and mass, the turbulent Schmidt number defined in FDS can be written as below. Both in the eddy viscosity term, μ_{LES} and the material diffusivity term, $(\rho D)_{LES}$ includes the molecular viscosity or the mass diffusivity which comes from the property of the fluid and the eddy diffusivity of momentum or mass which is determined by the turbulent motions in the flow.

$$Sc_{turb} = \frac{\nu + \varepsilon_M}{D_{AB} + \varepsilon_D} = \frac{\frac{\mu}{\rho} + \varepsilon_M}{D_{AB} + \varepsilon_D} = \frac{\frac{1}{\rho}\left(\mu + \rho\varepsilon_M\right)}{\left(D_{AB} + \varepsilon_D\right)} = \frac{\mu_{LES}}{\left(\rho D\right)_{LES}} \qquad \text{Eq. A.2.9}$$

$$\left(\rho D\right)_{LES} = \frac{\mu_{LES}}{Sc_{turb}} \qquad \text{Eq. A.2.10}$$

During the FDS simulations, the Sc_{turb} value decides the diffusivity of the materials within the fluid, $(\rho D)_{LES}$. One of the important roles of the $(\rho D)_{LES}$ value is that it influences the flame sheet location because FDS uses the mixture fraction approach to model the combustion. In order to find the proper value used for Sc_{turb} in the simulations the information from the fluid properties and the characteristics of the flow should be considered at the same time and hence the number is determined using empirical correlations due to the difficulties in analytically solving the turbulence of the flow.

However, few basic turbulent Schmidt numbers can be found by applying assumptions about the flow characteristics. By analogous to the turbulent Prandtl number, the turbulent Schmidt numbers can be derived for two different flow conditions; fully turbulent and laminar. Where the flow is fully turbulent the effects of the eddy viscosity and the material diffusivity are dominant compared to the molecular viscosity and mass diffusivity. Where the flow is laminar, the effects of the molecular motions becomes more important than the effects from eddies developed by the turbulence in the flow [**Error! Reference source not found.**]. Other than these two extreme cases, the turbulent Schmidt number must be found based on the comparison between the simulation results and the test data. The default setting of 0.5 was found by these exercises. In order to calibrate the use of the default value and to demonstrate the effects of changing the parameter, a sensitivity analysis has been performed in the following section. The simulations were done with a value of 0.4[5], 0.7[6] and 1.0 which are 20% smaller, 40% and 100% greater than the default setting respectively. The calculation results were compared with the actual test data and the default case run.

$$Sc_{turb}\big|_{fully\ turb} = \frac{\nu + \varepsilon_M}{D_{AB} + \varepsilon_D} = \frac{\varepsilon_M}{\varepsilon_D} \to 1 \quad \left(\nu << \varepsilon_M, D_{AB} << \varepsilon_D\right) \qquad \text{Eq. A.2.11}$$

$$Sc_{turb}\big|_{lam} = \frac{\nu + \varepsilon_M}{D_{AB} + \varepsilon_D} = \frac{\nu}{\alpha} \to Sc \quad \left(\nu >> \varepsilon_M, D_{AB} >> \varepsilon_D\right) \qquad \text{Eq. A.2.12}$$

A.2.2.2.1 Upstream region

Analogous to the results in the previous sensitivity analyses, extensive backflow had occurred in all four cases, SC = 0.4, 0.5(default), 0.7 and 1.0 compared to the test data. As before, the backflow caused the temperatures and the velocities of the gas phase to be higher than the actual test data near the ceiling. Figure A.2.6 shows that changing the turbulent Schmidt number in FDS does not affect the backflow in terms of its length and thickness. Also the velocity profile in Figure A.2.7 supports the findings discussed above.

A.2.2.2.1 Near-fire region

As expected, changing the turbulent Schmidt number had affected the calculation results of the flame length. Figure A.2.5 shows how the flame lengths stretched as the SC value used in the simulations had increased. With the SC of 0.4 and 0.5, the flame tips for these two cases had located in between Loop 304 and 303. For the other two cases, the flames were stretched from the fire base to the near ceiling area at Loop 303 which is about 12m downstream of the fuel location. In order to determine what the actual flame lengths were to compare with the simulation results, the approach taken by Ingason [7] was used. He assumed that the flame tip temperature in a tunnel fire was 600°C. Applying the assumption to the Memorial Tunnel Test 621A the flame tips were placed in between Loop 303 and 302, hence using a value greater than the default setting seems to give better results in terms of predicting the flame length. However, the influence of backflow that occurred in the simulation results must be accounted in the analyses also. Due to the excessive backflow, the flame blowing effect from the forced air stream is smaller than that in the real test conditions near the ceiling, which can possibly allow the flames to tilt less downstream.

The four different case runs were consuming the full amount of the heat release rate indicated in the input file. They were checked by comparing the total heat release rates from the simulation results to the input information. The total heat release rates from each runs showed oscillations as in other simulations done above. Interestingly, the SC = 0.7 and 1.0 cases had oscillations which were in the order of ±20MW at the early stage of the simulations from 80 seconds to 200 after ignition. The oscillations were from the energy loss through the solid boundaries. The reason behind these oscillations seems to be from the fact that the flames were in contact with the ceiling boundaries more often than the other two cases at this time period. The oscillation eventually damps out as the ceiling temperature increases to a point where there are less conductive heat loss through the boundaries. For the other two cases, SC = 0.4 and 0.5, the oscillations in the total heat release rate exists consistently throughout the simulation time. They are in the order of ±10MW.

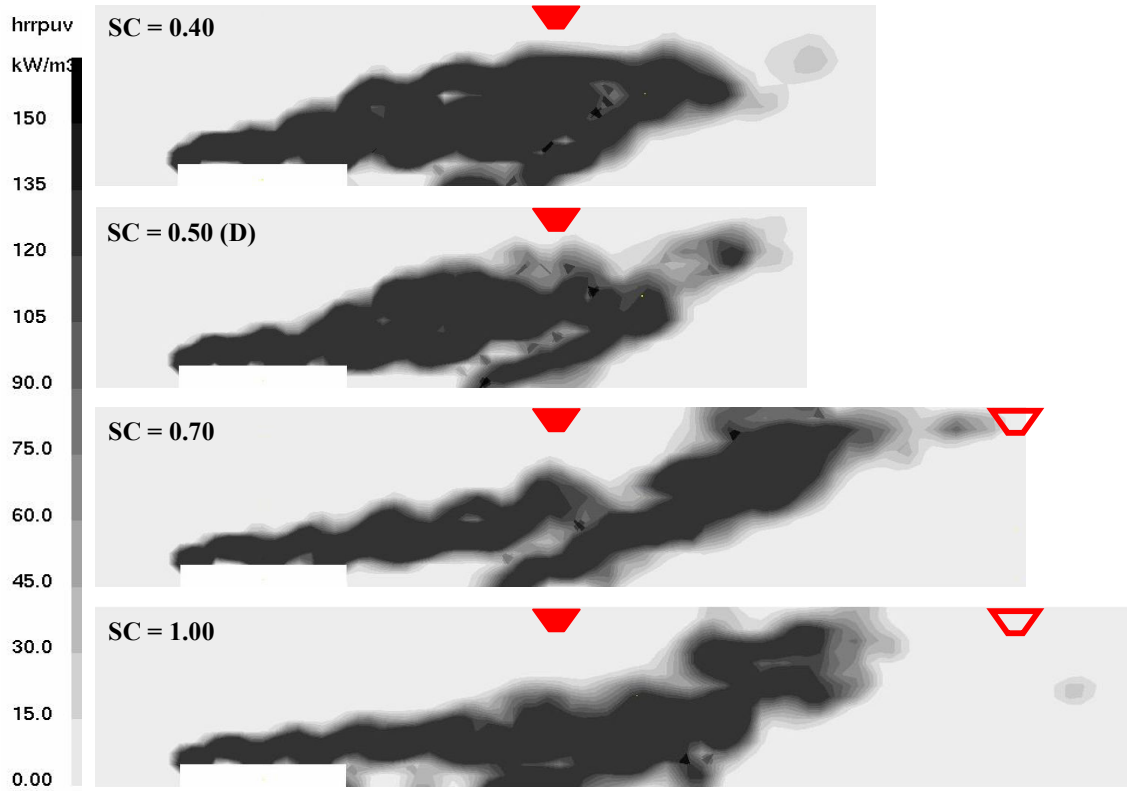

Figure A.2.5. **Heat release rate per unit volume (hrrpuv) at time = 16min. of Memorial Tunnel Test 621A; From the top, actual test data, SC of 0.40, 0.50 (default value), 0.70 and 1.00; Loop 304 marked as ▼ and Loop 303 marked as ▽.**

According to the actual test data, the maximum temperature within the tunnel locates near the ceiling at Loop 303 throughout the test, and its peak of 1502ºF exists around 430 seconds after ignition. The results from SC = 0.5(default) case had placed its maximum temperature around the center of the tunnel cross section area, rather than near the ceiling which was approximately at its flame surface. Also, the existence of the backflow caused the hot gases to travel upstream, and increased the temperature of the gas phase located above the fire base (see Figure A.2.6). There was a 35% reduction in the maximum temperature compared to the test data. The temperature distributions in the near-fire region of the other simulation runs were different due to the flame shapes in each case (see Figure A.2.5). The results from SC = 0.4 case were similar to the default case, but the hottest area had located closer to the fire base than that of the 0.5 case. With larger values of SC used in the simulations, the results showed that the hottest region had moved downstream and closer to the ceiling of the fire, and the low temperature area

above the fire base had increased. These results demonstrate that flame had stretched further downstream as the value used for the turbulent Schmidt number in FDS increased. The maximum temperatures in the time period of 430 ± 100 seconds for SC = 0.4, 0.7 and 1.0 cases were approximately 34%, 34% and 26% lower than the test value, respectively.

The velocity profiles at Loop 305, 304 and 302 (see Figure A.2.7) showed that the differences between four case runs were in the range of ±1m/s. The velocity deviation from the actual test data were within ±6m/s where backflow had occurred and ±1m/s for the rest of the flows in this region.

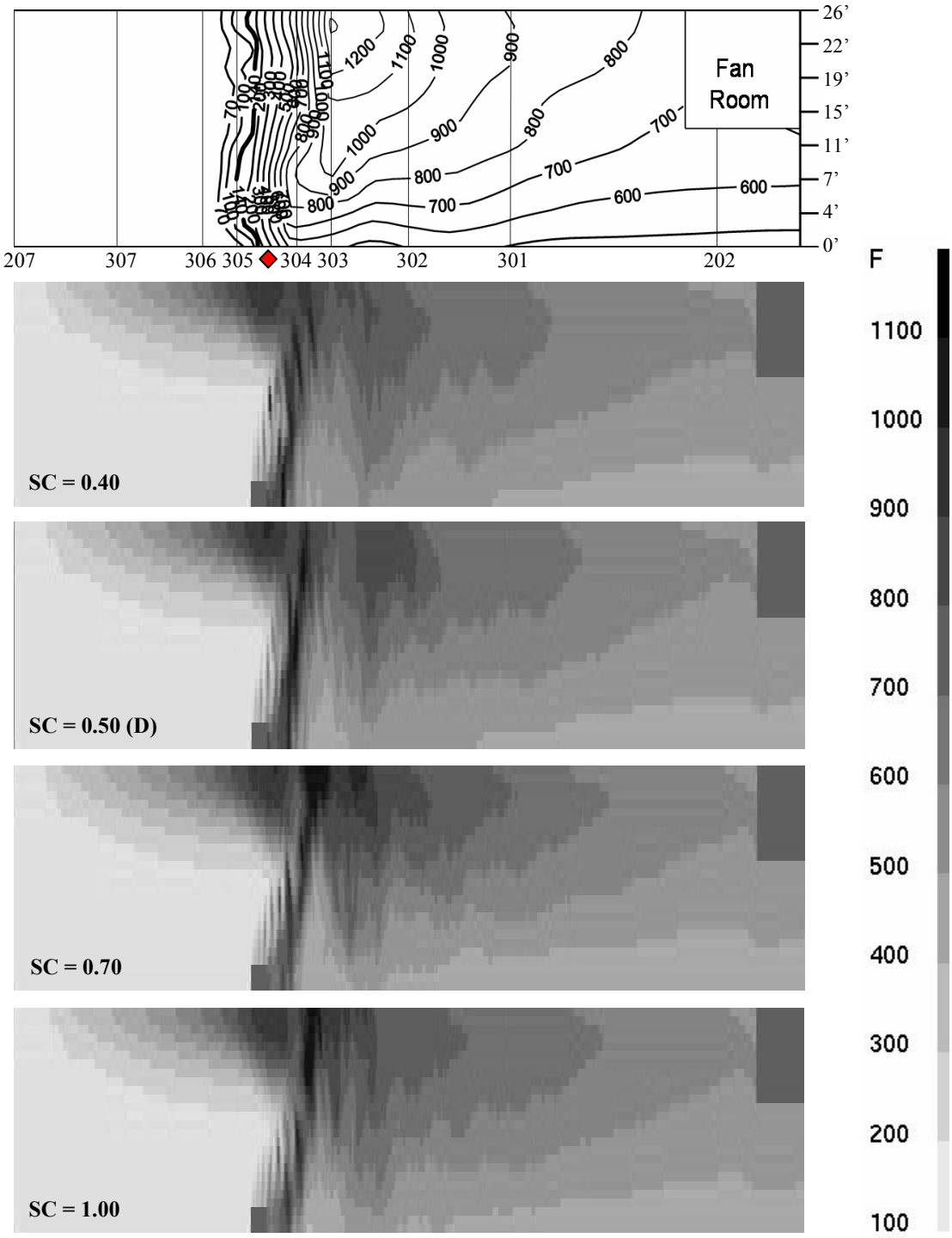

Figure A.2.6. **Temperature Profile at time = 16min. of Memorial Tunnel Test 621A; From the top, actual test data, SC of 0.40, 0.50 (default value), 0.70 and 1.00. The temperature distribution changes around the fire location as the SC varies.**

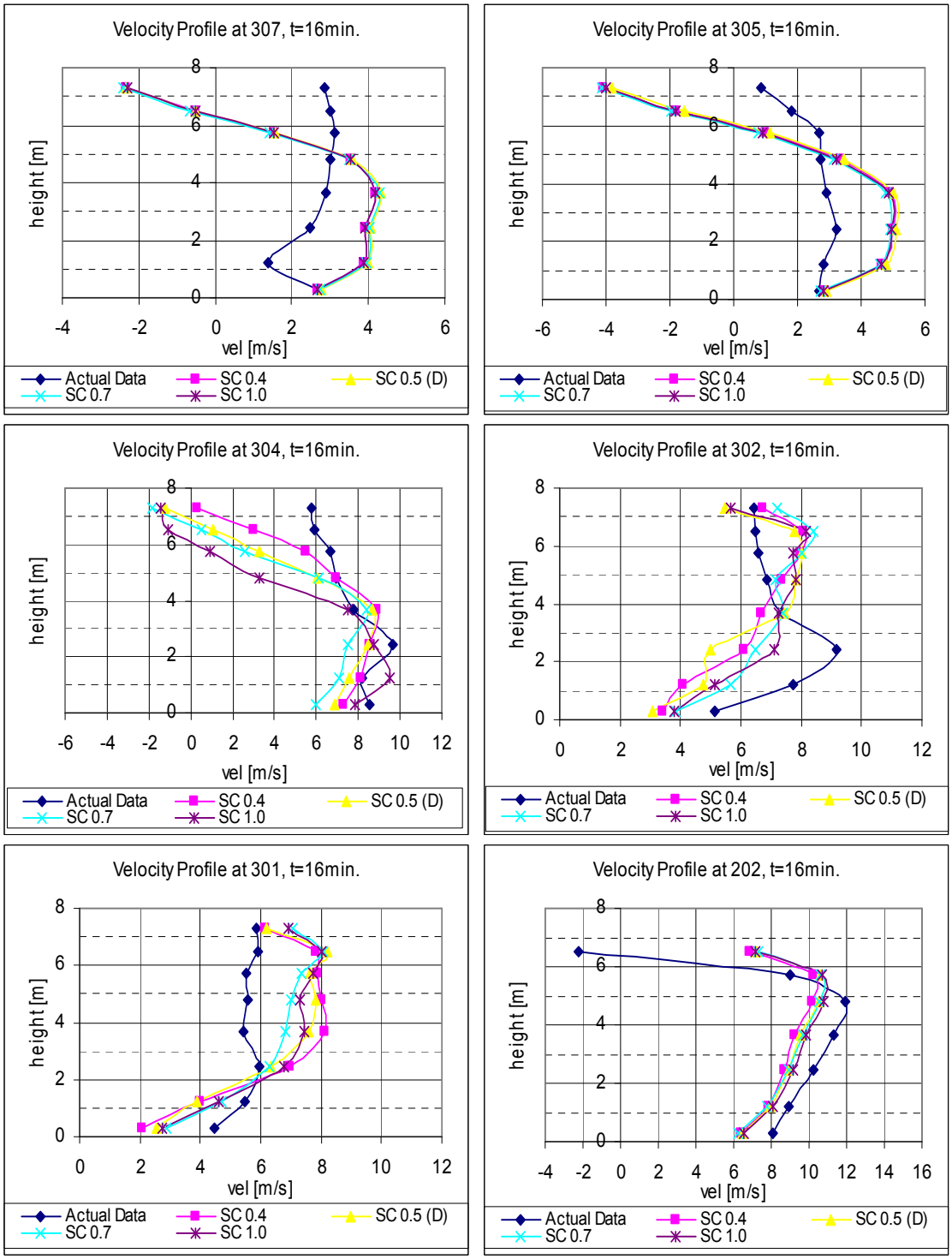

Figure A.2.7. Velocity Profiles using different SC values at time = 16min. of Memorial Tunnel Test 621A; From the top left, velocity at Loop 307, 305, 304, 302, 301 and 202. There are no significant differences in the velocity outputs between the four cases; SC = 0.4, 0.5(default), 0.7 and 1.0.

A.2.2.2.1 Downstream region

Similar to the other regions, the changes which occurred when using a different turbulent Schmidt number were due to the flame shapes. The temperature distribution pattern, from 400ºF to 600ºF are analogous to that of the default run, PR = 0.5 case. For the temperatures above 600ºF, the isothermal lines were placed differently depending on the location of the flame sheets. For cases with Sc_{turb} value greater than 0.5, the temperature line of 700ºF tended to be drawn closer to the ceiling. However, the overall shapes of the temperature distribution of three case runs were similar with each other and to the actual test data. As the distance from the fire increases further down to the tunnel exit, the gases became cooler from the floor area leaving relatively low temperatures around the tunnel exit.

The velocity profile at Loop 301 and 202 demonstrated that changing the Sc_{turb} value has a miner effect in FDS calculations for velocities. The difference between the actual test data and the simulation results were around ±2m/s for the simulations done for the turbulent Schmidt sensitivity analyses.

The turbulent Schmidt number sensitivity analyses demonstrated that changing the constant affects the length of the flame, and hence, alters the temperature distribution near the fire area. However, the suitable Sc_{turb} value cannot be clearly determined for the current simulations due to the existence of the unwanted backflow, even though the actual flame tip locations can be predicted from the fire test temperature measurements. Therefore, although using a larger value than the default setting of 0.5 seems to give better simulation results, this judgment may be incorrect, depending on the influence, which backflow factor is generating on the simulated flame tip position and flame length.

A.2.2.3 Smagorinsky constant, CSMAG

Over the years, studies have been conducted in validating the eddy viscosity subgrid-scale stress model used in LES, also known as the Smagorinsky model. The mathematical expression of eddy viscosity was introduced in the previous sections, where the definition of the total, molecular and Reynolds stress was given.

$$\left(\tau_{yx}\right)_{total} = \left(\tau_{yx}\right) + \left(\tau_{yx}\right)_{turb} = \rho\left(\nu + \varepsilon_M\right)\frac{d\overline{v_x}}{dy} = \left(\mu + \rho\varepsilon_M\right)\frac{d\overline{v_x}}{dy} = \mu_{LES}\frac{d\overline{v_x}}{dy} \qquad \text{Eq. A.2.13}$$

The flow viscosity used in LES calculation, is modeled using Smagorinsky model, because the simulation length scale is not sufficient to capture the details of the eddies generated by the flow turbulence. The model assumes that the turbulent energy in the length scales smaller than the grid is dispersed within the grid allowing no energy flow from the small to large scale, i.e. no backscatter.

$$\mu_{LES} = \rho\left(C_s\Delta\right)^2\left|S\right| \qquad \text{Eq. A.2.14}$$

where the C_s is the Smagorinsky constant, Δ is the grid length scale and S is the function of velocities.

$$\left|S\right|^2 = 2\left[\left(\frac{\partial u}{\partial x}\right)^2 + \left(\frac{\partial v}{\partial y}\right)^2 + \left(\frac{\partial w}{\partial z}\right)^2\right] + \left(\frac{\partial u}{\partial y} + \frac{\partial v}{\partial x}\right)^2 + \left(\frac{\partial u}{\partial z} + \frac{\partial w}{\partial x}\right)^2 + \left(\frac{\partial v}{\partial z} + \frac{\partial w}{\partial y}\right)^2 - \frac{2}{3}\left(\nabla\cdot\vec{u}\right)^2 \qquad \text{Eq. A.2.15}$$

As shown in the above expression, with the grid length scale, Δ, kept as a constant, increasing or decreasing the Smagorinsky constant, C_s, would increase or decrease the dynamic viscosity, μ_{LES} of the flow.

Because the dynamic viscosity, μ_{LES}, is used when calculating the turbulent Prandtl number, Pr_{turb}, and Schmidt number, Sc_{turb}, changing the Smagorinsky constant, , affects the thermal conductivity and mass diffusivity within the flow, allowing changes in the temperature distribution and the flame location.

$$k_{LES} = \frac{c_p\mu_{LES}}{\mathrm{Pr}_{turb}} \quad \text{and} \quad \left(\rho D\right)_{LES} = \frac{\mu_{LES}}{Sc_{turb}} \qquad \text{Eq. A.2.16}$$

Due to the eddy viscosity term in the total shear, the dynamic viscosity is determined by the turbulent motions of the flow, which can only be found empirically. The studies on the Smagorinsky constant have demonstrated that such values give better results in different cases. For example, using 0.23 gave reasonable results in simulating the

decaying turbulence. For mixing layer flows, a Smagorinksy constant used within the range of 0.12 to 0.14 produced the most suitable calculation results and 0.1 was required to simulate the turbulent channel flow [8]. For fire and smoke related flows in a standard fire room test model, 0.18 was considered to be appropriate depending on the resolution of the grid [10]. The researches demonstrate that there is no universal constant, which satisfies to model the turbulence of different flows, effectively. Hence, performing a sensitivity analysis with the Smagorinsky constant to study its effect on tunnel fire simulations was necessary. The Smagorinsky constants used in the first set of the simulations were 0.15, 0.20 (default value) and 0.25. Later two more cases were run using a value of 0.30 and 0.40. The values used for the later case runs did not have any reference for its applications. However, the results from the first set showed that increasing the Smagorinsky constant had a positive effect on reducing the backflow in terms of its length and thickness. Therefore, the values of 0.30 and 0.40 were used to run additional cases to test the connection between the constant and the backflow.

A.2.2.3.1 Upstream region

In the grid sensitivity analysis part, the extensive formation of the backflow in the upstream region was one of the significant differences between the simulation results and the actual data. Due to the backflows, the temperature distribution and the velocity profile of the simulation runs at the upstream area was much higher near the ceiling, comparing to the actual test data. Knowing that the simulations were done neglecting the tunnel slope, and the existence of the slope would encourage the backflow furthermore, the significance of the backflow was a problem. Therefore, the analyses for the upstream region were focused on reducing the backflow from the simulation results for better match with the test data. Interestingly, changing the values of the Smagorinsky constant had a positive effect in decreasing the backflow. As one may see in Figure A.2.8, the backflow reduces as the Smagorinsky constants used in the simulations increases. Hence, the temperature and the velocity distribution of the upstream simulations represent the actual test data better, when a relatively large Smagorinsky constant is used.

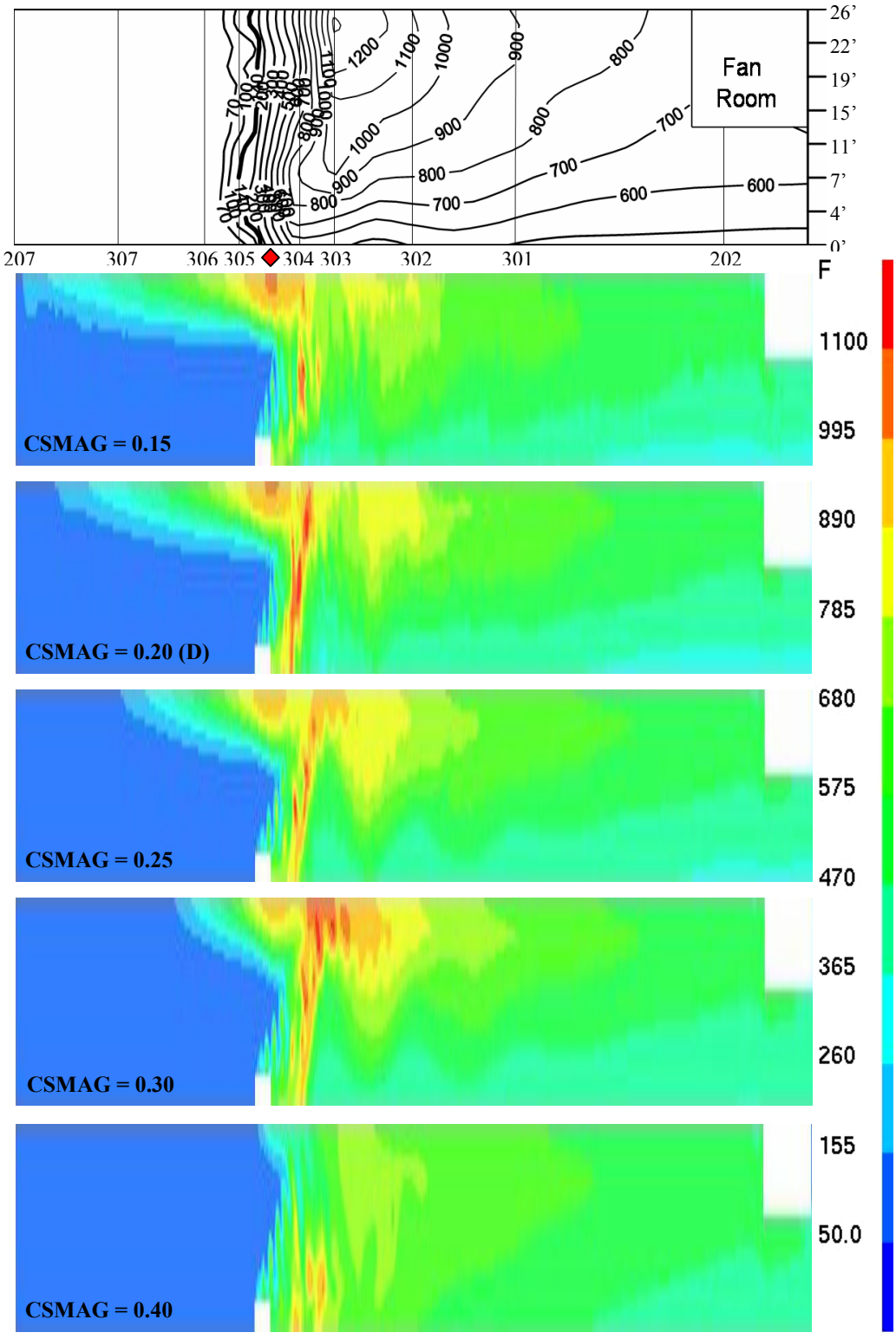

Figure A.2.8. **Temperature Profile at time = 16min. of Memorial Tunnel Test 621A; From the top, actual test data, CSMAG of 0.15, 0.20 (default value), 0.25, 0.30, and 0.4. The backflow in the upstream region decreases as the CSMAG increases.**

A.2.2.3.2 Near-fire region

All the total heat release rates in the hrr file, which is automatically generated during the calculations, were checked to see whether FDS was introducing the full amount of the heat release rate described in the input file. Although the total heat release rate curve from the simulations showed oscillations, the average heat release rates from each case run were close to the input information. The CSMAG = 0.15 and 0.20 (default) case runs had the most significant oscillations, both in the order of ±10MW. For the other cases, the oscillations had smoothed out as the Smagorinsky constant used in the simulations had increased. The total heat release rate for the CSMAG = 0.40 showed the least amount of oscillation, roughly in the order of ±2MW. Along with the reduction in the total heat release rate fluctuations as the Smagorinsky constant increases, the dynamics of the fire had smeared off which was visualized through Smokeview. Hence, instead of having flame sheets forming and deforming vorticities, the shape of the fire would stay almost stable.

The test data shows that the maximum temperature within the tunnel locates near the ceiling at Loop 303 throughout the test, and its peak of 1502˚F exists around 430 seconds after ignition. The CSMAG = 0.20 (default) had resulted in placing the maximum temperature around the center of the tunnel cross section. The flames from the tunnel floor to the ceiling were the hottest area. Also, the hot gases traveled upstream, leading to an increase in the temperature readings above the fire base. The maximum temperature had reduced 35% compared to the test data. The CSMAG = 0.15 case results were analogous to the CSMAG = 0.20 (default) case, but with increased backflow. The simulation runs with CSMAG = 0.30 and 0.40 were successful in suppressing the backflow. The CSMAG = 0.30 case shows the most appropriate representation of the actual test data in terms of the overall temperature distribution in the near-fire region, i.e. having high temperatures near the ceiling around Loop 303. However, the maximum temperature in the time interval of 430 ± 100 seconds was 35% lower than the reported value and the existence of the backflow issue remained. The maximum temperature and the temperature distribution pattern from the CSMAG = 0.40 case were approximately 47% lower and significantly different compared to the test data.

The velocity profile comparisons for Loop 305, 304 and 302 (see Figure A.2.9) shows that there are difficulties in selecting the most appropriate Smagorinsky constant for the Memorial Tunnel Test 621A simulations. Flows near the wall boundaries are calculated better using a relatively large Smagorinsky constant. Flows close to the centerline of the tunnel are well resolved when a relatively small Smagorinsky constant is used in the modeling process. However, note that the discrepancies between the actual test data and the simulated ones are within the range of ±6m/s for near-wall regions while ±2m/s for the flows located in the center of the tunnel meaning that varying the Smagorinsky constant did not affect the simulation results considerably for the flow calculations far from the solid boundaries.

A.2.2.3.3 Downstream region

Generally, the temperatures were low compared to the test data throughout the downstream area. The average difference between the simulation results and the test data were around 200ºF. However, the shapes of the temperature distribution of five case runs were similar with each other and to the actual test data. As the distance from the fire increases further down to the tunnel exit, the gases became cooler from the floor area leaving relatively low temperatures around the tunnel exit. It is fair to conclude that changing the Smagorinsky constant had modest impact on the temperature distribution in the downstream region of the fire.

The velocity profile comparison in the downstream region, Loop 301 and 202 displayed that CSMAG = 0.15 case produced the most realistic simulation results. The velocity distribution pattern is similar to the actual test data. The difference between the maximum flow rate near the centerline of the tunnel and the minimum flow rate near the solid boundaries are less than 2m/s for the CSMAG = 0.15 case while other case runs generates more than 2m/s. In other words, reducing the Smagorinsky constant led to a quasi-plug flow analogous to the given test data while increasing the value created more flow resistance near the tunnel walls causing the flow to have a shape close to a parabola.

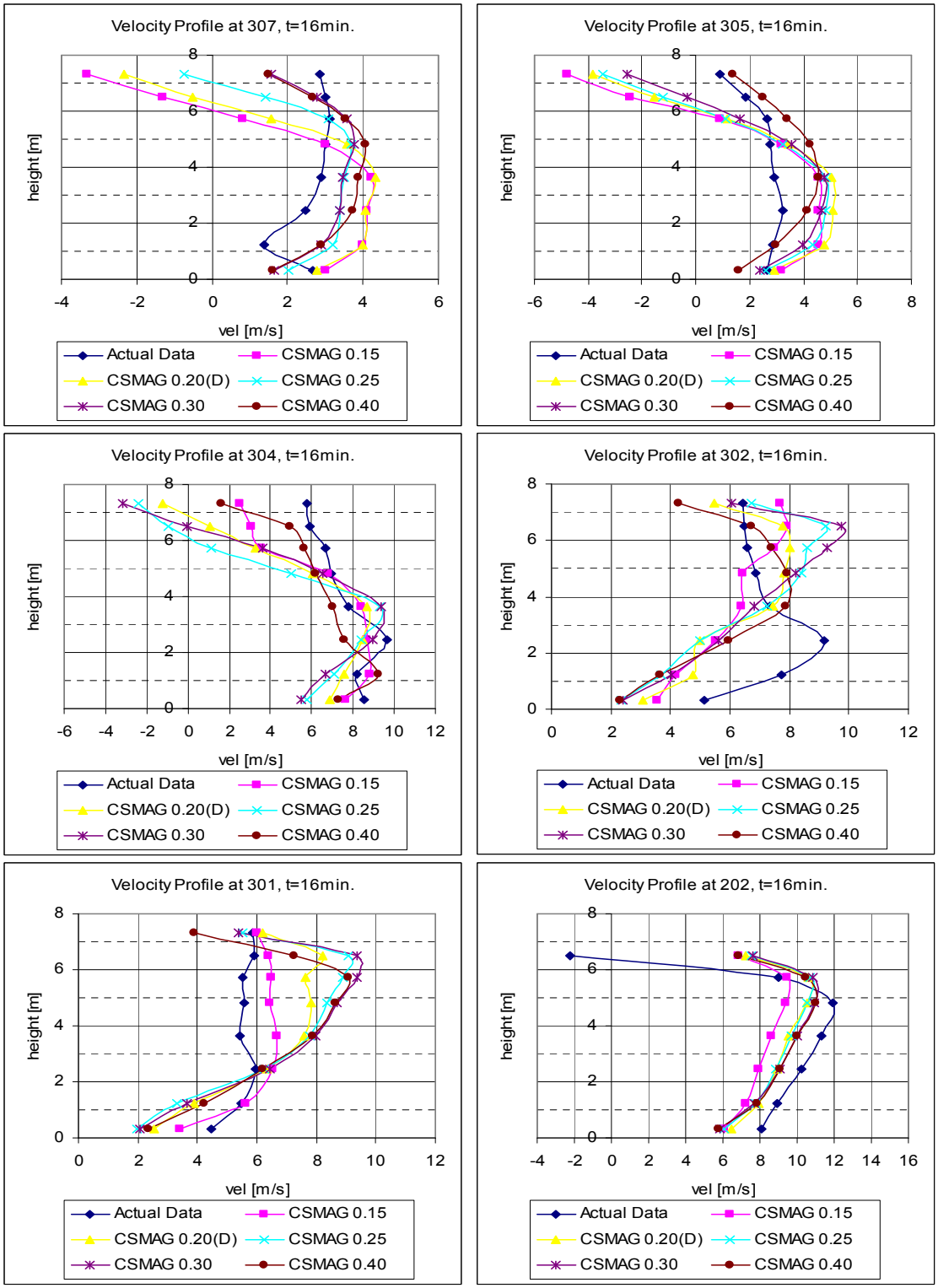

Figure A.2.9. Velocity Profiles using different CSMAG values at time = 16min. of Memorial Tunnel Test 621A; From the top left, velocity at Loop 307, 305, 304, 302, 301 and 202. Changing the CSMAG value affected the velocity outputs in the upstream region.

The Smagorinsky constant sensitivity analyses demonstrated that finding a single value which properly models the entire gas phase flow throughout the tunnel is impossible. As noted in the previous section, relatively large Smagorinsky constant is needed to reduce the backflow in the simulation results which does not exist in the test data. Because using a larger value of the Smagorinsky constant means adding artificial visocisty to the flow and forcing the flow to stick together, using a larger Smagorinsky constant helps the hot gases from the fire to travel less upstream. However, using a value greater than the default setting, 0.2, causes the fire to loose small scale dynamics, i.e. no vorticities like curvatures and fluctuations are formed at the flame sheets. For the downstream region, where the hot gases continuously mix with the cold lower gas layer and flow through the tunnel towards the exit, a Smagorinsky constant of less than 0.2 is required for satisfying simulation results. Therefore, instead of searching for the ideal Smagorinsky constant that presents good modeling results for the whole tunnel, the constant should be selected depending on the purpose of the simulations. The value, which resolves the flow or the phenomena of interest most appropriately, should be applied to the calculations, based on the findings provided by the analyses performed above.

A.3. REFERENCE

1. McGrattan, K., Large eddy simulations of smoke movement, Fire Safety Journal 30(2), 161-178, 1998
2. Drysdale, D., An Introduction to Fire Dynamics, 2nd edition, John Wiley & Sons, ©1998
3. Welty, J.R., Wicks, C.E., Wilson, R.E., Rorrer, G., Fundamentals of Momentum, Heat, and Mass Transfer, 4th ed., John Wiley & Sons, Inc., New York, NY, ©2001
4. Zhang, W., Hamer, A., Klassen, M., Carpenter, D., Roby, R., Turbulence statistics in a fire room model by large eddy simulation, Fire Safety Journal 37(8), November (2002), 721-752
5. W. Zhang, N. Ryder, R.J. Roby, and D. Carpenter. Modeling of the Combustion in Compartment Fires Using Large Eddy Simulation Approach. In *Proceedings of the 2001 Fall Technical Meeting, Eastern States Section*. Combustion Institute, Pittsburgh, Pennsylvania, December (2001)
6. H. Pitsch, H. Steiner, Large-eddy simulation of a turbulent piloted methane/air diffusion flame (Sandia flame D), Physic of Fluids, Volume 12, Number 10, October (2000)
7. N. Branley, W.P. Jones, Large Eddy simulation of a turbulent non-premixed flame, Combustion and Flame 127 (1-2) (2001) 1914-1934
8. Lönnermark, A., Ingason, H., Fire Spread and Flame Length in Large-Scale Tunnel Fires, Fire Technology, In Press
9. Yoshizawa, A., Eddy-viscosity-type subgrid-scale model with a variable Smagorinsky coefficient and its relationship with the one-equation model in large eddy simulation, Phys. Fluids A 3(8), August (1991), 2007-2009
10. The SFPE Handbook of Fire Protection Engineering, 3rd ed., National Fire Protection Association, Quincy, MA, ©2002